Università degli Studi di Padova
Dipartimento di Ingegneria Industriale
Corso di laurea Magistrale in Ingegneria Energetica

Technical University of Denmark
International Centre for Indoor Environment and Energy

THE USE OF PHASE CHANGING MATERIALS FOR COOLING OF BUILDINGS COMBINED WITH NIGHT SKY RADIANT COOLING

RELATORE: CH.MO PROF. MICHELE DE CARLI
CORRELATORE: CH.MO PROF. BJARNE W. OLESEN

LAUREANDO: FABIO GROSSULE
MATRICOLA: 1061387

ANNO ACCADEMICO 2014/2015

A Marika, per avermi costantemente sostenuto e incoraggiato durante questa esperienza e per aver sopportato la mia assenza nel corso di questi ultimi mesi.

Un sentito grazie ai miei genitori Paolo ed Emanuela per avermi dato la possibilità di intraprendere questa meravigliosa esperienza e per aver sempre riposto la massima fiducia in me.

Kongens Lyngby, Aprile 2015

Fabio

Acknowledgements

First and foremost, I would like to express my sincere gratitude to Professor Bjarne W. Olesen, without whom this great experience in Denmark would not have been possible.

Furthermore, I would like to thank my supervisors Eleftherios Bourdakis and Ongun Berk Kazanci for the constant guidance and the precious advice provided all along the work carried out for this thesis.

A special thanks to Marcos García for the effort in building the control system of the experimental setup and for the extraordinary cooperation during the last stages of this work.

I wish to thank Nico Henrik Ziersen for the effort and support in building up the experimental setup and for helping me increasing my practical knowledge through the patient explanations provided.

Many thanks to Luca Gennari, Thibault Péan and Georgi Krasimirov Pavlov for their helpfulness and for the precious information provided throughout my work.

Also I would like to thank my colleagues at the International Centre for Indoor Environment and Energy for the warm welcome and for making me feel part of the team since the very first day.

And last but not least, a heartfelt thanks to all my flatmates for the great time spent together. It has been a wonderful experience!

Abstract

The world energy consumption has increased rapidly in the last decades, mainly due to the population growth and to the industrial development. Since the global warming has become a widespread concern, many countries are making efforts to slow it down, through proper energy policies.
The enhancement of the energy efficiency is considered to be one of the most practical ways to reduce the energy consumption and the building sector is shown to be the one with the highest potential. Indeed, the energy use in buildings accounts for over 40% of primary energy consumption in many IEA member countries and the most of it is required for heating and cooling purposes.

In the present study an application combining night sky radiant cooling with phase changing materials (PCM) for cooling of a room in an office building is investigated. The thesis comprises of a review of existing literature in the fields of phase changing materials and night sky radiant cooling for cooling applications in buildings, an experimental study and a parametric study, employing the dynamic simulation software TRNSYS 17.

The experimental data have been employed for the validation of the simulation model, which was used afterwards to assess the performance of the system providing cooling to a 2-persons office room. The summer climates of Copenhagen, Milan and Athens have been selected for the purpose.

The simulation model developed exhibited satisfactory accuracy in describing the thermal conditions of the indoor space and the behaviour of the phase changing material embedded in the suspended ceiling. The representation of the night sky radiant cooling process was in general less precise; the gap between the results of the simulation and the experimental study, in terms of overall cooling power provided by the solar circuit, ranged from less than 4% to 34% of the experimental value.

The coupling between phase changing materials and night sky radiant cooling shows good potential in Copenhagen and Milan, since a significant portion of the energy required to discharge the PCM (35% and 30% respectively) was covered by the nocturnal cooling output of the solar collectors. Contrarily, limited performances were achieved for the warm climate of Athens.

The average cooling power per unit area provided by the photovoltaic-thermal collectors (PV-T) varies between 30 and 35 W/m^2 in Copenhagen and Milan, whereas a value of approximately 20 W/m^2 is assessed under Athens' climate conditions. The nocturnal cooling output of the unglazed solar collector is negligible for the first two locations while heating is provided during the whole night in Athens.

Finally, it has been highlighted that in all three reference locations only the radiative heat exchange contributes to the cooling effect during summertime, thus justifying the name "night sky radiant cooling" assigned to the considered technology.

Sommario

Il consumo energetico mondiale ha subito un notevole incremento negli ultimi decenni, principalmente a causa della crescita demografica e dello sviluppo industriale. Poiché il riscaldamento globale è divenuto una preoccupazione diffusa, molti Paesi stanno tentando di rallentare questo fenomeno attraverso l'adozione di opportune politiche energetiche.
L'incremento dell'efficienza energetica è considerato essere una delle modalità più facilmente attuabili per ridurre il consumo di energia e il settore edilizio è quello con il maggior potenziale. Infatti, la domanda di energia negli edifici è responsabile di oltre il 40% del consumo complessivo di energia primaria in molti Stati membri dell'IEA e la maggior parte di essa è richiesta per il riscaldamento e il raffrescamento degli ambienti.

Il presente studio analizza il funzionamento di un'applicazione che combina la tecnologia del *night sky radiant cooling* con materiali in cambiamento di fase (PCM) per il condizionamento di un ufficio. La tesi comprende una revisione della letteratura esistente nell'ambito dei materiali in cambiamento di fase e in quello del *night sky radiant cooling* per applicazioni di condizionamento degli edifici, uno studio sperimentale e un'analisi parametrica effettuata con il software di simulazione dinamica TRNSYS 17.

I dati sperimentali sono stati impiegati per la validazione del modello di simulazione, utilizzato per valutare le prestazioni dell'impianto il cui scopo era condizionare un ufficio di 2 persone; le condizioni meteorologiche estive di Copenaghen, Milano ed Atene sono state scelte come riferimento.

Il modello di simulazione sviluppato ha mostrato sufficiente accuratezza nella descrizione delle condizioni termiche della camera climatica e del comportamento del materiale in cambiamento di fase contenuto nel soffitto. La simulazione del processo di *night sky radiant cooling* era in generale meno fedele alla realtà; la differenza tra il *cooling output* sperimentale e quello risultante dalla simulazione variava tra il 4% e il 34% del valore misurato.

L'integrazione tra la tecnologia PCM e quella del *night sky radiant cooling* rivela un buon potenziale per i climi di Copenaghen e Milano, giacché una porzione rilevante dell'energia richiesta per espletare la fase di scarica del PCM (35% e 30% rispettivamente) era fornita dai collettori solari. Al contrario, il potenziale dell'impianto si è rivelato limitato nelle condizioni climatiche di Atene.

Il carico di raffrescamento per unità di superficie esposta dei collettori fotovoltaico-termici (PV-T) varia tra 30 W/m^2 e 35 W/m^2 a Copenaghen e Milano, mentre presenta un valore di circa 20 W/m^2 nelle condizioni climatiche di Atene. La potenza di raffrescamento del collettore piano non vetrato è esigua per i primi due siti mentre un effetto di riscaldamento del fluido termovettore è stato riscontrato per Atene.

In conclusione, è stato evidenziato che nel periodo estivo la potenza di raffrescamento è prodotta interamente dal processo di scambio termico radiativo con la volta celeste; questa considerazione giustifica il nome "*night sky radiant cooling*" assegnato alla tecnologia considerata.

Table of Contents

1 Introduction

The world energy consumption has increased rapidly in the last decades, mainly due to the population growth and to the industrial development. Since the global warming has become a widespread concern, many countries are making efforts to slow it down, through proper energy policies. The reduction of the worrying trend of the climatic change can be pursued primarily in three ways:

- reducing the overall energy demand
- improving the energy efficiency of processes and systems
- increasing the amount of energy produced by renewable resources.

The last two modalities are mentioned in the 20-20-20 European plan and energy package, which defines the EU's targets to reduce climate impact and energy consumption [1]. Specifically, these targets aim to achieve by 2020 a 20% reduction in EU greenhouse gas emissions from the level of 1990, a 20% improvement in the EU's energy efficiency and raising the amount of EU energy consumption produced from renewable resources to 20%.

The enhancement of the energy efficiency is considered to be one of the most practical ways to pursue the prefixed goal and the building sector is shown to be the one with the highest potential. Indeed, a recent study from International Energy Agency (IEA) [2] reported that energy use in buildings accounts for over 40% of primary energy consumption in many IEA member countries and the most of it is required for heating and cooling purposes.

There are several measures which can be adopted in order to increase the energy efficiency of a building, mainly related to the building's envelope and the cooling/heating system's performance.

In the last years, a lot of effort has been put to provide a better insulation for the buildings' structures, such as incorporating high performance insulation materials in the walls and adopting multiple-layer windows [3].
Furthermore, the importance of having a good interaction between the building's envelope and the sun, both in winter and in summer, has been remarked [3]. Modern houses are able to optimally manage the solar heat gains, in order to reduce the heat demand in winter and avoid overheating during the warm season. This can be done basically through a proper positioning and sizing of the windows (which have to present optimal optical properties) or by means of shading devices.

The efficiency of the conditioning plant can be perfected in different ways, such as by substituting the old components with modern ones or by improving the control mechanism. Moreover, the coupling of the existent systems with renewable sources and the use of passive heating/cooling techniques can lead to a significant reduction of the energy demand.

In order to exploit the great energy saving potential in the buildings sector, several innovative technologies have been studied during the last years. Among these, phase changing materials and night sky radiant cooling have been shown to have a good potential in terms of energy consumption reduction in civil applications. The present study intends to evaluate the performance of a cooling system combining these two technologies for an office building.

2 Introduction to PCMs

Phase changing materials (PCMs) are thermal energy storage substances, used to control temperature fluctuations in different applications, such as buildings and clothes. Their peculiarity is the ability to store latent heat by changing their physical state. This allows them to store a much larger amount of thermal energy per unit mass or unit volume than conventional materials. They can accumulate between 5 and 14 times more heat per unit volume than sensible storage materials such as water, masonry, or rock [4].
Although these materials have been studied since the 80's, they never succeeded in reaching a wide usage in buildings due to different reasons, such as costs, chemical compatibility with other building materials and flammability issues [5].

2.1 Classification

PCMs can be classified in four categories regarding the physical states involved in the phase transition:

1. Solid-liquid
2. Solid-gas
3. Liquid-gas
4. Solid-solid.

The transitions involving gas phase are not practical because of the large volumes or high pressures required to store the materials, while solid-solid PCMs have typically a very slow phase change and low heat of transition.
Hence, solid-liquid PCMs are the most suitable technology for storing thermal energy in buildings.
Solid-liquid phase change substances can be as well categorized in:

1. organic, such as paraffins, fatty acids and sugar alcohols;
2. inorganic, such as salt hydrates.

Strengths and weaknesses of these substances will be pointed out later in the text, and a short comparison between the two classes will be provided.
This report will focus on organic solid-liquid PCMs since the test room used for the experimental study is equipped with panels containing microencapsulated[1] paraffin.

2.2 Principle of operation of a solid-liquid PCM

One of the aims of the present work is to study the behavior and the effects of the use of PCMs in an office room during the cooling season.
The mechanism which stands at the base of this technology is the following: during daytime the PCM absorbs heat by melting (charge phase), thus resulting in a reduction of the cooling load of the building, while during the night it is cooled down and solidifies, so it releases the thermal energy previously stored (discharge phase). Figure 2.1 shows the working principle of a microencapsulated phase changing material.

[1] Microencapsulation is a technique by means of which the PCM particles are enclosed in a thin polymeric coating; the capsules obtained are then embedded in the construction material.

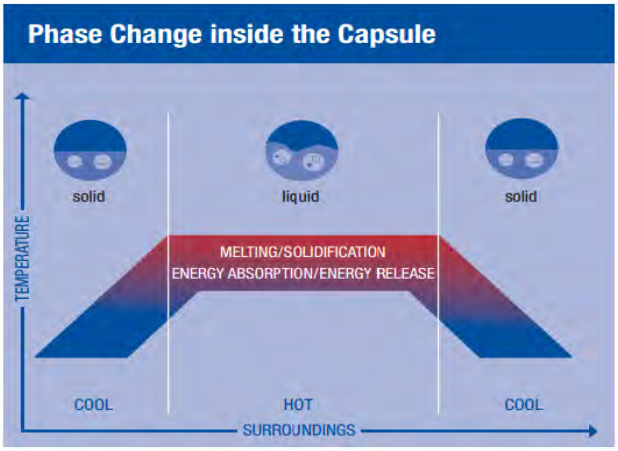

Figure 2.1 – Schematic representation of the phase change in a microencapsulated PCM [6]

The process explained is based on the so called "Thermal mass activation" concept, which can be divided in two main categories [7]:

- Passive (or Surface) Thermal Mass Activation;
- Active (or Core) Thermal Mass Activation.

In the first one, the thermal energy is stored during daytime by a direct heat exchange between the surface of the material and the indoor environment. The penetration depth of the stored heat depends on the thermal properties of the building's fabric. During the night the energy previously absorbed by the structures, which may be provided with PCMs, is released to the external environment through natural or mechanical ventilation.
Active thermal storage is similar to the passive concept, but here the thermal energy is removed from the building structure during the night by a fluid circulating inside a duct or pipe system embedded in the building envelope; these systems are labelled with the name TABS (Thermo-Active Building Systems) [7]. The thermal energy absorbed by the heat carrier during night can be released to the external environment through different methods, such as using a chiller or by means of night-time radiative exchange with the sky.
Figure 2.2 shows a typical structure of PCM panel, both for passive and active applications.

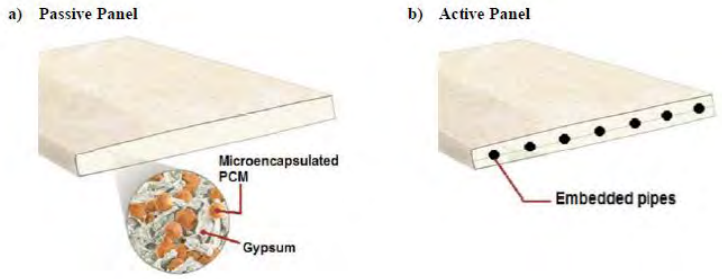

Figure 2.2 – PCM-gypsum ceiling panels [7]

This report will focus on the use of an active system, in which the discharge of the PCM will be ensured by night sky radiant cooling. The radiative heat exchange process between the panels and the sky will be further investigated later in the text.

2.3 Advantages and drawbacks of using PCMs

The enhancement of the thermal mass of the building due to the adoption of PCMs in the envelope has several advantages, both for heating and cooling. Since this study is focused on a cooling application, only the benefits and the weaknesses concerning the cooling mode will be taken into consideration. The adoption of phase changing materials allows pursuing:

- a reduction of the peak cooling load by shifting part of the cooling demand from peak to off-peak periods, as shown in Figure 2.3 (this process is called peak-shaving);
- a reduction of the peak electrical power supply (electricity is necessary if the cooling is provided by a chiller or a heat pump), thus allowing the customers to subscribe more convenient contracts with the electrical energy provider[2];
- the shift of part of the electrical energy demand during night, when the price of the electricity is lower in many countries;
- an attenuation of the indoor temperature fluctuations, thus leading to an improvement of the thermal comfort, as illustrated in Figure 2.4;
- a reduction of the size of the HVAC system, which allows to have:
  - lower initial cost
  - lower operation and maintenance cost
  - greater compactness of the plant;
- a greater coupling with renewable energy cooling techniques (such as solar cooling or night sky radiant cooling), since generally they cannot supply a high peak power;
- the chance to increase the supply temperature[3], if the cooling energy is provided by a mechanical plant (for example an electrical chiller), thus leading to:
  - improvement of the energy efficiency of the plant (COP[4]), that implies a lower energy consumption
  - the possibility of having free cooling, if the outside temperature is low enough (it has to be lower than the supply temperature).

The last concept mentioned needs further investigation. In order to maintain a constant indoor temperature, the power provided by the plant installed (P_{plant}) must match the cooling load of the building ($P_{demanded}$) every time of the day. The power generated by the chiller can be expressed as:

$$P_{plant} = \dot{m} \cdot c \cdot (t_{supply} - t_{return})$$

where:

- $\dot{m}$ [kg/s] is the flow rate of the fluid used as heat carrier
- c [kJ/(kg K) is the specific heat of the heat carrier
- t_{supply} [K] is outlet temperature of the chiller
- t_{return} [K] is the inlet temperature of the chiller.

Assuming to have constant flow rate and specific heat, if the power required by the building decreases, the temperature difference can be reduced. Hence, if the chiller is set to ensure a fixed return temperature, the supply temperature drops and so does the one in the evaporator of the cooling machine. Since the higher the evaporation temperature is, the higher the COP is, increasing the supply temperature leads to an improvement of the efficiency of the refrigeration cycle [3].
In conclusion, the adoption of PCM in the building's structures may result in an improvement of the chiller operation.

[2] In some countries, Italy included, once a year costumers pay a tariff depending on the maximum power required from the grid, defined in the contract subscribed with the energy provider; the higher the maximum power set is, the higher the related fare is.
[3] The supply temperature has to be suitable for the complete discharge of the PCM.
[4] The Coefficient of Performance (COP) of a chiller is the ratio between the cooling power produced ($P_{cooling}$) and the electrical energy consumed by the pumps and the compressor (P_{el}):

$$COP = \frac{P_{cooling}}{P_{el}}$$

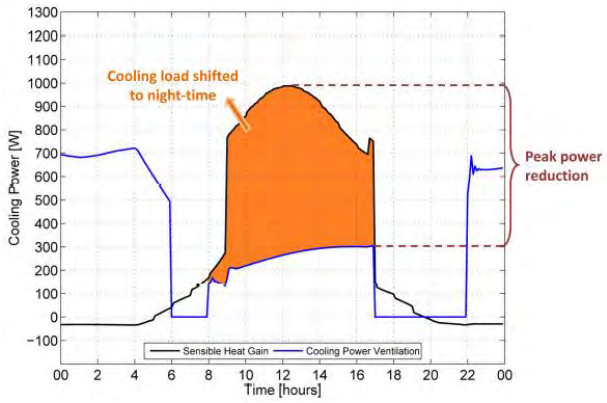

Figure 2.3 – Load shifting and peak shaving effects in an office with passive PCM-gypsum ceiling panels [7]

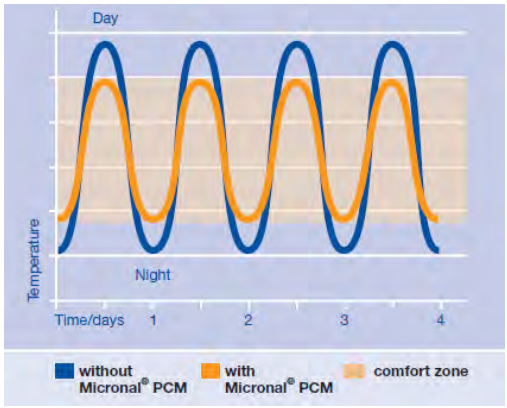

Figure 2.4 – Attenuation of the indoor temperature fluctuation due to the PCM [6]

As every technology, PCMs present some drawbacks, among which:

- higher cost than conventional building materials
- flammability issues
- incompatibility with other materials, such as metals, due to corrosion issues.

2.4 Desired characteristics in a PCM

The aim of this paragraph is to present the main requirements of a phase changing material to be suitable for cooling applications. The desired features can be categorized in three classes [8]:

- Thermal properties:
  - suitable phase change temperature (the value depends on the application)
  - large latent heat of fusion, to achieve high storage density
  - high thermal conductivity, to be able to absorb and release the heat in a short time
  - reproducible phase change, also called cycling stability, to store the heat as many times as necessary
  - small subcooling[5] (see Figure 2.5), to avoid the need of temperatures below the solidification point to discharge the PCM

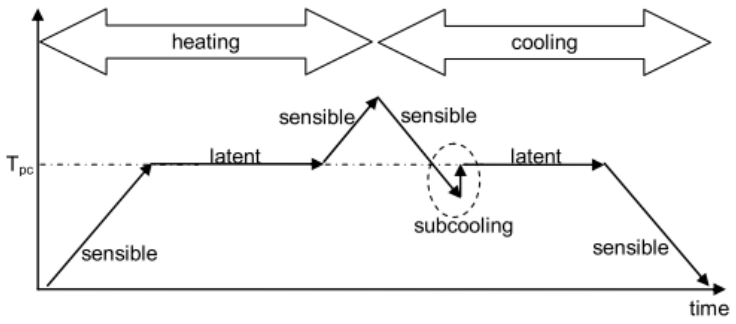

Figure 2.5 – Schematic temperature change during heating and cooling of a PCM with subcooling [8]

[5] Subcooling (also called supercooling) is the effect that a temperature significantly below the melting temperature has to be reached, so that a material begins to solidify and release heat (fig.6.2). If that temperature is not reached, the PCM will not solidify and thus only store sensible heat.

- Chemical properties:
  - chemical stability, to assure long lifetime of the PCM
  - compatibility with constructional materials
  - lack of corrosivity
  - lack of flammability
  - lack of toxicity

- Other requirements:
  - low volume change during the transition phase, to reduce mechanical stress on surrounding materials
  - low price
  - high availability
  - high recyclability, for environmental and economic reasons.

There is no material which fulfils all the requirements presented.
Most of the early studies on latent heat storage in buildings focused on inorganic materials, above all on salt hydrates, because they are cheaper than organic PCMs and they have higher melting enthalpy per volume, due to their higher density. However, they have many drawbacks ([4], [7], [8]):

- incompatibility to metals, due to corrosion issues
- tendency to subcool
- higher volume change during the transition than organic PCMs (up to 10%)
- they do not melt congruently because they are made of several components (at least one salt and water) and they can potentially separate into different phases.

Phenomena such as supercooling and phase separation alter the thermal behaviour of these materials and cause random variation of the transition zone over repeated phase-change cycles.

In an effort to avoid the problems inherent to inorganic PCMs, interest has turned towards organic substances such as fatty acids and their derivatives and paraffins. Those materials are more costly than common salt hydrates, and they have lower heat storage capacity per unit volume. However, some of these materials have strong advantages, such as physical and chemical stability, good thermal behaviour, and adjustable transition zone.
Paraffins show good storage density with respect to mass and they melt and solidify congruently with little or no subcooling. Furthermore, their compatibility with metals is very good.
Fatty acids show almost the same characteristics as paraffins but they present a worse compatibility with metals.
Organic PCMs' drawbacks are mainly related to flammability. Moreover, most PCMs suffer from the common problem of low thermal conductivity, being around 0.2 W/mK for paraffin wax and 0.5 W/mK for hydrated salts and eutectics, which prolongs the charging and discharging phases' duration. Inadequate heat transfer and overall reduction in thermal conductivity during energy recovery are identified as the main barriers affecting the performance of a PCM wallboard system.

In spite of these limitations, paraffins seem to be for now the most suitable substances for thermal storage building applications as PCMs; this is the reason why the test room used for the experiments has been equipped with panels including microencapsulated paraffin. From now on the report will focus mainly on this specific technology.

2.5 Potential

Many studies about PCMs can be found in literature, most of them trying to identify new substances which may be suitable for latent thermal energy storage. Probably thousands of single materials and mixtures of substances have been investigated for their use as PCM in the past decades [8].
Hereafter a short literature review is provided, focusing on the potentialities of these materials in cooling applications.

With regards to the storage capacity, Hawes et al. [9] conducted some tests on PCM wallboards and PCM concrete blocks in order to provide a comparison with conventional wallboards and concrete blocks. They tested a wide range of phase change materials, including some paraffins for the case of concrete blocks. They found that the concrete walls including PCM showed an energy storage capacity in the order of 200-230% of conventional blocks through a 6 °C change.

A research [10] highlighted that the diurnal energy storage achievable with wallboards impregnated with phase change materials is limited to about 300-400 kJ/m^2, even if the wallboard is manufactured with a greater latent capacity.

Regarding the melting/solidification temperature range, some researches [7], [11] show that in building thermal mass enhancement applications it should be in the comfort temperature range. PCMs with a phase change temperature between 18 and 30°C are expected to meet the need of thermal comfort.

An innovative concrete including a commercial microencapsulated polymeric phase change material, called Micronal®, was studied in order to evaluate its ability in terms of temperature fluctuation control [5]. The experimental setup, located in Spain, consisted of two identically shaped cubicles, one made of conventional concrete while the second one built with the modified concrete (it contained 5% in weight of phase change material in the south and the west walls and in the ceiling).
The results obtained demonstrated a great potential of the encapsulation of PCMs in concrete in terms of increase of the thermal inertia of the structure. In fact, considering the south façade under summer conditions, the cubicle without PCM had a maximum temperature 1 °C higher and a minimum temperature 2 °C lower than that with phase change material. In addition, the maximum temperature in the wall with phase change material appeared about 2 hours later compared to the case without PCM. The effect of the higher thermal inertia appeared in the afternoon due to the solidification of the PCM, but also earlier in the morning due to its melting.

Other researchers assessed the thermal performance of a composite PCM wallboard constituted by microencapsulated paraffin in a copolymer, through an experimental study carried out in a test cell located in Lyon (France) [12]. Two series of experiments were conducted: in the first one the test room was made of conventional building materials, while for the second one three of its walls were modified to include the PCM. The results obtained show that the presence of PCMs in the wallboards allows to reduce significantly the temperature fluctuations of the room: for the summer case the maximum air temperature value decreases of about 3.9 °C (from 36.6 °C to 32.7 °C) while the minimum one increases of about 0.9 °C (from 18.9 °C to 19.8 °C). Furthermore, the employment of phase change materials determines a reduction of the wall surface temperatures fluctuations. Last but not less important, it seems that the natural convection inside the room was enhanced by the PCM. In fact, a thermal stratification existed in the case of regular wallboards, which did not occur with the walls including the PCM. This effect improves the thermal comfort.

A similar study [13] provides a comparison between a room equipped with ordinary wallboards and one with PCM wallboards, operating in cooling mode. The tests were performed in Montreal (Canada) and the PCM utilized was a mixture of fatty acid esters, constituted of 50% butyl stearate and 48% butyl palmitate.
The rooms were cooled to a temperature around 10 °C and then the cooling system was switched off, in order to assess the ability of the walls to maintain a comfortable room air temperature as long as possible. Results show that, under the stated conditions, the temperature in the room equipped with ordinary wallboards rose from 16°C to 22°C in 27.2 hours, while in the PCM wallboards room the temperature was maintained below 22°C for 50 hours. The times required to raise the temperature from 18°C to 22°C were 24.1 hours and 45.6 hours respectively. These times represent an increase of the performances of 84% and 89% respectively by using PCM wallboards instead of the conventional ones.

In closing, another research work [7] investigated, both through simulations and experiments, the effects of the integration of PCMs in a lightweight building. The study considered panels for suspended ceiling installations made of plasterboard and clayboard combined with a microencapsulated paraffin wax. Both a passive and an active system were taken into consideration: the first one consisted of night-time ventilation cooling and was studied under Copenhagen's summer weather conditions, while the active panels with embedded pipes were considered for the hot summer climate of Madrid.
For passive PCM-gypsum and PCM-clayboard ceiling panels combined with night-time ventilative cooling energy savings of up to 70% and peak cooling load reduction up to 70% were achieved.

For thermally-activated panels, peak power reduction of 32% was achieved. The cooling demand shifted from peak to off-peak hours was up to 67% of the total daily cooling load.
Results also show the importance of the choice of the phase change material with a suitable melting temperature range. Selection of PCMs with optimum melting temperature may decrease the diurnal temperature swings by 1-2 K and reduce the daytime peak temperatures by 1-3 K, in comparison to PCMs with higher or lower melting temperatures than the optimum.

The results presented in the studies mentioned above show the enormous potential of integrating phase change materials in thermally activated construction for increasing buildings thermal mass.
Important benefits can be achieved in terms of:

- energy storage capacity
- indoor air temperature and wall temperature fluctuations control
- peak power reduction
- reduction of the thermal stratification.

The added thermal mass allows decoupling the heating and cooling demand of the building from the heat and cold production.

3 Introduction to night sky radiant cooling

Night sky radiant cooling is a passive cooling technique based on the radiative heat exchange which occurs between two surfaces with different temperature facing each other. Since the effective sky temperature is lower than the one of the air during night, every object placed in the external environment tends to release energy toward the sky in the form of electromagnetic waves. This phenomenon can be exploited to draw away the thermal energy stored by materials during daytime.
Radiative cooling of buildings has attracted considerable research over the years, mostly focused on the evaluation of the cooling potential of the technology for different locations [14]–[17] .

3.1 Classification

Several techniques of radiative cooling have been investigated in the past decades, among which roof ponds, movable insulation, air based systems and open or closed water-based systems. Hereafter a description and a short literature review regarding these applications are provided, in order to show the historical development of the radiant cooling technology.

3.1.1 Movable insulation systems

Movable insulation systems are one of the first applications of radiative cooling, tested about 50 years ago. They consist of an insulating layer covering the roof which is removed during the night in order to enhance the radiative heat exchange toward the sky and cool down the building. The principle of working is illustrated in Figure 3.1.
The main weakness of such systems is the motor-operated mechanism to remove and replace the insulation panels [14]. Furthermore, since the method is completely passive, it is not interesting for multi-storey buildings because only the spaces directly under the roof will benefit from it [18].

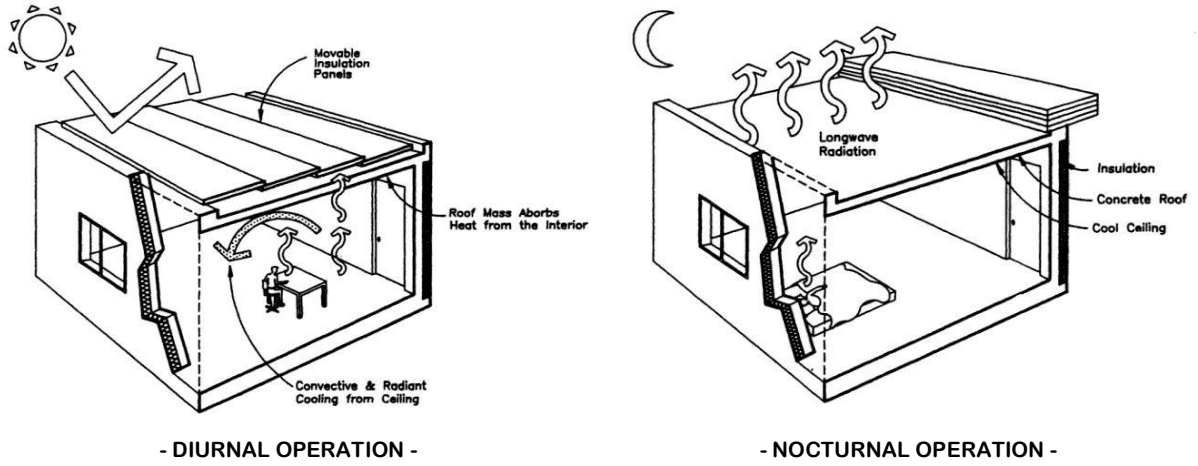

Figure 3.1 – Principle of operation of a movable insulation system [18]

A particular movable insulation system is the so called roof pond (Figure 3.2); it consists essentially of a pool of water stored on a flat roof (either as an open pond or contained in plastic bags) and a movable insulation. The operation is identical to the other movable insulation systems but the presence of the water allows storing a larger amount of thermal energy, absorbed through the ceiling (the pond works as a heat sink). In addition to the radiative and the convective heat exchange mechanisms, the evaporation of the water allows increasing the amount of the thermal energy released. The main limitations of this cooling technique are the requirement of additional structural support for the roof and the need to replenish the water lost during the evaporative process. Furthermore, there may be public health concerns associated with standing water (mosquitoes etc.).

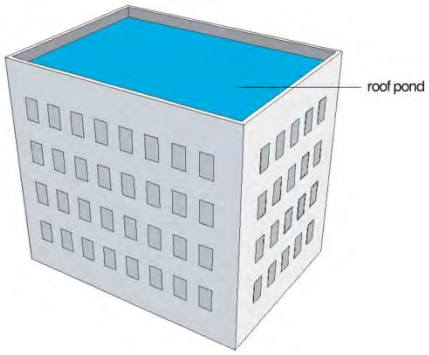

Figure 3.2 – Schematic representation of a roof pond system [19]

Figure 3.3 – Roof pond system [20]

3.1.2 Air-based systems

Some of the earliest experiments on air-based systems were carried out in Israel at the beginning of the 70's; the air was cooled down by means of radiative heat exchange while passing through a narrow channel [14].
Among others, an application of air radiative cooling was performed in Italy in 1998 [21]; the system consisted of a lightweight metallic radiator covered by a single polyethylene wind screen; the air was cooled by circulating under the surface of the radiator before being directed into the building to provide instantaneous cooling during the night and to cool the interior mass of the building by convection, thus creating a cold storage for the following day. The simulation model built estimated for the months of July and August a daily useful cooling energy between 30 and 56 Wh/m^2 for a clear sky and from 27 to 45 Wh/m^2 for a cloudy sky.

3.1.3 Open water-based systems

Open water-based systems let the water flow on a tilted surface, in direct contact with the atmosphere. Since there is no additional thermal resistance between the water and the ambient, the cooling outputs are higher than those of closed applications. Measurements carried out in Germany show that a specific cooling power of 120 W/m^2 can be achieved [14].
Although the power they can provide is larger than the closed ones, open systems present some drawbacks related to their integration in the distribution system. Indeed, the water is at atmospheric pressure, therefore it is necessary to decouple the radiant cooling loop from the building distribution system, by inserting a heat exchanger between these two circuits. Moreover, since the water is in direct contact with the external air, a filter is necessary to prevent dust entering the plant. Finally, the water consumption due to evaporation is not negligible.

3.1.4 Closed water-based systems

These systems use water as heat carrier but, in contrast to open systems, it is not in direct contact with the external air but it flows through pipes. Literature and actual projects, including this thesis, focus on two categories of devices suitable to release the heat through radiative exchange to the sky: flat plate solar collectors (Figure 3.4) and photovoltaic-thermal panels (PV-T, Figure 3.5).

Unglazed collectors are simple and cheap systems in which the absorbing plate is in direct contact with the air, and they are usually used in domestic applications of pool heating. Their simple design and the high emissivity of the material are a source of considerable heat losses, which are undesirable for heating applications, but a strength for cooling applications, where high heat losses are sought for [22]. This is the reason why research on radiative cooling moved from glazed to uncovered collectors. In fact, the presence of the glass layer is an obstacle to the radiative heat exchange with the sky and also strongly reduces the convective exchange with the atmosphere.

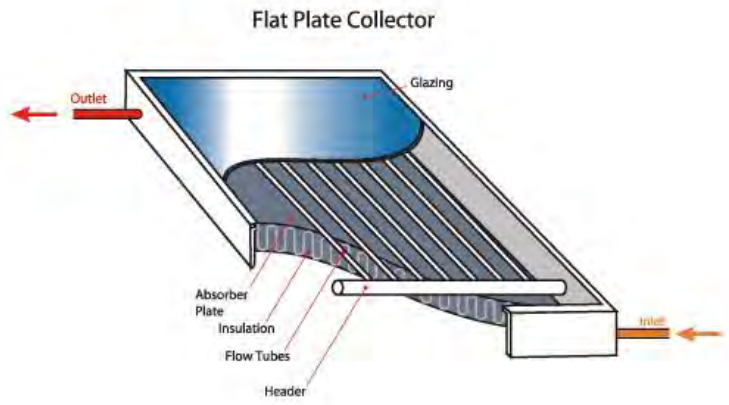

Figure 3.4 – Schematic representation of a glazed flat plate collector [23]

PV-T stands at the other side of the existing range of solar technologies: they are relatively expensive and at the state-of-the art of this field [22]. These systems combine photovoltaic cells, which convert the incoming solar radiation into electricity, with a solar thermal collector, which captures the waste heat from the PV module and turns it into exploitable thermal energy.
The integration of the solar collector is, most of the time, realized via metal tubes welded to the PV panels (see Figure 3.5); in this way PV panels act as an "absorber plate" for the thermal part. A crucial issue with this application is to assure good thermal contact between the tubes and the absorber plate.

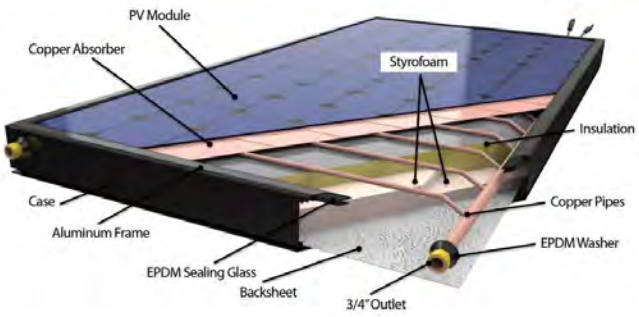

Figure 3.5 – Schematic representation of a PV-T panel [24]

The presence of the thermal collector allows a double benefit: firstly, it recovers thermal energy which would be wasted with an ordinary PV cell, to produce domestic hot water or to cover part of the space heating demand; secondly, it keeps the photovoltaic cells performance close to the rated efficiency by removing the excess heat. Indeed, a well-known problem with the photovoltaic panels is that the electrical conversion efficiency levels tend to drop significantly as the cell temperatures increase [25].
PV-T panels can be as well used to provide cooling, if combined with cooling radiant systems: during night the water absorbs heat from the structures of the building (walls, ceiling or floor) and it is circulated through the loop of the panel, where it releases the thermal energy previously stored by radiative exchange towards the sky. In addition, the energy exchange is enhanced by the convective contribution.

3.2 Advantages and drawbacks of using night sky radiant cooling

The adoption of a night sky radiant cooling system allows achieving many benefits, among which:

- energy saving, since it is a free cooling technique;
- if the surface temperature of the collector is lower than the one of the external air, the amount of the heat released is increased by the convective heat exchange mechanism;

- a higher utilization factor for solar panels and PV-Ts, since they can be exploited both during day and night in the cooling season;
- generally, cooling demand and availability are in phase: higher amount of radiative exchange can be achieved in summer, since clear night skies occur more often;
- it can be coupled with high thermal storage materials, such as PCMs.

The main disadvantages related to this technology are:

- the cost to install the collectors
- the disposal of the panels at the end of their operating life
- the need of maintenance (for example panels need to be cleaned)
- the need of arrangements to avoid freezing of the liquid in the loop
- aesthetic issues
- the amount of energy dissipated is not constant but it is strongly influenced by the weather conditions
- the need of a supplementary device (often an electrical chiller) able to provide the additional power demanded by the user; the integration of the two devices implies a more complex system, either to build or to control.

Since the cooling and the heating mode require opposite features of the panel (as mentioned in the previous paragraph), it is not always possible to use the same collector for both the applications. However, sometimes this solution is feasible, such as with unglazed flat plate collectors. In this case it is worth pointing out that most of the drawbacks mentioned are related to the presence of the panels themselves and not to the night-time operation. Therefore, if the roof is already provided with solar collectors, these disadvantages occur without the cooling mode as well.

3.3 Potential

Hereafter a literature review concerning the potential of nocturnal radiative cooling in terms of cooling production and economical affordability is presented. Since the experimental and the simulation study involve a system adopting flat plate solar collectors and photovoltaic-thermal panels, the discussion below will mainly focus on these devices.

As regards to the first technology mentioned, the performance of unglazed polymer flat plate radiators with water as heat carrier were investigated, both experimentally and theoretically, under Oslo climatic conditions [15]. The first significant outcome highlighted that the cooling power is strongly influenced by the presence of clouds in the sky: considering the same conditions, the cooling power related to a clear night sky is around 50 W/m^2 higher than nights when the sky is completely covered by clouds.
A simulation program to evaluate the potential of a radiative cooling system for a typical residence building was built during this research. The case study referred to a one-family house of 150 m^2 living area provided with a hydronic radiant floor which used water cooled through a 50 m^2 roof radiator. The system included also a 2 m^3 reservoir volume.
Results show that for a dry clear night in October the storage temperature dropped from 20°C at 20:00 to approximately 10.5 °C at 5:00, thus corresponding to a stored energy of 22 kWh: the radiative cooling system provided sufficient energy to cool the building. The behaviour of the plant has also been modelled for a humid clear summer night; in this case a cooling energy of around 7 kWh was stored in the tank at 5:00, which covered approximately 56% of the cooling demand of the following day.

In another research [16] a nocturnal radiative cooling system with a flat plate solar collector in a humid area, Babol, Iran, was assessed both experimentally and numerically. The system consisted of two unglazed radiators with a surface of 2 m^2 each connected in parallel, and a storage tank. During the night the water circulated through the unglazed radiators to be cooled, while during day-time it flew through the air-conditioning coils to cool the indoor air.
The experiments were carried out during summer and fall at various mass flow rates and in different weather conditions and the results have been compared to those of the theoretical model. The results indicate that under clear sky the water temperature decreased 7-8 °C during night and the average net cooling ranged from 23 to 52 W/m^2, as the mass flow rate increased from 0.01 to 0.05 kg/s.

Furthermore, although a detailed economic analysis was not performed in this research it is remarked that, since the very low pumping costs due to the low flow rate and pressure drop in the loop, the system is able to perform the task in an economically viable manner.

Cooling power in the same range were achieved in experiments carried out in Israel [17]. The experimental set-up consisted of a water pond on a roof of a test chamber (ground surface of 4 m^2) linked through pipes to two unglazed flat plate collectors with the exposed surface painted white. Water from the roof pond absorbed heat from the room during day-time and was circulated at night through the collectors, where it was cooled by means of radiative and convective heat exchange.
Two series of experiments were performed, in order to assess the influence of the water flow rate on the system performances. The average cooling power obtained with a water flow rate of 0.17 m^3/h was 31.9 W/m^2 while by circulating 1.1 m^3/h an average cooling power of 55.8 W/m^2 was achieved. Peak power of 90 W/m^2 was reached.

In the matter of photovoltaic-thermal panels, very few projects using these devices for night-time radiative cooling applications can be found in literature. One of the first studies related to this topic [14] tested the performances of 12 PV-T modules integrated in a residential Zero Energy Building (ZEB) under Madrid's summer climatic conditions.
Measured cooling power levels were between 60 and 65 W/m^2 when the PV-T collectors were used to cool a warm storage tank and 40-45 W/m^2 for the case that the energy was directly used to cool a ceiling. The COP, ratio of the cooling energy produced by the energy required for pumping water through the PV-T collector at night, had values between 17 and 30.
Moreover, the authors carried out some simulation studies to compare the behavior of the collectors under different climatic conditions. The simulated annual cooling energy production for Madrid and Shanghai climatic conditions was between 50 and 55 $kWh/(m^2y)$, which adds to the electrical energy generated by the photovoltaic effect.

In a work carried out in Kgs. Lyngby, Denmark [22] the cooling power and the performances of both PV-T panels and unglazed flat plate collectors are evaluated, and a comparison between the two technologies is provided. The experiments, which took place during August 2014, tested three PV-T panels assembled in series and one unglazed solar collector.
As regards to PV-T, the obtained cooling power ranged from around 30 W/m^2 during an overcast night until 60 W/m^2 during a clear sky night. The COP showed values ranging from 13 to 33 depending on the outside conditions. The energy production in 12 hours of operation was between 1 kWh and 3.5 kWh.
The unglazed collector showed similar potentialities, with an average cooling power ranging between 20 W/m^2 and 70 W/m^2, but the efficiency of such systems was lower, presenting a COP between 6 and 23. Comparing the energy production of the corresponding nights, the difference between PV-T and unglazed collectors was negligible (less than 0.1 kWh/m^2 per night).
The authors provided also a simple economical evaluation concerning the technologies previously mentioned. In terms of economic feasibility, night sky radiant cooling shows a good potential even in Denmark, where the need of cooling is limited. In fact, all the initial costs investigated were amortized in less than 15 years. For the most expensive technology, the PV-T, a payback time of 14 years was achieved just considering the cooling potential; adding the heating and electricity production it could be drastically reduced. The potential could be even more relevant for public buildings like offices, where the cooling demand is higher and a bigger installation would reduce the initial cost per m^2.

The works above investigated allow drawing important conclusions on night sky radiant cooling.
At first, the parameters that mostly affect the cooling production due to the radiative exchange are:

- effective sky temperature
- humidity
- cloud cover of the sky
- water flow rate.

Maximum cooling occurs under clear skies, light winds and dry conditions. Indeed, vapour and clouds tend to reflect the high wavelength electromagnetic waves toward the earth surface, thus resulting in a drop of the overall amount of energy exchanged through the radiative mechanism.

Furthermore, high COPs are achievable with PV-T and solar collector systems, since they are able to produce up to 30 times the amount of energy consumed, thus making radiant cooling an even more efficient cooling process than a traditional heat pump (COP usually not higher than 5).
In terms of economic feasibility, night sky radiant cooling is a very interesting technology, allowing to cover a significant part of the cooling demand of domestic buildings and offices in a great variety of climatic conditions, from the Nordic climates (such as the one of Denmark and Norway) to the warmer ones (such as the ones of Spain and Israel).

4 Integration of PCM and night sky radiant cooling

The main purpose of this report is to evaluate the performances of a system integrating phase change materials with night sky radiant cooling. These technologies can be combined by means of a heat carrier which removes the thermal energy stored in the PCM embedded in the building's structures before being sent to the solar collectors, where it gives off the heat through the radiative exchange mechanism with the sky. Generally, the fluid used as heat carrier is water [14], [26], [27] but air flowing in ducts can be employed as well [28].
Not many works combining these two technologies can be found in literature, since the concept is relatively recent. Hereinafter some studies regarding this topic are gathered.

An interesting application integrating PCM with night sky radiant cooling consists of using phase change materials to cool concentrated photovoltaic modules [26]. In fact, as previously mentioned about PV-T panels, thermal control of photovoltaic cells is necessary to reduce the temperature-related efficiency drop and avoid material degradation. The idea is to store the waste heat released from the PV cells during the daytime in the PCM, in order to prevent their overheating. During night the heat is removed from the phase change material by water circulating into pipes embedded in the PCM modules and dissipated by means of natural convection and night sky radiation. The PCM to which the article refers is Polyethylene Glycol (PEG), which has a melting temperature of less than 40°C. In Figure 4.1 the set-up of the system and its operation principle are shown.

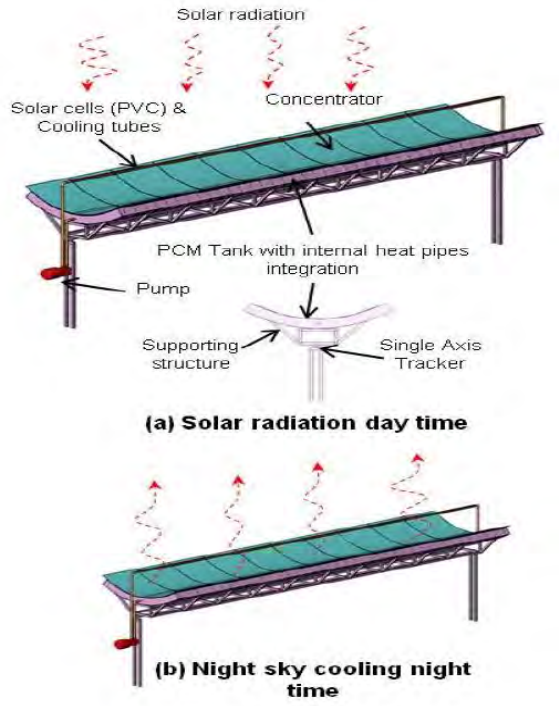

Figure 4.1 – Concentrated photovoltaic cooling using PCM and night-time sky radiation [26]

Another particular application combining night sky radiant cooling to PCMs consists of a system integrating a storage tank containing a PCM slurry, a nocturnal sky radiator and a mechanical chiller, used as supplemental cooling source [27]. The plant was designed to cover the cooling demand of a one-floor-building, by means of a radiative ceiling with embedded pipes. Two heat exchangers were immersed in the tank to absorb or release the cooling energy: at night-time, cooling obtained by the radiative exchange was stored in the slurry tank, while during daytime the cooling energy was released to cool the indoor environment.
A feasibility analysis of such a system was conducted for five typical cities across China, from South to North, Hong Kong, Shanghai, Lanzhou, Beijing and Urumqi, based on local meteorological data.

With the introduction of the nocturnal radiation concept, the load of charging the PCM slurry at night was mainly participated by the nocturnal sky radiator, which means the chiller energy consumption was greatly reduced at night. Results show that Lanzhou and Urumqi have the most evident annual energy saving effect and largest cooling capacity of utilizing nocturnal sky radiative cooling system. The energy saving potential can reach 77% and 62% in the two cities, which exhibits a strong attractiveness for building energy conservation and emission reduction. Hong Kong has the weakest effect under the same operating conditions due to the hot and humid climate conditions. The utilization potential in Shanghai and Beijing is also considerable and cannot be ignored.

One of the few works integrating night-time radiative collectors with PCMs embedded in the building's structures is the one carried out in the framework of the student competition Solar Decathlon 2010 by the team from the University of Stuttgart [14]. The building they built was a highly insulated passive standard house provided with 12 uncovered PV-T collectors mounted on the horizontal roof, covering a total surface of 38 m^2. The ceiling contained a phase change material, having a total surface area of 18 m^2 and a melting temperature of about 22 °C.
During one night the PV-T collectors were directly used to discharge the PCM ceiling; their cooling power production was around 40 W/m^2, thus allowing the supply water temperature going down as far as 11 °C at the end of the night, with return temperatures of the radiant floor 2 °C higher and from the phase change material ceiling 5 °C higher (the flow rate was about 10 $kg/(m^2h)$). The return temperature from the chilled ceiling dropped from 21 °C at the beginning of the discharge down to about 15 °C at the end of the night.
Under Madrid's climate conditions, the specific cooling energy delivered from the PV-T collectors to the PCM ceilings is 16.5 $kWh/(m^2 a)$ during summer, thus covering 27% of the total building cooling energy demand of 39 $kWh/(m^2 a)$.

In conclusion, a paper [28] presents the development and performance evaluation of a novel ceiling ventilation system integrated with PV-T collectors and phase change materials. The PV-T collectors (with an overall surface of 40 m^2) were used to generate electricity and provide low grade heating and cooling energy by using winter daytime solar radiation and summer night-time sky radiative cooling, respectively. The house concerned in this study is a Net Zero Energy House with a ground surface of 70 m^2, with a ceiling integrating the PCM panels.
The performance of the proposed system was numerically evaluated under Sidney's climate. Different operation modes were tested in summer, that were simple ventilative cooling, night-time direct cooling by means of the PV-T panels and night-time PCM charging through the PV-T. In the last case mentioned, during night-time the PV-T outlet air was used to discharge the PCM after being cooled by the radiative effect of the PV-T collectors.
It can be seen that the average temperature reduction of the ambient air flowing through the PV-T collectors during the night-time was 2.4 °C, when the proposed ceiling ventilation system was employed. The indoor temperature was lower than that using the PCM natural ventilation system without using PV-T collectors and the original house without using PV-T and PCM layers. This was because the night-time sky radiative cooling of the PV-T collectors increased the amount of cool energy stored in the PCM layers. Therefore, the integration of the PV-T technology with latent heat storage improved the indoor thermal comfort.
The PCM natural ventilation system without using the PV-T collectors could also provide a lower indoor temperature as compared to that of the original house without using the PCM panels.

Since night-time cooling energy is intermittent and has a low energy density, the integration of PCMs with such a technique could represent a worthy solution to effectively use nocturnal radiant cooling. Although the concept needs to be further investigated, the above studies demonstrate that the combination of night sky radiant cooling with phase change materials is able to enhance energy efficiency and thermal comfort of buildings.

5 Experimental study

The experiment was carried out at the ICIEE Laboratory at the Technical University of Denmark (DTU) in Kongens Lyngby, Denmark (55°47'02.5"N 12°31'19.9"E), during the month of March 2015.

The main purpose of the experimental study was to evaluate the potential of a cooling system combining phase changing materials and night sky radiant cooling, employed to provide space cooling to a 2-persons office.
The experimental results were used afterwards to validate a simulation model built with the software TRNSYS 17. The present model will be fully described in Chapter 6.

5.1 Experimental setup

The general system consisted primarily of 5 subsystems:

1. a climatic chamber, simulating a 2-persons office room
2. a PCM-clayboard active suspended ceiling, located inside the chamber
3. a water supply circuit for the suspended ceiling
4. a solar circuit, constituted by three PV-T panels and one unglazed collector
5. an intermediate loop, connecting the solar circuit to the PCM panels' water supply system.

The main purpose of the system was to provide the cooling energy required to completely discharge the phase changing material contained in the suspended ceiling of the climatic chamber. Furthermore, the system produced electrical energy by means of the photovoltaic-thermal panels and thermal energy which could be used to provide space heating during the cold season or to supply domestic hot water during the whole year.

The system alternates two operating modes every day:

- during daytime operational mode (Figure 5.1) the water stored in the hot water tank is heated by means of the radiation absorbed by the solar collectors
- during the nocturnal mode (Figure 5.2) the water contained inside the cold tank is cooled through nighttime radiative exchange with the sky and it is used to discharge the PCM embedded in the chamber's suspended ceiling; an auxiliary system is connected to the storage tank and provides the additional cooling load requested to ensure the complete discharge of the PCM during the night.

The switch between the two operating modes was automatically implemented by the control system and was based on the difference between the temperature of the stored water at the middle of the cold tank and the outlet temperature of the solar panels' loop: when this value rose above the set point the nocturnal mode was activated. Further details concerning the operation of the control system will be provided later in the text.

Since the present work focuses on the coupling between phase changing materials and night sky radiant cooling, the daytime operation is not examined in depth and just a few results are analysed.

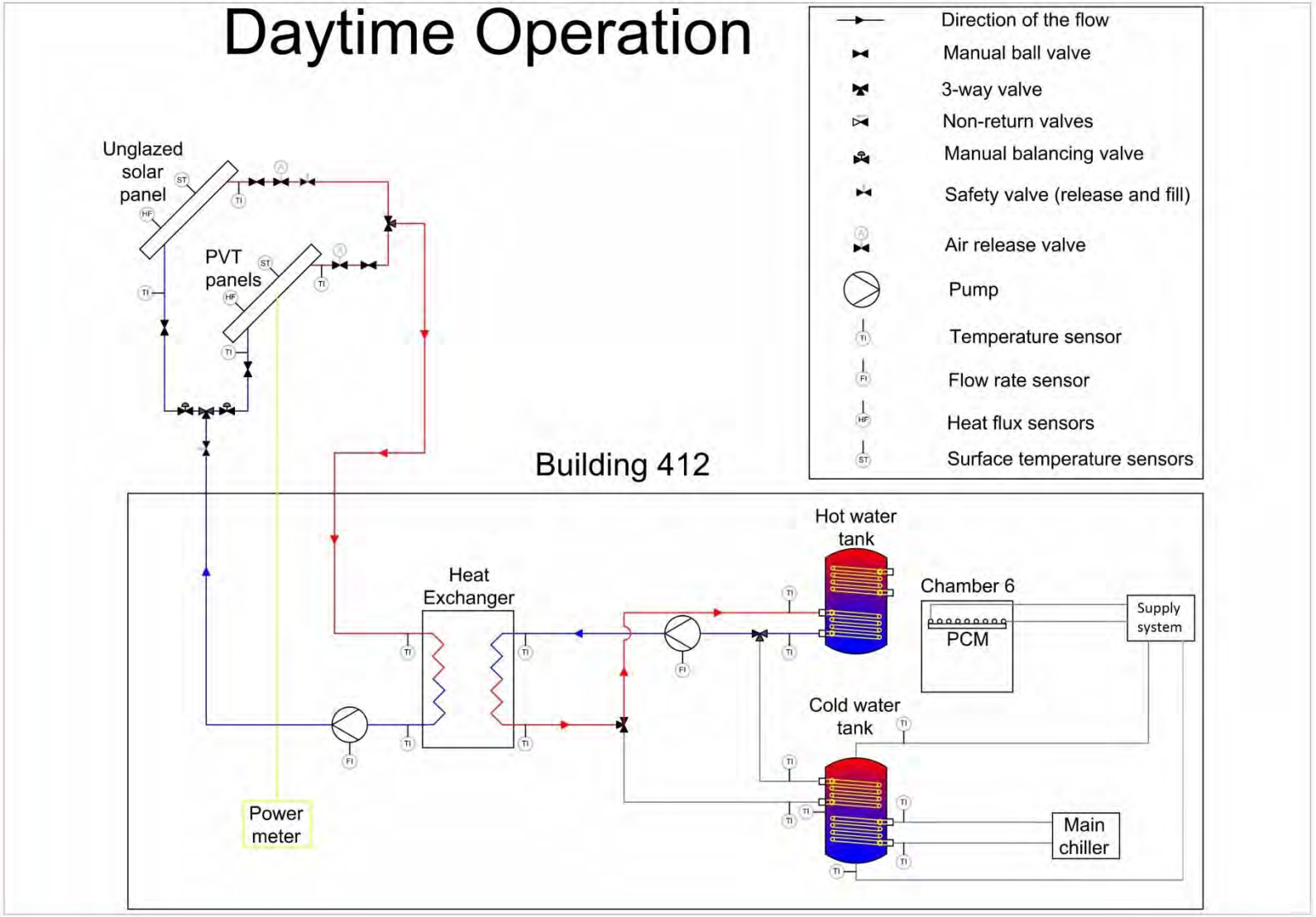

Figure 5.1 – Scheme of the experimental setup during daytime operation

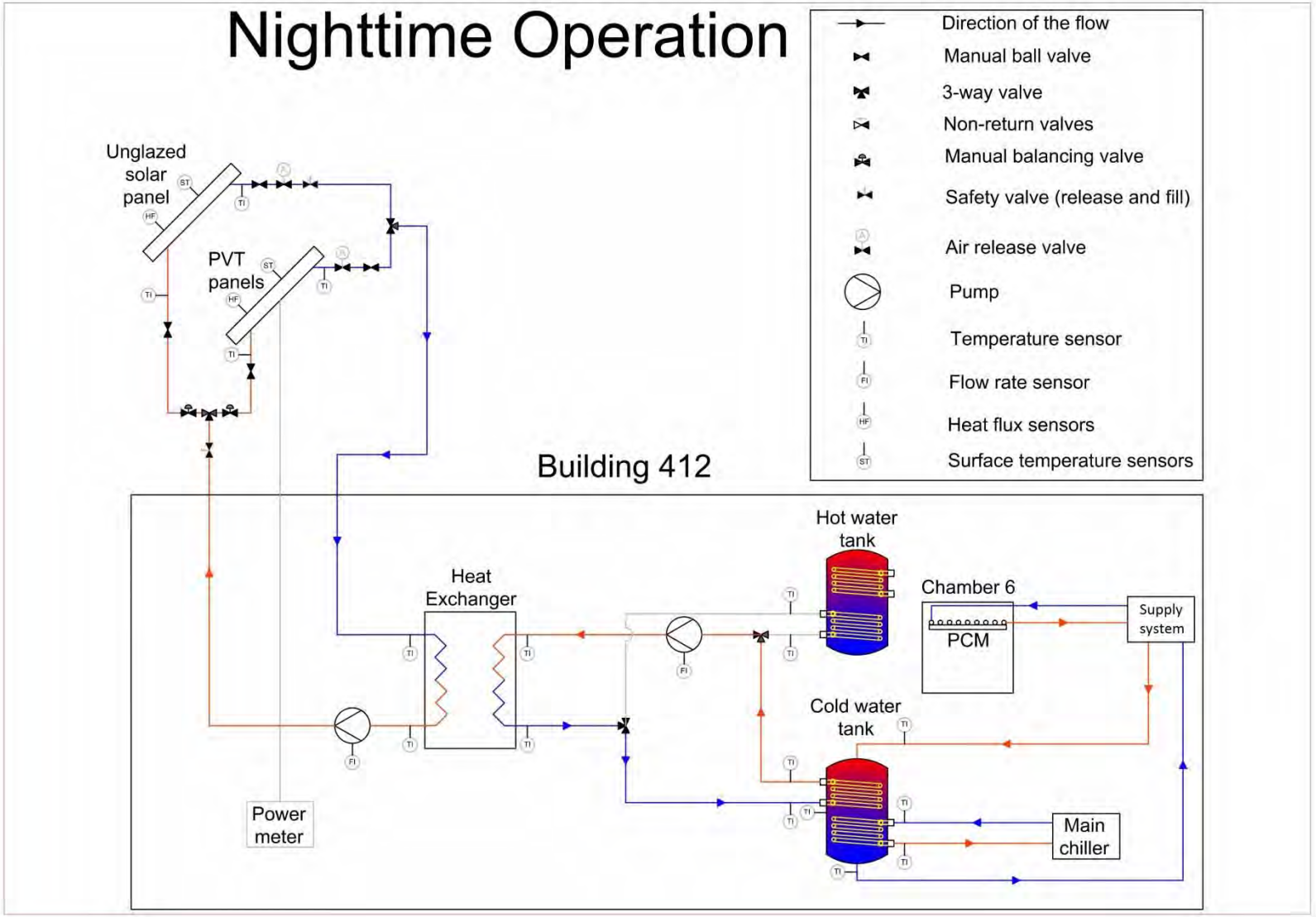

Figure 5.2 – Scheme of the experimental setup during nighttime operation

Hereinafter a description of the subsystems involved in the experimental setup is provided.

5.1.1 Climatic chamber

Climatic chamber number 6 of ICIEE Laboratory was selected for the experimental purpose. The chamber was designed to simulate a 2-persons office room with floor dimensions of 5.4 x 4.2 m and height[6] of 2.5 m, thus resulting in a total floor area of 22.7 m^2 and a volume of 56.7 m^3. The test room was equipped with a suspended ceiling constituted by clayboard panels containing a phase changing material. Between the PCM-clayboard ceiling and the roof of the chamber there was an additional space of 0.5 m height which was used as a plenum for the ventilation air supply.

The experimental layout of the climatic chamber is shown in Figure 5.3 and Figure 5.4. The solar radiation simulator (the grey panel attached to the wall in Figure 5.3) was not used in the present study.

Figure 5.3 – Experimental setup of the climatic chamber

[6] This value is referred to the distance from the office floor to the bottom surface of the suspended ceiling

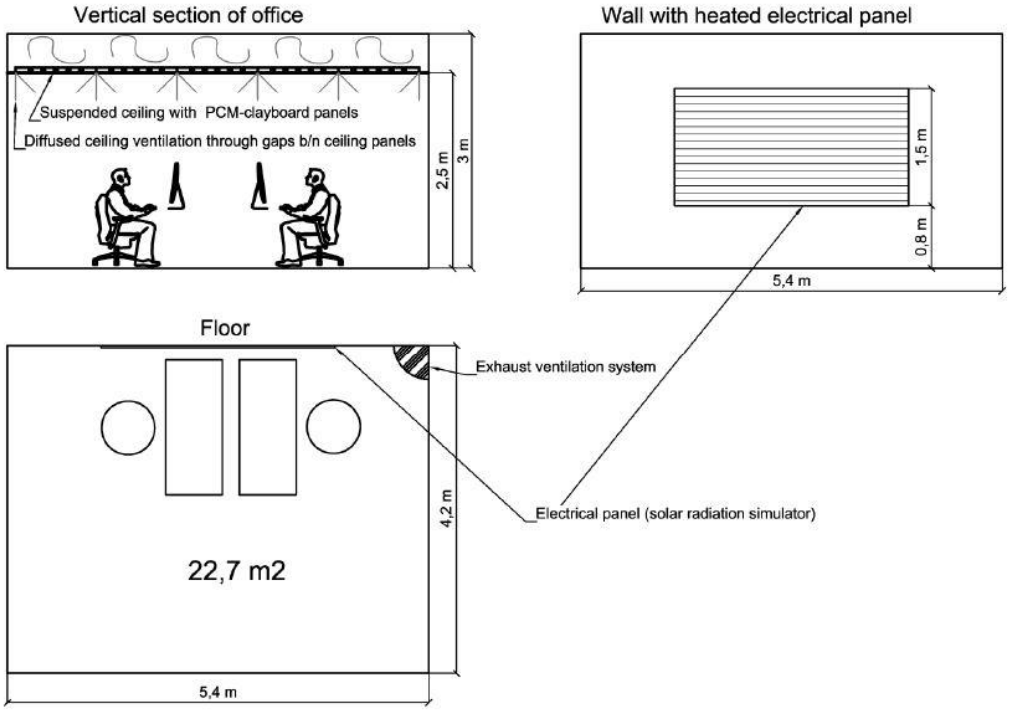

Figure 5.4 – Climatic chamber layout [7]

The walls and the roof of the chamber were made of two steel sheets separated by 10 cm of mineral wool (insulation material), while the floor corresponded to the slab of the building where the chamber was situated.

Since the climatic chamber was used simultaneously for another experimental study involving human subjects, a compromise on the indoor operative conditions was found in order to satisfy both the parties involved.
Hereinafter a description of the required internal conditions is provided.

5.1.1.1 Indoor thermal conditions and ventilation

A constant indoor air temperature was required from 9.00 a.m. to 6.00 p.m. Two different cases were analysed: in Case A the internal air temperature was kept constantly at 26 °C while in Case B a value of 28 °C was set. This parameter was measured by means of a thermoresistance PT100 placed at a height of 1.30 m from the floor in the middle of the room.

The ventilation system of the room was used to ensure the requested indoor thermal conditions. The air flow was provided to the chamber by means of a diffuse ceiling ventilation system: the air was supplied to the space between the suspended ceiling and the chamber's roof (Figure 5.5), used as a plenum, and it flew towards the occupied environment through the gaps between the PCM panels. The exhaust was located on the floor in one corner (Figure 5.6) and the indoor air flew spontaneously through it since the chamber was in overpressure.

Figure 5.5 – Ventilation supply duct

Figure 5.6 – Ventilation exhaust

The ventilation was turned on manually every morning at 7.30. The supplied air temperature was not constant during this phase but it was subjected to manual regulation in order to reach the pre-set air temperature by 9.00 a.m. The air temperature was varying between 26 and 30 °C for Case A and between 28 and 32 °C for Case B. In both cases the flow rate had an approximately constant value of 0.2 m^3/s. Two heated dummies (with a power of 75 W each) and a heat blower were used during this time interval to speed up the heating process.
Between 9.00 a.m. and 6.00 p.m. small adjustments on the ventilation supply temperature were made to keep the indoor air temperature constant. During this interval the supplied air temperature was varying between 25.5 and 26.5 °C for Case A while assumed values in the range 27.5 - 28.5 °C for the other scenario. The ventilation air flow rate was constant at 0.2 m^3/s.
Before 7.30 a.m. and after 6.00 p.m. the ventilation was off, therefore the indoor temperature was not controlled during nighttime.

A review on the ventilation operating parameters is presented in Table 5.1.

Table 5.1 – Supplied air parameters for the considered case studies

Time interval	CASE A		CASE B	
	air temperature [°C]	air flow rate [m^3/s]	air temperature [°C]	air flow rate [m^3/s]
00.00 – 7.30	/	0	/	0
7.30 – 9.00	26 - 30	0.2	28 - 32	0.2
9.00 – 18.00	25.5 – 26.5	0.2	27.5 – 28.5	0.2
18.00 – 24.00	/	0	/	0

5.1.1.2 Internal heat gains

The lighting was provided by four electrical bulbs hanging from the suspended ceiling and two desk lamps, each of them with 40 W of electrical power. The lights were turned on and off automatically by the control system at 7.00 a.m. and 7.00 p.m., respectively.

As regards to the occupancy, one person was present in the room for half an hour duration every 1.5 hours (9.00-9.30, 11.00-11.30, 13.00-13.30, 15.00-15.30).

The operation time of the ventilation supply and the lighting and the occupancy profile during one day are illustrated in Figure 5.7.

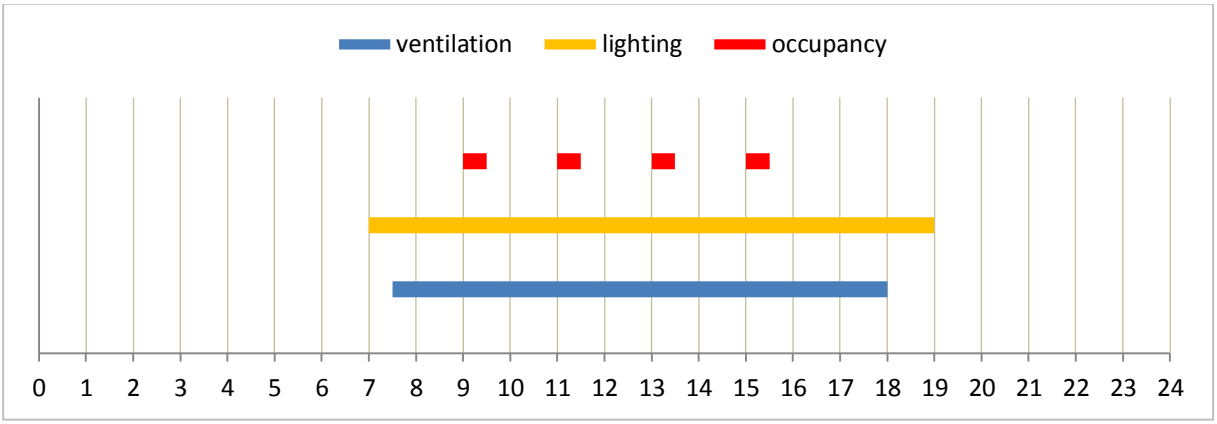

Figure 5.7– Ventilation, lighting and occupancy profile for the climatic chamber

5.1.1.3 Environment surrounding the chamber

The climatic chamber was not directly exposed to the external weather conditions, since it is located inside building 412. The space surrounding the room was conditioned by means of the main ventilation system of ICIEE Laboratory and the air temperature was measured by a sensor located above the main door of the chamber. Fluctuations between 21.5 °C and 24 °C were observed.

5.1.2 PCM-clay ceiling panels

As mentioned before, the experimental chamber was equipped with a suspended ceiling, constituted by 2.5 cm thick panels placed at a height of 2.5 m from the floor. Among the 27 panels employed, 24 were built of clayboard containing a phase changing material, while the other 3 and the remaining surface at the edges were made of gypsum. Each panel had dimensions of 125 x 62.5 cm.
Figure 5.8 illustrates the suspended ceiling layout.

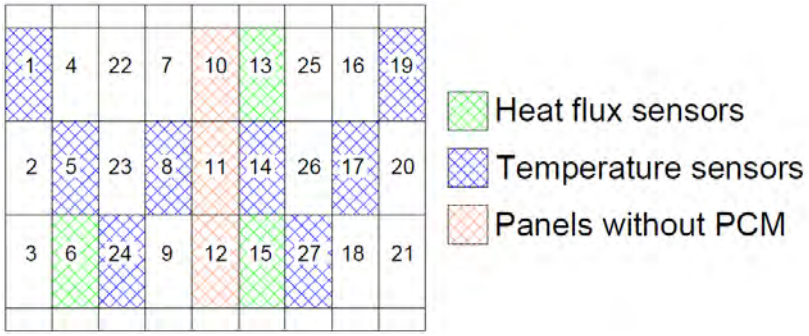

Figure 5.8 – PCM-clayboard ceiling layout and sensors' location [29]

The PCM panels were made of two 10 mm thick clayboard layers containing microencapsulated paraffin (26% in weight), separated by a 5 mm thick cardboard layer, inserted to provide structural support (a paper structure was inserted in both the clay layers for the same reason). The clayboard layer facing the chamber's roof was equipped with regularly arranged embedded Alu-Pex pipes (8 mm external diameter, 10 cm pipe spacing), used to actively discharge the PCM during night-time.
Figure 5.9 illustrates the PCM panels' structure.

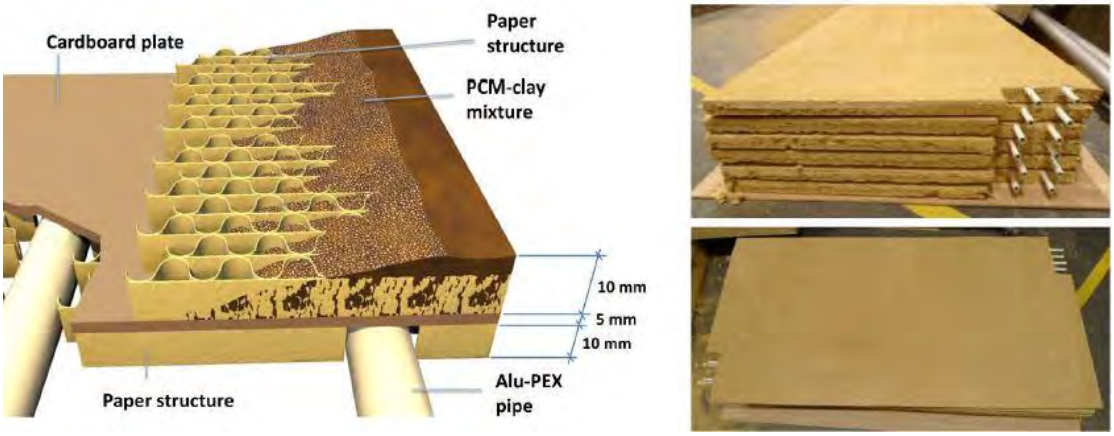

Figure 5.9 – PCM-clay panels (upwards facing the office room) [7]

The PCM incorporated in the ceiling panels was microencapsulated paraffin BASF Micronal® PCM type DS 5040X, with a melting range between 21 °C and 25 °C and a fusion temperature of 23 °C. The internal structure of the PCM-clayboard panels is presented in Figure 5.10, while Table 5.2 details their thermal and physical properties.

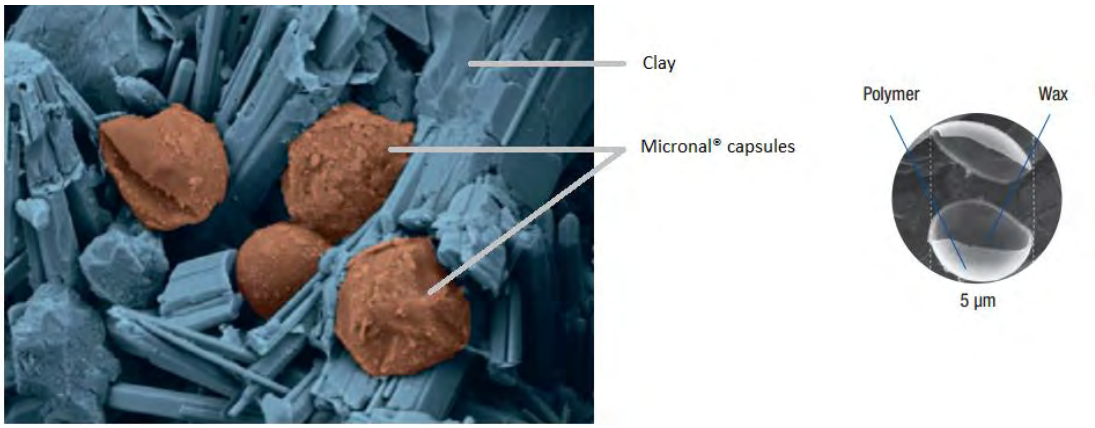

Figure 5.10 – PCM-clayboard panels' internal structure [6]

Table 5.2 – Thermal and physical properties of the PCM ceiling panels' components [7]

Material	PCM	Cardboard	Clayboard
Density [kg/m^3]	980	270	1300
Melting range [°C]	21-25	-	-
Fusion temperature [°C]	23	-	-
Specific latent heat [kJ/kg]	110	-	-
Specific heat capacity [kJ/kgK]	-	2.1	1.0
Thermal conductivity [W/mK]	0.14	0.14	0.47

The data concerning the specific heat capacity of the phase change material has not been reported in the previous table because it is subject to a relevant change when its temperature varies into the melting range. Contrarily, the specific heat capacity of cardboard and clayboard is approximately constant in the temperature interval considered (16-30 °C).
The specific thermal capacity of the PCM panels utilized for the present study has been experimentally evaluated in [7] and is illustrated as function of the internal temperature of the panels in Figure 5.11.

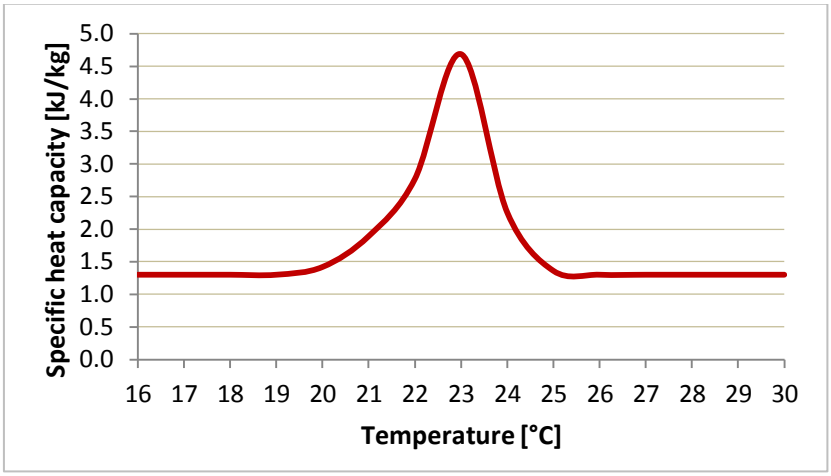

Figure 5.11 – Measured specific heat capacity of the PCM-clayboard ceiling panels

The hydraulic scheme of the active ceiling was arranged in 8 parallel branches, each of them consisting of three panels in series, as shown in Figure 5.12.

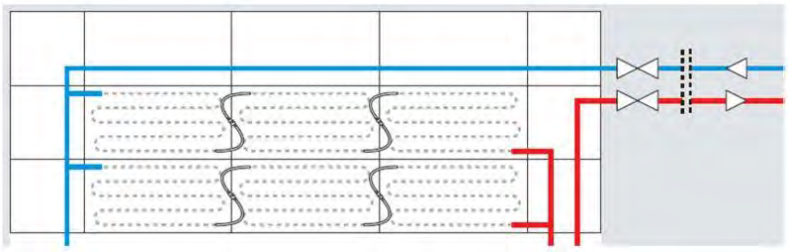

Figure 5.12 – Hydraulic scheme of the suspended ceiling [7]

5.1.3 Active ceiling's water supply system

The water supply circuit was responsible for providing cold water to the suspended ceiling in order to discharge the phase changing material during the night. The fluid was extracted from the bottom of the cold water tank and re-inserted at the top of it, after flowing through the suspended ceiling's internal loop. The operation of the pump was submitted to the conditions imposed by the control system, which will be detailed later in the text.

A recirculation valve was installed before the pump to keep the supply temperature at the constant value set by the control system, by varying the recirculating fraction of return water from the PCM panels. The supplied flow rate was constantly at 150 l/h when the pump was working.

Figure 5.13 and Figure 5.14 show the layout and the hydraulic scheme of the ceiling water supply system, respectively.

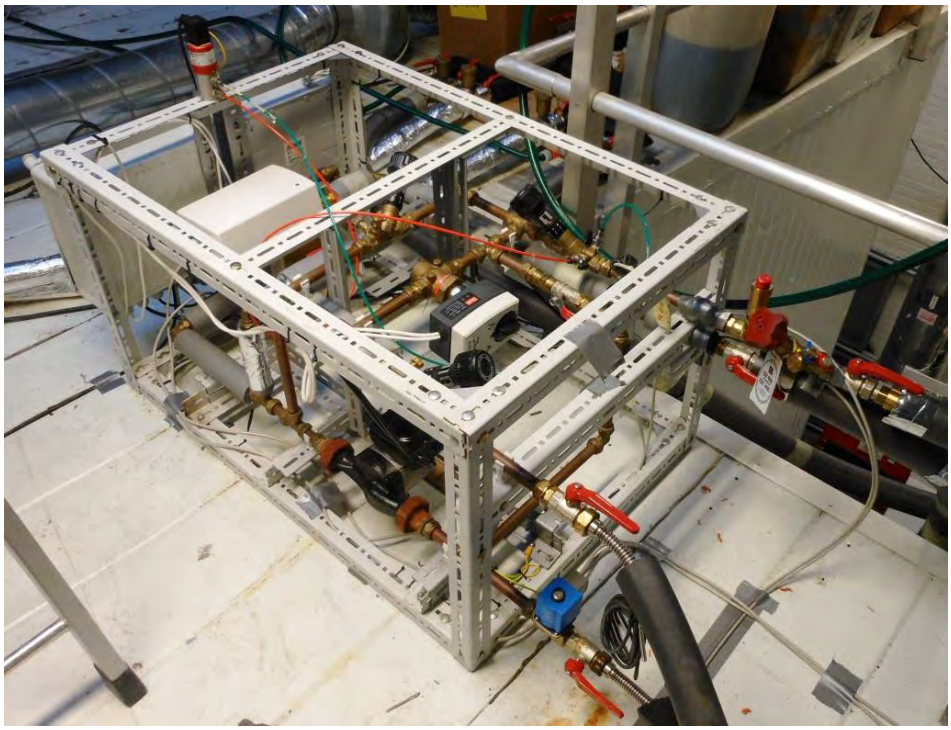

Figure 5.13 – Layout of the ceiling water supply system

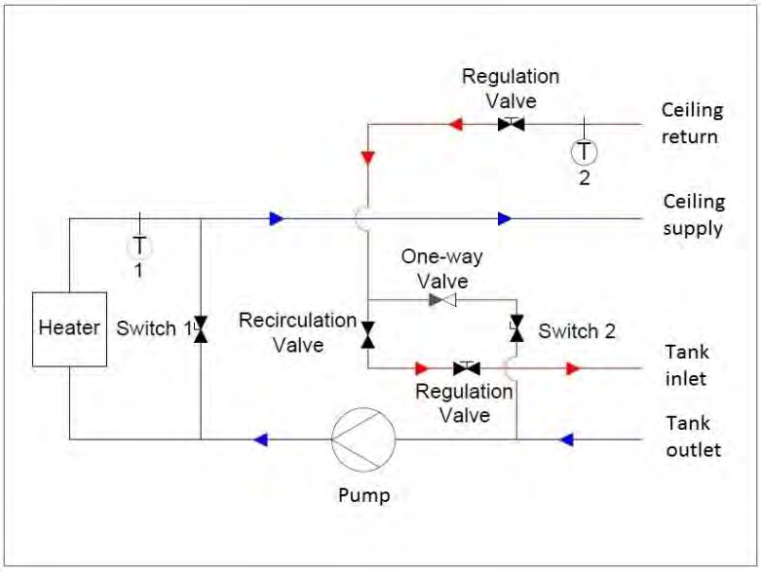

Figure 5.14 – Hydraulic scheme of the ceiling water supply system

An electrical heater was included in the system but was not used for the present experiment.
The internal connections of the supply subsystem were built of copper pipes with an 18 mm external diameter. No insulation was installed for these pipes.

The cooling power was provided to the tank by means of two immersed heat exchangers, the first one linked (although not directly) to the solar circuit, while the other one was supplied by the chiller of the general cooling system of building 412.

The electrical chiller provided water at 12 °C with an approximately constant flow rate of 150 l/h. The supply control system was designed in such a way to exploit as much as possible the potentialities of the nocturnal radiative cooling, whereas the chiller was used as ancillary cooling system[7].

5.1.4 Solar circuit

The solar collectors used for the experiments are situated on the horizontal roof of building 412 at the Technical University of Denmark. The circuit consisted of two branches connected in parallel, the first one including three PV-T panels in series and the second one an unglazed collector. All four collectors were facing South. The layout of the solar circuit is shown in Figure 5.15 and Figure 5.16.

The unglazed solar collector, made of polypropylene, had a surface area of 2.4 m^2 and a tilt angle of 45°. The fluid supply was located at the top of the collector while the return pipe was at the bottom of it. The internal loop was built by PVC pipes with external diameter 18 mm (Figure 5.17).

Each PV-T (Figure 5.18) had an overall surface area of 1.3 m^2 and a tilt angle of 45°. The fluid supply was located at the top of the first collector while the return was at the bottom of the third panel. The internal pipes were made of copper with 18 mm external diameter.

All four collectors were covered by a 7 cm thick polyurethane insulation layer on the back side, in order to limit the back heat losses.

The fluid circulating through the solar loop was a mixture of water and glycol (40% of mass fraction), used as anti-freezing. The total flow rate of the circuit was 180 l/h, of which 108 l/h (60% of the total) flew through the PV-T branch while approximately 72 l/h (40%) circulated through the unglazed loop. The flow rates were distributed in order to have approximately the same specific flow rate (flow rate per square metre of the collectors' surface) in the two branches, thus allowing comparing the performances of the two types of collectors utilized. This regulation was made manually by changing the position of the two balancing valves located in the two branches.

[7] A complete description of the logic of the control system is provided in paragraph 5.2

Figure 5.15 − Front view of the solar collectors

Figure 5.16 − Rear view of the solar collectors

Figure 5.17 – Internal structure of the unglazed solar collector [22]

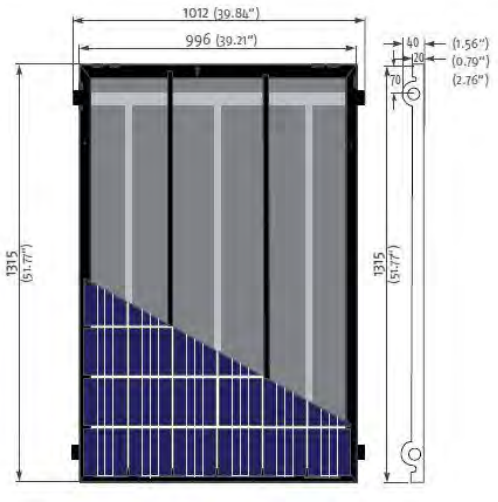

Figure 5.18 – Photovoltaic-Thermal collector [24]

The pipes of the solar circuit were made of copper (external diameter 18 mm, pipe wall thickness 1.5 mm).

5.1.5 Intermediate loop

The solar collectors' circuit was not directly linked to the two tanks but an intermediate loop was installed between them. This expedient was made in order to decouple the two hydraulic circuits, thus allowing setting different pressure values in the pipes. Indeed, the unglazed collector was not able to withstand more than 0.5 bar of relative pressure while in the heat exchangers inside the storage tanks a higher value was required.

A plate heat exchanger (Metro Therm type 2720 230-16) was used for the thermic coupling of the two circuits. The technical details are presented in Table 5.3.

Table 5.3 – Heat exchanger technical data

Parameter	Value
Number of plates	16
Heat exchange surface [m^2]	0.37
Rated heat transfer coefficient [kW/m^2K]	2.626[8]

The flow rate in the present circuit had an approximately constant value of 190 l/h during both the cooling and the heating operative modes. As for the solar loop, the fluid circulating inside the intermediate circuit was a mixture of water and glycol (40% in volume).

Figure 5.19 and Figure 5.20 show the arrangement of the intermediate circuit and the structure of the heat exchanger, respectively. As illustrated, inlet and outlet on the rear side of the heat exchanger were connected to the solar circuit (source side) whereas the front connections were linked to the intermediate loop (load side).

[8] The heat transfer coefficient has been calculated referring to the following parameters:
- Heat exchange rate: 7 kW
- Hot fluid temperature range: 70 – 40 °C
- Cold fluid temperature range: 35 – 60 °C

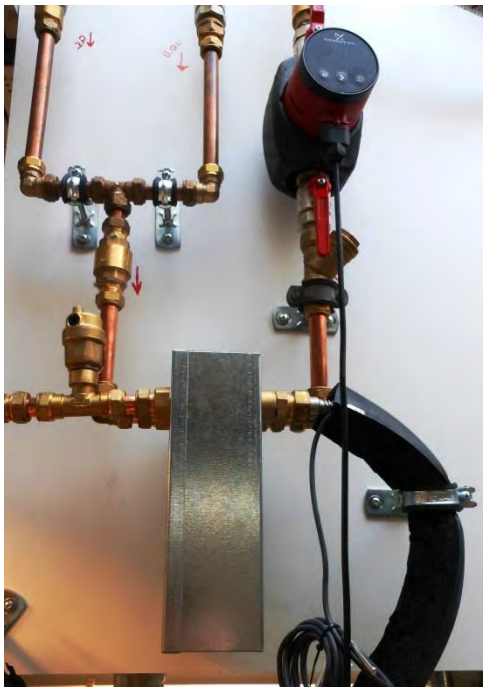

Figure 5.19 – Intermediate circuit arrangement

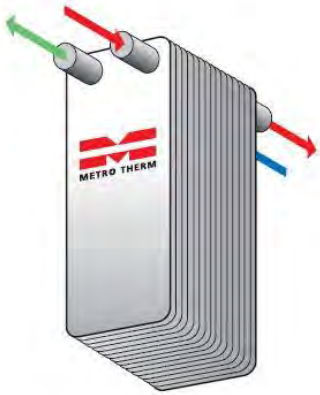

Figure 5.20 – Schematic layout of the intermediate heat exchanger

Two storage tanks were included in the experimental layout (Figure 5.21): the first one (Metro Therm type 2242 U2 7A) was utilized to store the water heated by the solar panels during the day, while the other one (Metro Therm type 2242 2) was used to collect the water cooled by the nighttime radiative cooling process. Both tanks had a volume of 255 l and contained two immersed copper spiral heat exchangers, each with a 0.75 m^2 thermal exchange surface.

As previously described, the heat exchanger located at the top of the cold water tank was connected to the intermediate loop, while the one at the bottom was supplied by the main chiller of ICIEE Laboratory. This layout was chosen in order to exploit as much as possible the cooling energy provided by the solar panels, taking advantage of the water stratification inside the tank[9].

With regards to the hot water reservoir, only the heat exchanger located at the bottom was used; the decision of exploiting this one instead of the one at the top was done in order to have a greater temperature difference between the two fluids involved in the thermal exchange[10].

[9] The water with the highest temperature is located at the top of the tank, due to the stratification phenomenon; therefore, the greatest temperature difference between the water of the tank and the intermediate loop is the one existing with the top of the tank. By connecting the intermediate circuit to the top heat exchanger the sky radiant cooling source is exploited more than by using the one at the bottom. Indeed, the control system turned on the tank supply system only when the temperature difference mentioned rose above a prefixed value.

[10] Due to the stratification inside the tank, the coldest water is located at its bottom.

Figure 5.21 – Cold (on the left) and hot (on the right) water storage tanks

From now on, the abbreviations CWT and HWT will be used to indicate the cold water tank and the hot water tank, respectively.

5.1.6 Hydraulic components

Several hydraulic elements were included in the experimental plant, such as pumps and valves. The location of each component is presented in the general system layout, illustrated in Figure 5.1 and Figure 5.2.
A brief description of the hydraulic elements is presented hereinafter.

5.1.6.1 Pumps

Four hydraulic pumps were included in the system:

- one in the collectors' circuit, circulating water through the solar panels and the source side of the intermediate heat exchanger (from now on, it will be named P1)
- one in the intermediate circuit, pumping the water between the load side of the heat exchanger and the two storage tanks (P2)
- one in the ceiling supply system, extracting water from the CWT and circulating it through the pipes embedded inside the PCM panels (P3)
- one in the main chiller of the department (P4)

Table 5.4 presents the models of the four pumps and the flow rates set in the different parts of the system.

Table 5.4 – Plant flow rates and pump models

Subsystem	Flow rate [l/h]	Pump model
Solar circuit	180	Grundfos Alpha 2 15-40 130
Intermediate circuit	190	Grundfos UPS 15-40
Ceiling supply circuit	150	Grundfos UPM2 25-75 180
Chiller circuit	150	/

5.1.6.2 Connecting Pipes

Two kinds of pipes were used to connect the different parts which composed the overall system, all of them wrapped in 15 mm thick insulation material (λ=0.04 W/mK).

The connections between the CWT and the supply subsystem and the ones between the latter and the suspended ceiling internal loop were built of flexible stainless steel pipes with external diameter 18 mm and wall thickness 1.5 mm. The same type of pipes was utilized for the intermediate loop and to link the heat exchanger at the bottom of the CWT and the main chiller.

Copper pipes 18 x 1.5 mm were used to build the solar circuit.

5.1.6.3 Valves

Several valves were included in the system, the most of them performing safety and control purposes; in more detail the following types of valve has been employed:

- one-way valves
- regulation valves
- recirculation valves
- safety valves
- one 3-way valve
- two-way valves
- balancing valves
- air release valves

Given their importance for the correct operation of the plant, the operational principle of the valves controlled directly by the control system deserves a further investigation.

As explained before, the recirculation valve (Danfoss AHU3 V1) fulfilled the task of maintaining the water supplied to the suspended ceiling loop at a constant temperature. This regulation was performed by the control system, which was continuously changing the position of the valve based on the measured supply water temperature (retroactive regulation). When the supply water temperature was lower than the set value, the valve was commanded to increase the span of the passage section in order to enhance the amount of fluid recirculated.

The 3-way valve (Danfoss AMZ 113) was located below the CWT and was in charge of switching between the cooling and the heating operational mode, whenever commanded by the control system.
The outlook and the principle of operation of this device are illustrated in Figure 5.22 and Figure 5.23.
The valve received the fluid coming from the intermediate heat exchanger (port AB) and directed it either to the CWT (when in position B) or to the HWT (when in position A).

A 2-way valve (Danfoss VS 2) was used to regulate the flow rate of the water supplied by the chiller to the CWT. The present valve was commanded to open the passage every time the temperature of the water in the middle of the CWT rose above the respective set point, whereas it was closed in the opposite case.

Figure 5.22 – Outlook of the 3-way valve

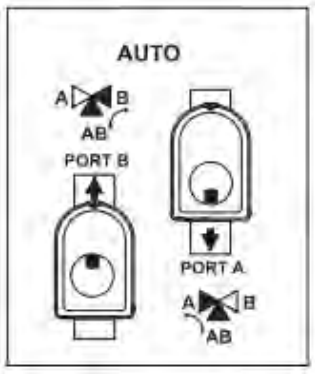

Figure 5.23 – Principle of operation of the 3-way valve

5.1.7 Measurement equipment and sensors

In the present paragraph a description of the measurement equipment is provided.
Several measurement tools were installed in order to monitor the reference parameters for the control system and to evaluate the performances of the plant and the conditions of the surrounding environments.

5.1.7.1 Weather station

The external weather conditions were monitored by means of Weather station Vantage Pro2 (Figure 5.24), which contains a sensor suite measuring, among others, the following parameters:

- Wind speed [m/s]
- Wind direction [°]
- Rain amount [mm]
- Air relative humidity [%]
- Air temperature [°C]
- Dew point temperature [°C]
- Atmospheric pressure [hPa]
- Solar radiation on horizontal surface [W/m^2]

Figure 5.24 – Weather station Vantage Pro 2

5.1.7.2 Temperature sensors

Several temperature values were measured during the experiment, all of them by means of Platinum Thermoresistances PT1000 class A.

Two sensors were employed to monitor the top surface temperature of the solar collectors. One was attached to the unglazed collector (Figure 5.26) while the second one was placed on the middle PV-T. Both of them have been welded to the surface of the collectors with thermal glue and they have been covered with water proof thermal insulation and a low emissivity foil, in order to minimize the influence of the surrounding (radiation, wind, air temperature).

Other 16 PT1000 were used to measure the PCM ceiling panels' surface temperature. Each sensor was fixed on a small copper plate and attached on the ceiling panels' top and bottom surfaces, as illustrated in Figure 5.25. Surface temperature was measured on the panels numbered with 1, 5, 8, 14, 17, 19, 24, 27, according to Figure 5.8.

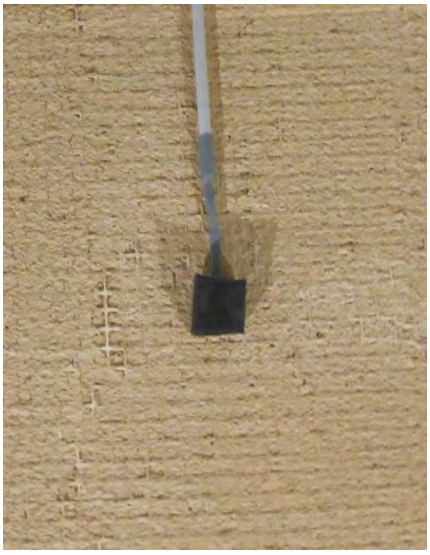

Figure 5.25 − Surface temperature sensor at the bottom of one PCM panel

Figure 5.26 − Temperature sensor on the top surface of the unglazed collector

Two stands with temperature sensors (Figure 5.27) attached on them were employed to evaluate the indoor thermal conditions. The air temperature of the climatic chamber was measured at four heights: 0.1 m, 0.6 m, 1.1 m (ankle, abdomen and head level for a seated person), and 1.7 m (head level for a standing person) while the operative temperature was measured only at a height 0.6 m (abdomen seated person), according to the recommendations for measuring heights of the physical parameters of an indoor environment given in EN ISO 7726 [30].

Figure 5.27 − Stand for measuring the air and the operative temperature inside the chamber

In addition to the thermal parameters of the indoor environment, the air temperature in the space surrounding the chamber was measured by means of a sensor place right above the door of the climate chamber. This value was recorded to have the possibility to estimate the influence of heat gains/losses due to transmission through the chamber's envelope.

The temperatures of the fluids flowing along the hydraulic circuits were measured in all the spots considered relevant either for overviewing the operation of the system or for later calculation purposes. Temperature sensors were placed underneath the insulation material covering the hydraulic circuit, welded to the pipes with thermal glue. In more detail, the following parameters were measured:

- inlet and outlet temperature of the unglazed collector
- inlet and outlet temperature of the PV-T series
- inlet and outlet temperature of the intermediate heat exchanger, on both sides (source and load side)
- temperature at top, middle and bottom of the CWT
- temperature at the top of the HWT
- supply and return temperature of the active ceiling's loop
- supply temperature of the main chiller

The tanks had been prearranged to facilitate the contingent insertion of sensors measuring the stored water temperature.

Finally, the supply and return temperature of the ventilation air was monitored through the general control of the ventilation system of ICIEE Laboratory. The supplied air relative humidity and flow rate were monitored by this system, as well as the relative humidity inside the climate chamber.

5.1.7.3 Heat flux sensors

The heat flux absorbed and released by the active ceiling was measured by Type M55A heat flux sensors by ETO DENKI (Figure 5.28), placed on the surface facing the room of the panels with numbers 6, 13, 15, according to Figure 5.8.

The heat flux flowing through the solar collectors' top surface was measured by means of two thin film heat flux sensors model Omega HFS-4, one placed on the unglazed collector and the other attached on the PV-T located in the middle (Figure 5.29).

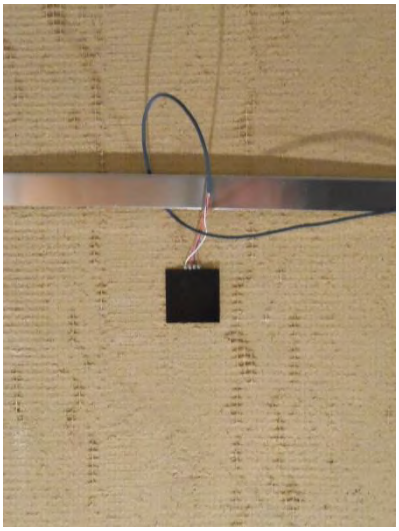

Figure 5.28 − Heat flux sensor at the bottom of one ceiling panel

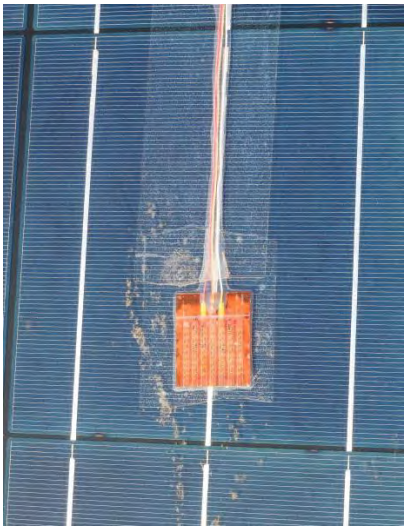

Figure 5.29 − Heat flux sensor on the middle PV-T collector

5.1.7.4 Flow rate sensors

Vortex flow sensor[11] Grundfos VFS 1-12 QT was utilized to measure the total flow rate of the water supplied to the solar collectors' loop. The present device was located right before the diverter splitting the fluid into the two branches of the solar circuit. The temperature recorded by the VFS was not taken into consideration since the value shown was affected by relevant fluctuations[12].
An identical VFS was employed to monitor the flow rate in the intermediate circuit.

The flow rate in each of the solar branches was measured by a digital flow rate reader (IMI Hydronic TA Scope) whose sensing element was inserted inside one of the cavities of the balancing valves. The same approach was used to evaluate the flow rate of the water supplied to the PCM ceiling. The values recorded were kept constant during the whole experiment.

5.1.8 Data logger

All the measured parameters were logged on a server and were extracted and visualized by means of software Historian Enquire by Schneider Electric. The data logger recorded for each parameter a number of samples dependent on the sampling rate of the related sensor. The user has the possibility to extract automatically averaged values over time ranges of 1 minute, 15 minute and 1 hour.

[11] VFS is a series of combined flow and temperature sensors (two-in-one) based on the principle of vortex shedding behind a bluff body.
[12] Two of the PT1000 mentioned in the previous paragraph were employed because of the lack of accuracy of the present VFS.

5.2 Control system

The control system was implemented by means of a PLC (Programmable Logic Controller, Schneider Electric model M340), which controlled the different sections of the experimental system and more specifically the 3-way valve, the pump and the recirculation valve of the supply system and the 2-way valve regulating the flow rate supplied by the chiller. Furthermore, the control was responsible of implementing the schedule for the lighting of the climatic chamber.

A description of the control logic of each component is presented below.

5.2.1 3-way valve control

As previously explained, the 3-way valve was in charge of switching between the cooling and the heating mode by modifying its position. The cooling operation was active when the temperature difference between the middle of the CWT and the water at the outlet of the solar panel's circuit (Δt) was above the set point (Δt^*).

The set point value was fixed to 3 °C in order to ensure that the water exiting the solar collectors provided cooling to the water inside the CWT, taking into account the cooling power losses along the way to the reservoir[13]. This choice was not optimal for the heating mode since cooling energy was provided to the HWT during some hours of the day. However, since the main aim of the plant was discharging the PCM contained in the suspended ceiling, priority was given to the cooling mode.

5.2.2 Water supply system control

The supply system's pump was operating as long as all the following conditions were fulfilled simultaneously:

- the time was between 8.00 p.m. and 7.30 a.m.
- the temperature at the middle of the cold water tank (t_{mt}) was below 18 °C (t^*_{mt}), thus assuring the stored water was able to provide cooling to the PCM ceiling panels
- the operative temperature in the room (t_o) was above 21 °C (t^*_o) , thus preventing having too low indoor temperatures in the morning[14]
- the average temperature at the bottom of the ceiling panels (t_{b_PCM}) was above 21 °C ($t^*_{b\_PCM}$); this condition was implemented in order to prevent circulating water in the ceiling's hydraulic loop after the PCM was completely solidified (21 °C represents the lower boundary of the PCM's melting temperature range).

The logic of the PCM ceiling' supply control is illustrated in Figure 5.30.

Monitoring the temperature of the water at the middle of the tank (instead the one the bottom) ensured to have a sufficient amount of water at a lower temperature than the set one (due to stratification phenomenon), thus reducing the number of starts/stops of the pump and therefore assuring a higher stability of the control.
On the other hand, the temperature at the top of CWT was not considered because the related sensor was located close to the inlet of the water coming back from the ceiling loop. Hence, the measured value was much higher than the average temperature of the tank.

[13] The cooling power losses occur along the connection pipes and at the intermediate heat exchanger and are due to the heat absorption from the surrounding environment.
[14] If the temperature dropped below 21 °C, longer time would be necessary to reach the steady thermal conditions required in the room by 9.00 a.m.

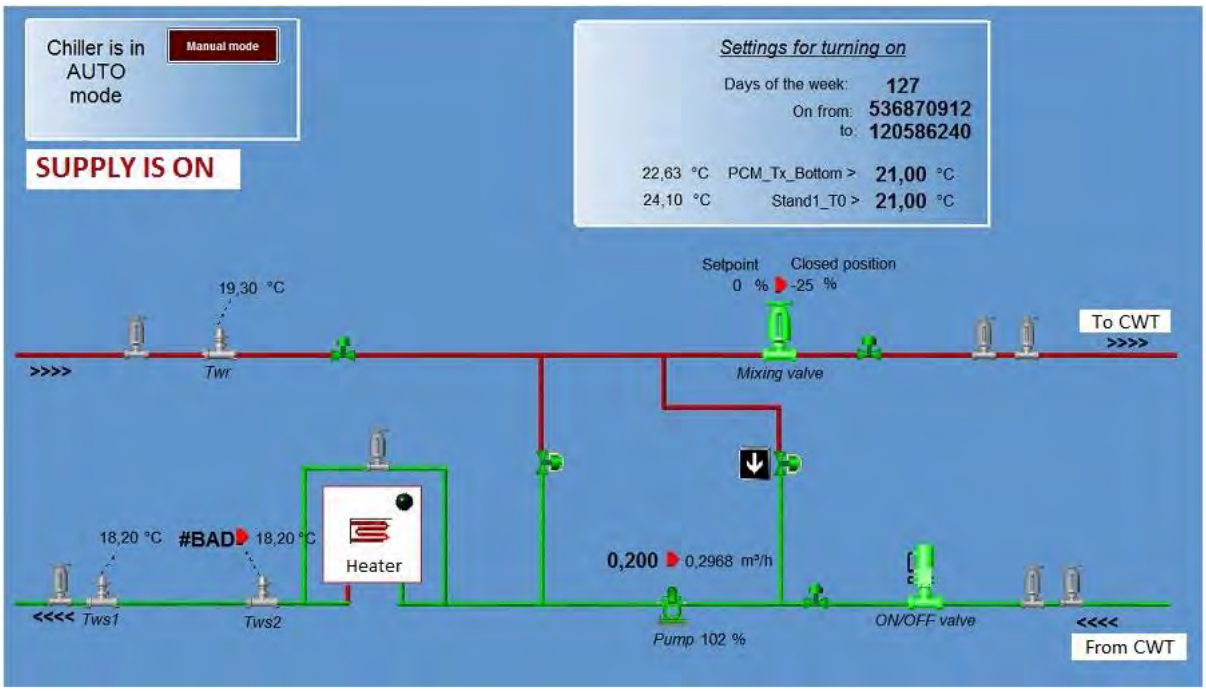

Figure 5.30 – Control of the ceiling water supply system

5.2.3 Recirculation valve control

The position of the recirculation valve installed in the ceiling's water supply system was controlled by the PLC, with the aim of keeping constant the water supply temperature (t_{supply}).

The set point value for the present regulation (t^*_{supply}) was chosen taking into account the following aspects:

- the condensation of the water vapour contained in the indoor air on the ceiling panel's surfaces needs to be prevented; considering an indoor air temperature of 28 °C and a relative humidity of 30%[15], local surface condensation phenomena could occur if the air temperature drops below 8 °C [31]
- on the other hand, the supply temperature had to be low enough to cool the ceiling panels until the completion of the PCM discharge process, which occurred at 21 °C.

Based on these considerations, the water supply temperature was set to 18 °C.

5.2.4 Chiller control

Water from the main chiller of ICIEE Laboratory supplied the PCM ceiling loop when the temperature at the middle of CWT (t_{mt}) rose above 17 °C (t^{**}_{mt}) during the time interval between 0.00 a.m. and 7.30 a.m.
The temperature at the middle of CWT was chosen as reference parameter for the same reasons explained in paragraph 5.2.2.

A review on the set points of the control system is presented in Table 5.5.

[15] The internal relative humidity was always kept below this value by the main ventilation control system

Table 5.5 – Set points for the control system

Controlled device	Parameter	Set point value [°C]
3-way valve	Δt^*	3
Supply system	t^*_{mt}	18
	t^*_{o}	21
	$t^*_{b\ PCM}$	21
Recirculation valve	t^*_{supply}	18
Chiller	t^{**}_{mt}	17

5.3 Results

In the present section the results of the experimental study are presented and discussed. Particular emphasis will be given to the performances of the PCM ceiling and the night sky radiant cooling system, whose combination is the main subject of the thesis. The experimental results concerning these two technologies are presented separately in order to guarantee a better clarity. Hence, the present paragraph has been subdivided in two sections.

All the reported graphs represent data averaged over 1 minute time step.

5.3.1 Climate chamber and PCM ceiling

The temperature profiles of the climate chamber and the PCM panels are shown for a 24-hour time interval, from 7.30 a.m. to 7.30 a.m. of the following day. The time interval between the 14th and the 15th of March was chosen as a representative day for Case A, while the 24 hours over 13th and 14th March were selected for Case B.

The average temperature at the bottom surface of the ceiling panels, the air temperature[16] and the operative temperature of the room are illustrated in Figure 5.31 and Figure 5.32 for Case A and B, respectively. The first and the last parameter mentioned were taken as reference by the control system for the operation of the pump which was supplying water to the ceiling's loop.

In both the studied cases the cooling energy provided by the supplied water was enough to fully discharge the phase change material during the night. Indeed, the end of the discharge process of the PCM occurred approximately at 1.30 a.m. for Case A and at around 2.30 a.m. in Case B. This difference can be ascribed to the fact that more sensible heat was stored in the panels in Case B since their temperature during daytime was approximately 2 °C higher than for Case A. Considering the supply and return temperature of the water, the cooling energy provided to the ceiling during nocturnal operation was assessed to be about 2 kWh in Case A and 2.15 kWh for Case B.

It is worthwhile remarking that the fluctuation of the air and the operative temperatures during daytime was more marked than the temperature variation of the PCM panels' bottom surface. This can be attributed to the surface thermal resistance of the ceiling, which represents an obstacle to the heat exchange. On the other hand, the drop of the downwards surface temperature of the ceiling was faster than the one of the air during the night because the cooling source, that is the supplied water, was located inside the panels.

The sudden drops of the air and operative temperature which can be observed during daytime are due to the opening of the entrance door of the climate chamber, which was needed by the researchers carrying out the experiment involving human subjects.

[16] From now on, the air temperature at a height of 1.1 m will be considered, since it was the closest to the one used to control the indoor temperature during daytime

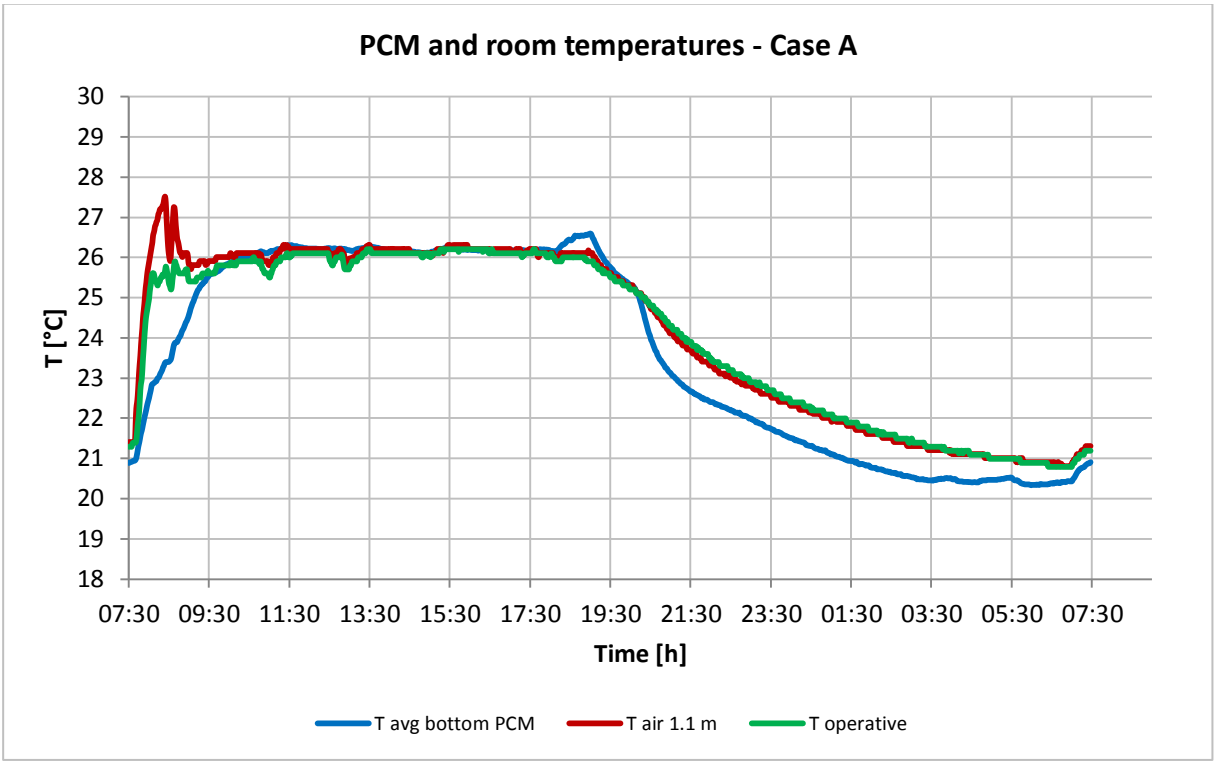

Figure 5.31 – PCM panels and room temperatures measured for Case A

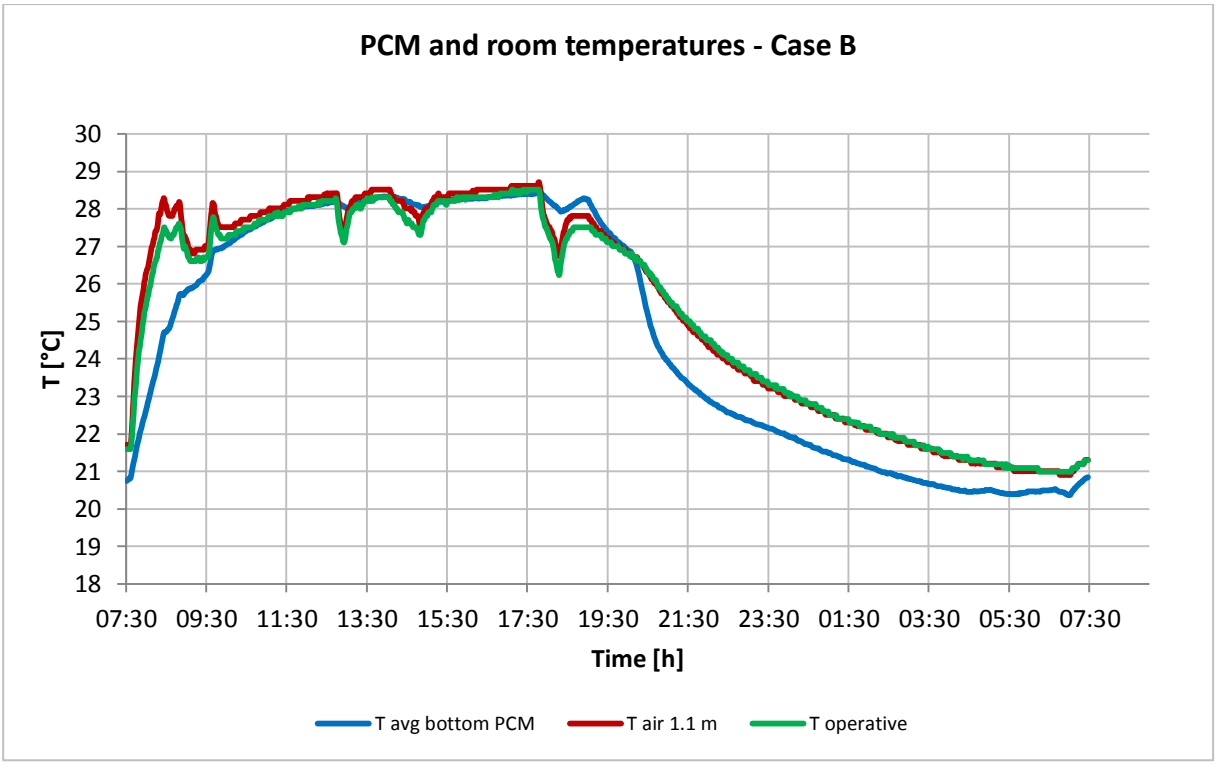

Figure 5.32 – PCM panels and room temperatures measured for Case B

As a consequence of the different amount of energy stored in the PCM in the two case studies, the first turning off of the water supply pump, which occurred when the average temperature at the bottom surface of the PCM panels dropped below 20.5 °C[17], happened about 1 hour before in Case A. Indeed, the supply pump was switched off at 3.10 a.m. in Case A and at about 4.20 a.m. in the other scenario, as illustrated in Figure 5.33 and Figure 5.34.

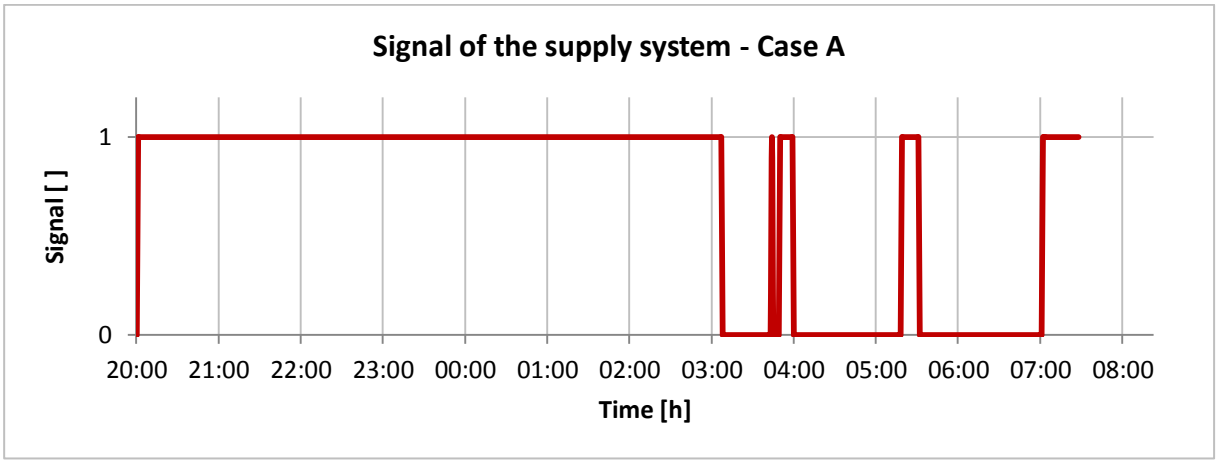

Figure 5.33 – Input signal to the pump of the water supply system (1=ON, 0=OFF) for Case A

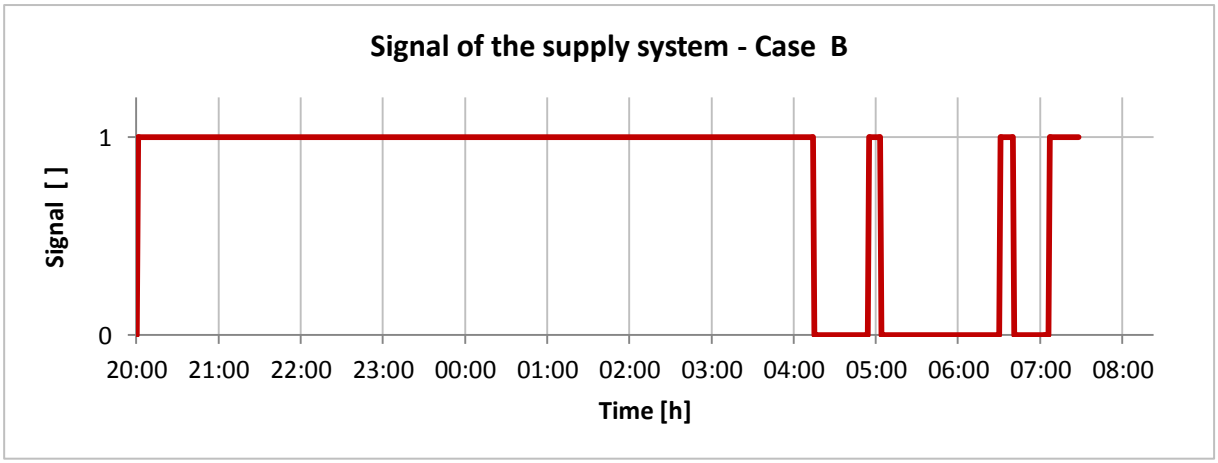

Figure 5.34 – Input signal to the pump of the water supply system (1=ON, 0=OFF) for Case B

The bottom surface temperature of every single PCM panel is reported in Figure 5.35 and Figure 5.36, in order to underline the non-homogeneity of the PCM's charge and discharge phases in the different parts of the ceiling. The panels number 5, 8, 14 and 17, which were located in the intermediate row of the suspended ceiling (see Figure 5.8), shown higher temperature values than the other elements during the occupancy period. This could be due to the position of the electrical bulbs hanging from the ceiling, which were installed near the first mentioned panels. This non-uniformity was particularly evident between 6.00 p.m. and 7.00 p.m., when the ventilation was off and the lights were the only heat sources in the chamber. During this period, the temperature of the surface facing the floor was almost constant for panels 1, 19, 24 and 27 while it was rising considerably for the remaining ones. The highest increase in this time interval was observed for panel number 17, being approximately 2 °C and 1.5 °C for Case A and B, respectively.

[17] A dead-band of 0.5 °C below the set point of 21 °C was set to ensure the complete discharge the PCM contained in each panel by the end of the night.

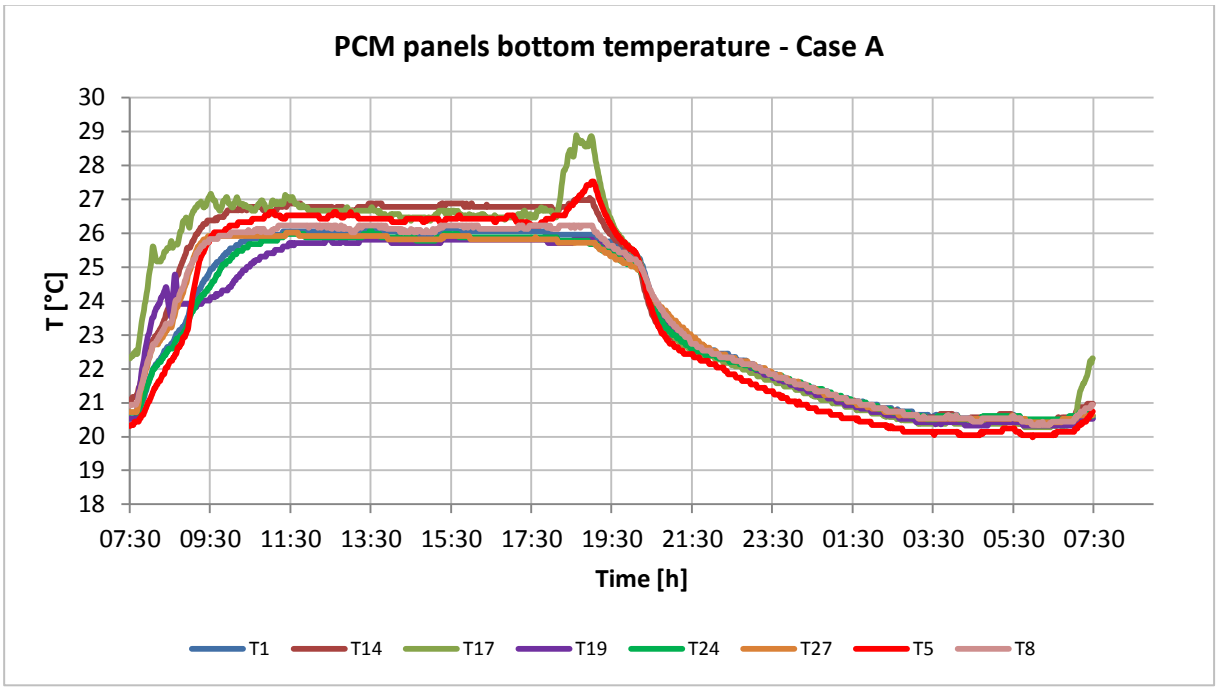

Figure 5.35 – PCM panels' bottom surface temperature for Case A

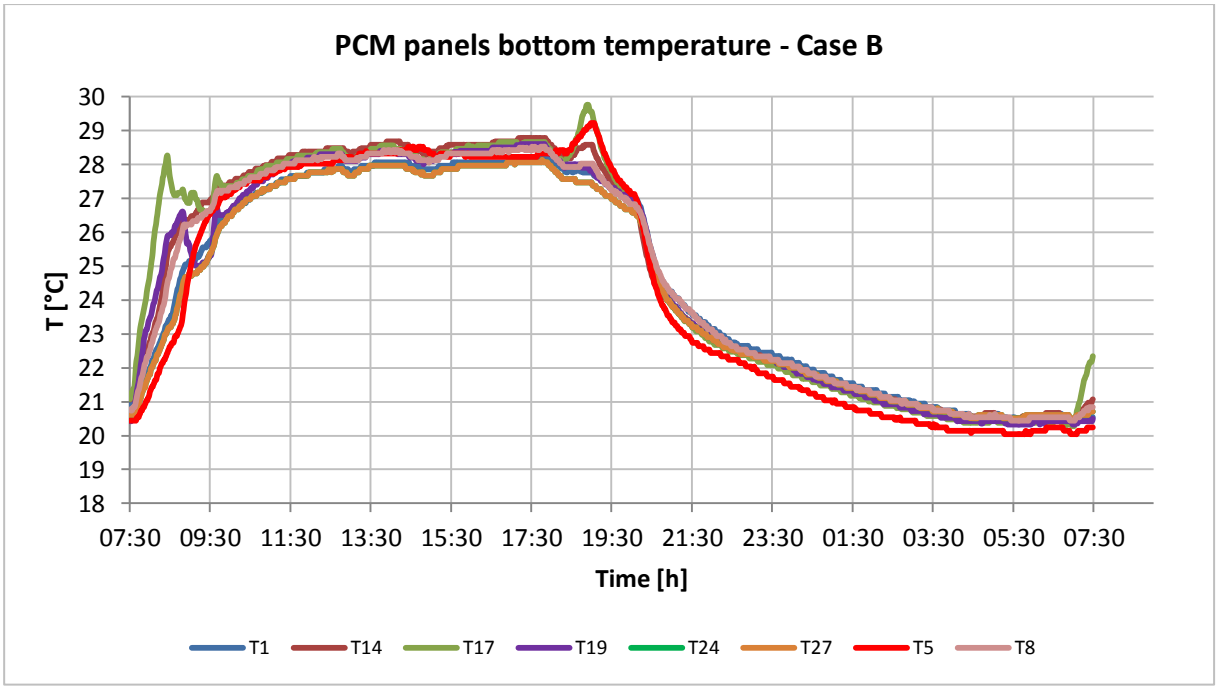

Figure 5.36 – PCM panels' bottom surface temperature for Case B

The temperatures of the PCM panels' surface facing the roof of the chamber are shown in Figure 5.37 and Figure 5.38. During daytime the present values were lower than the ones of the bottom surface because they were not affected directly by the heat gains inside the room, since the suspended ceiling worked as a thermal resistance. The temperature difference between top and bottom surfaces of corresponding panels was approximately 1 °C during the occupancy period (from 9.00 a.m. to 6.00 p.m.).

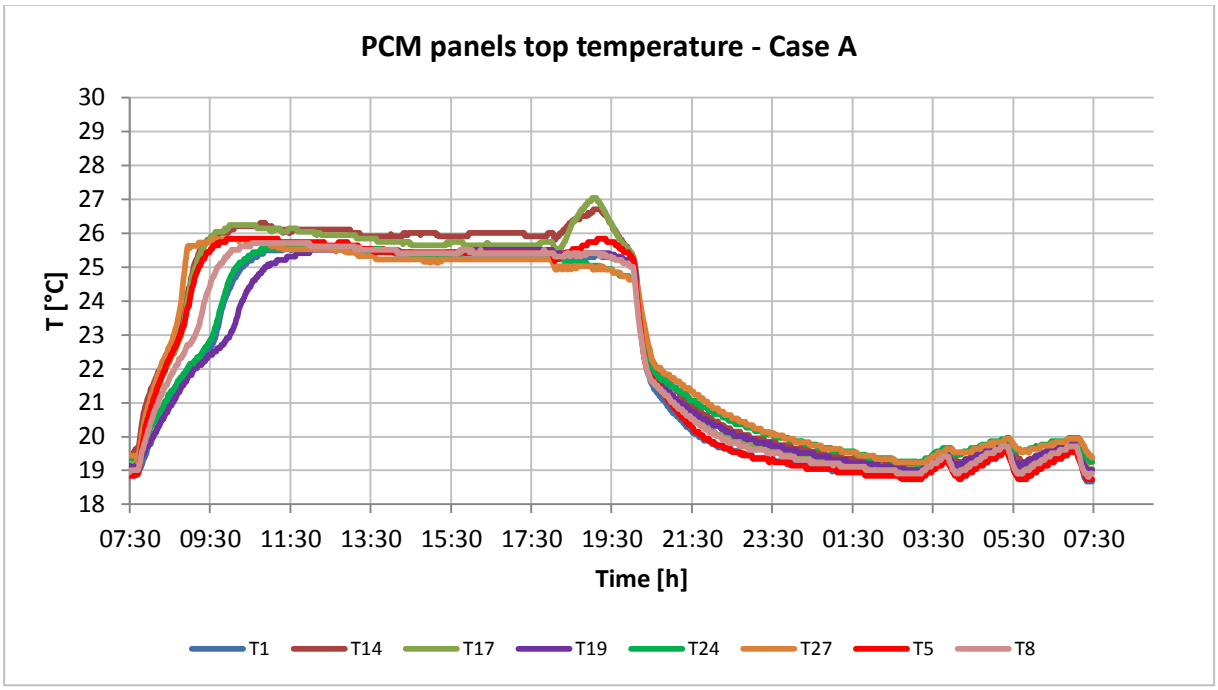

Figure 5.37 – PCM panels' top surface temperature for Case A

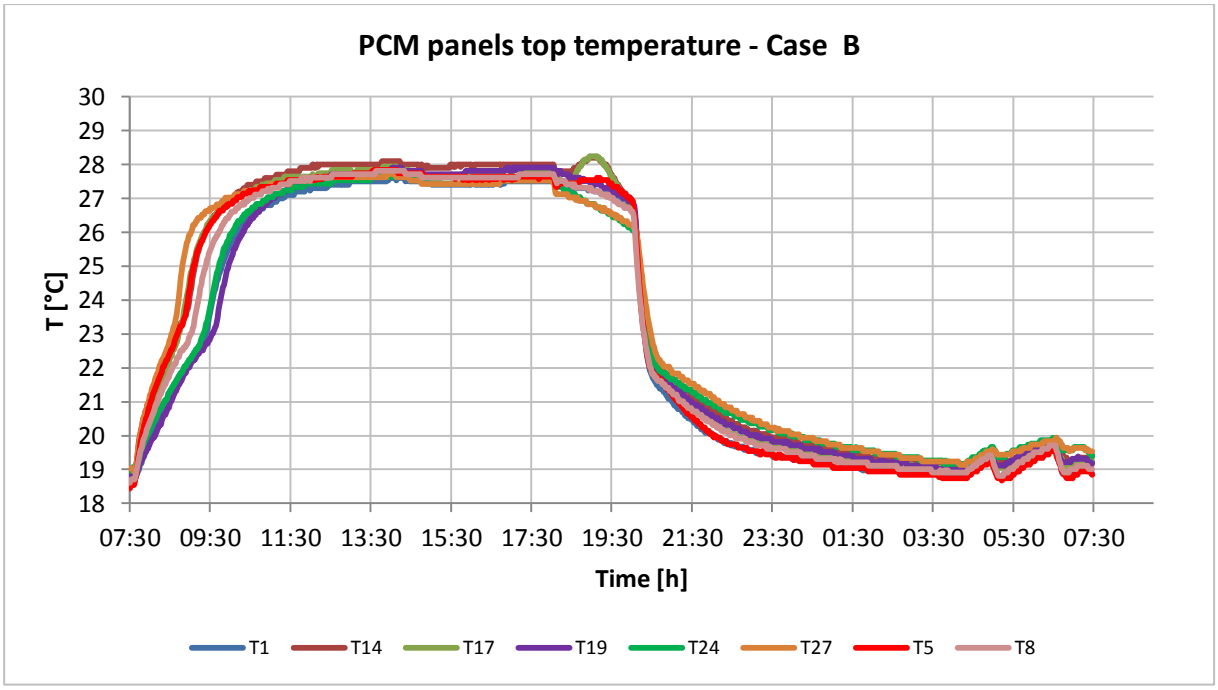

Figure 5.38 – PCM panels' top surface temperature for Case B

However, the temperature drop resulting after the starting of the water circulation was much faster for the upper part of the ceiling. Indeed, it was already below 21 °C by 10.00 p.m. for both the case studies. This may be due to the location of the embedded pipes, which were situated above the cardboard layer, which was functioning as a significant thermal resistance.

5.3.2 Night sky radiant cooling

In the present section the performances of the solar collectors are investigated, mainly focusing on the cooling power provided during night-time.

The useful cooling power supplied to the water flowing through the solar circuit has been evaluated by means of two different approaches. In the first case the temperature sensors at inlet and outlet of the two branches of the circuit were employed and the specific cooling power per surface area was calculated as:

$$P_{cool,spec} = \frac{\dot{m} \cdot c_p \cdot (T_{supply} - T_{return})}{A_c} \qquad [W/m^2]$$

where A_c is the frontal surface area of the considered collector (in m^2). A value of 3.35 kJ/kg K was found in literature for the specific heat capacity of the water-glycol mixture in the solar circuit [32].

The second method was based on the measurements of the heat flux sensors placed on the top surface of the solar collectors. Since the present sensors measure just the heat flux passing through the top surface of the collectors, the bottom and edges heat losses were added to this value in order to estimate the useful cooling power provided to the water. In this way, the results of the two experimental methods can be compared.
The specific cooling power was calculated by means of the following equation:

$$P_{cool,spec} = P_{HF\ sensor} + (U_{bott} + U_{edges}) \cdot (T_{surf} - T_{air}) \qquad [W/m^2]$$

where:

- $P_{HF\ sensor}$ is the value measured by the heat flux sensor, in W/m^2
- U_{bott} and U_{edges} are the bottom and edges heat loss coefficients, respectively (W/m^2K)
- T_{surf} is the surface temperature of the considered solar collector, in °C.

The method used for the evaluation of the bottom and edges heat loss coefficients is explained in detail in Annex 12.1.2.

The results are shown for the nights between 7th and 8th and between 10th and 11th of March. The sun set at around 6.10 p.m. and rose at about 6.45 a.m. In order to provide an unbiased comparison between the two selected nights, the results are presented for the time interval between 10.00 p.m. and 6.00 a.m. This choice ensured that the cooling power was supplied to the CWT since the cooling mode was always active during the mentioned time range for the considered nights[18].

Figure 5.39 and Figure 5.40 illustrate the specific cooling power provided by the unglazed and the PV-T collectors during the selected nights.

[18] When the 3-way valve switches from the cooling mode to the heating mode, the inlet temperature to the solar collectors rises considerably and so does the heat released to the external environment.

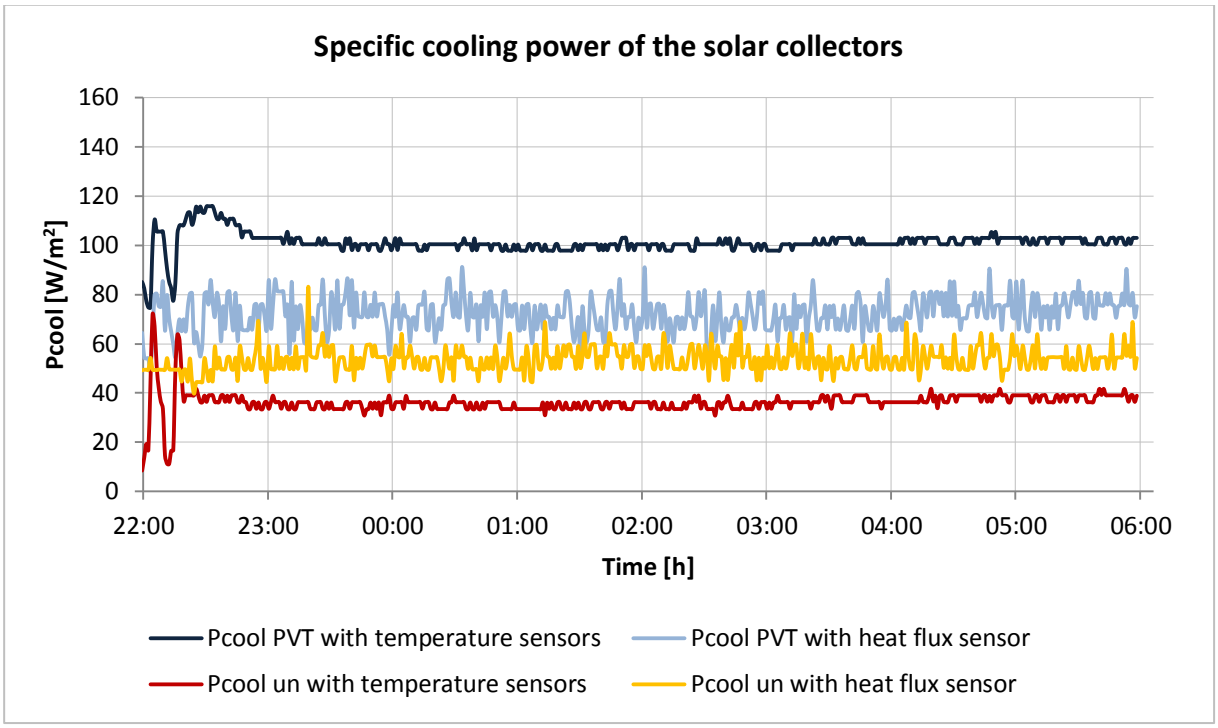

Figure 5.39 – Specific cooling power provided by the collectors during the night between 7th and 8th March

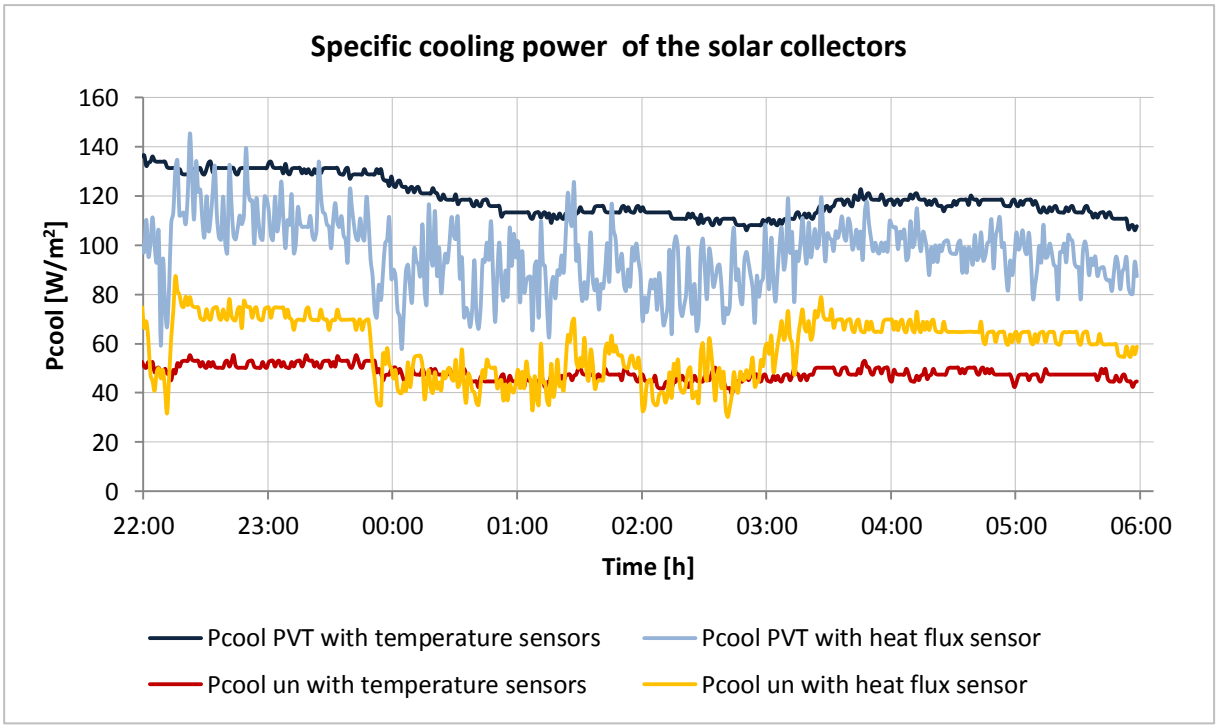

Figure 5.40 – Specific cooling power provided by the collectors during the night between10th and 11th March

As regards to the unglazed collector, it can be noticed that the cooling power evaluated by means of the het flux sensor was overestimated for the most of the time if compared to the one assessed with the temperature sensors.

This difference could be partially explained by the uncertainty in the calculation of the bottom and back heat losses coefficients. Indeed, not all the technical parameters (such as thickness and thermal conductivity of the frame material) were available and therefore some assumptions were made.
Furthermore, the measurements of the heat flux sensors could have been moderately affected by the wires extensions which were performed. Indeed, although in the datasheet it was specified that no calibration was needed for wires' length below 10 m (it was 8 m in the experimental setup), the accuracy of the measured value may have been conditioned by the wires' extension.
Finally, it has to be taken into account that the heat flux sensor measures the heat flux passing through a restricted portion of the collector's surface. However, the measured value may differ from the heat flux of other parts of the absorber plate due to different local thermal conditions, such as the temperature of the fluid flowing through the internal loop. Indeed, the fluid temperature is supposed to decrease going from the top (where the fluid inlet is located) to the bottom of the collector, thus reducing the heat released to the external environment.

Figure 5.41 shows the average specific cooling power provided by the unglazed collector for both the employed calculation approaches. The nights between the 5th and the 11th of March (time range 10.00 p.m. - 6.00 a.m.) are considered.

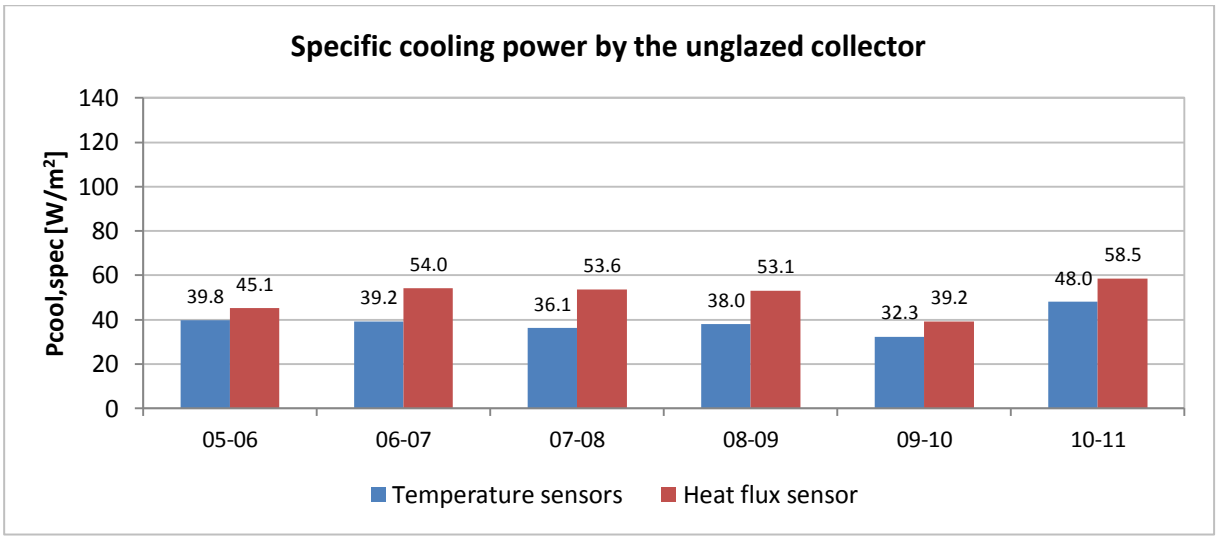

Figure 5.41 – Average specific cooling power of the unglazed collector from 10.00 p.m. to 6.00 a.m.

The previous considerations concerning the gap between the cooling powers assessed with the two methods are verified for all the 6 nights presented. The average specific cooling power evaluated with the heat flux sensor is always higher than the one assessed by means of the temperature sensors. A difference ranging from 5.3 W/m^2 to 17.5 W/m^2 is observed between the two methods. In terms of relative values, the cooling power evaluated considering inlet and outlet temperatures of the fluid varies from 68% to 88% of the one calculated with the other approach.

In the matter of the Photovoltaic-Thermal solar collectors, the cooling power given by the two methods was significantly different for both nights. However, contrarily to what observed for the unglazed collector, the value calculated using the heat flux sensor is lower than the one estimated with the other approach. The present statement is confirmed for all the 6 nights considered in Figure 5.42.

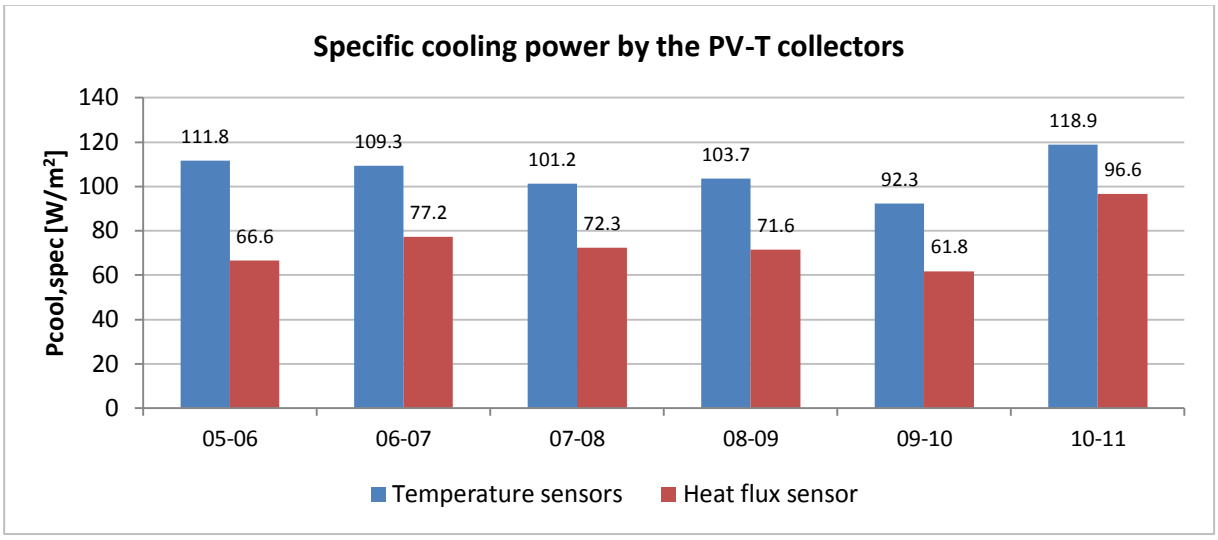

Figure 5.42 – Average specific cooling power of the PV-T collectors from 10.00 p.m. to 6.00 a.m.

The specific power measured by means of the heat flux sensors was between 60% and 81% of the one calculated with the temperature difference. The same reasons mentioned for the unglazed collector could explain the noticeable dissimilarity between the two experimental approaches. Even more uncertainty of the measured heat flux has to be taken into account in this case, since just one single sensor was used and its measurement was considered representative for all three collectors. In fact, not the same thermal conditions can be assumed for the different portions of the collectors' top surface and therefore the hypothesis of homogeneous heat flux has to be considered inadequate.

In order to verify the supposed inaccuracy of the heat flux sensors, the average cooling power released in correspondence to the intermediate heat exchanger has been calculated. The average value refers to the time range from 10.00 p.m. to 6.00 a.m. The following equation has been employed:

$$P_{cool} = \dot{m} \cdot c_p \cdot (T_{outlet,HE} - T_{inlet,HE}) \qquad [W/m^2]$$

where $T_{outlet,HE}$ and $T_{inlet,HE}$ are respectively the inlet and outlet temperatures to the heat exchanger of the fluid circulating in the solar circuit. The present value has been compared with the power evaluated with the previous two approaches, as shown in Figure 5.43.

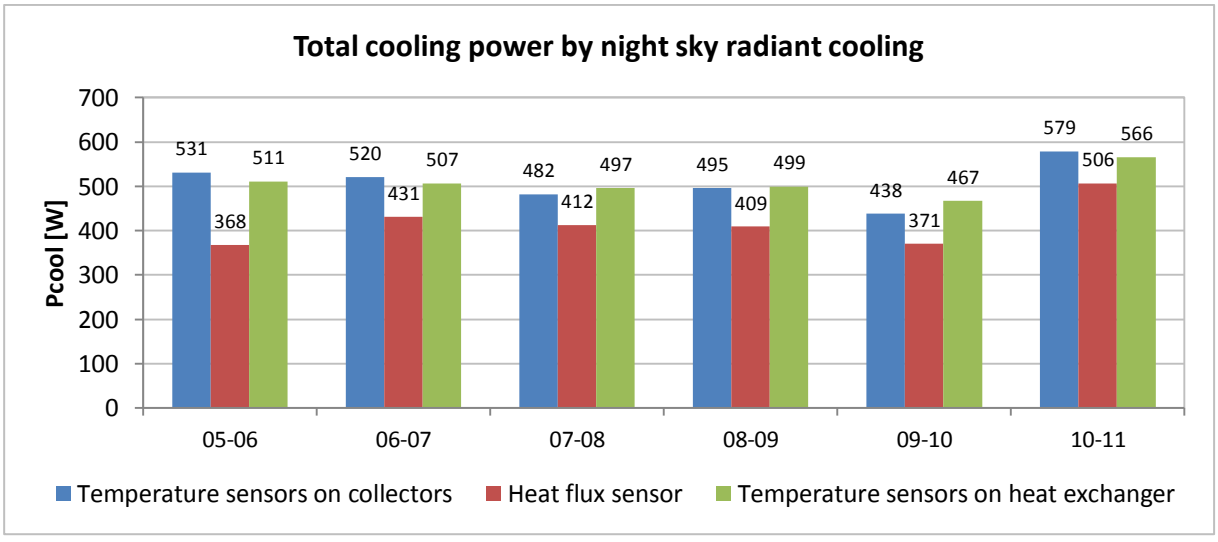

Figure 5.43 – Total cooling power provided by night sky radiant cooling

As can be noticed, the cooling power calculated with the two approaches employing PT1000 sensors matches remarkably well, while the one evaluated by means of the heat flux sensors is noticeably lower. Hence, the latter approach cannot be considered reliable and the related results will not be utilized from now on. The divergence between the first two methods is due to the heat losses/gains affecting the fluid along its way from the collectors to the heat exchanger and vice versa, which were not taken into account in the calculations.

Considering the total cooling power assessed by means of the temperature sensors on the inlets and outlets of the two hydraulic branches, values between 438 W and 579 W were observed (Figure 5.44). The useful cooling power provided by the PV-T collectors was always more than 80% of the overall value of the solar circuit.

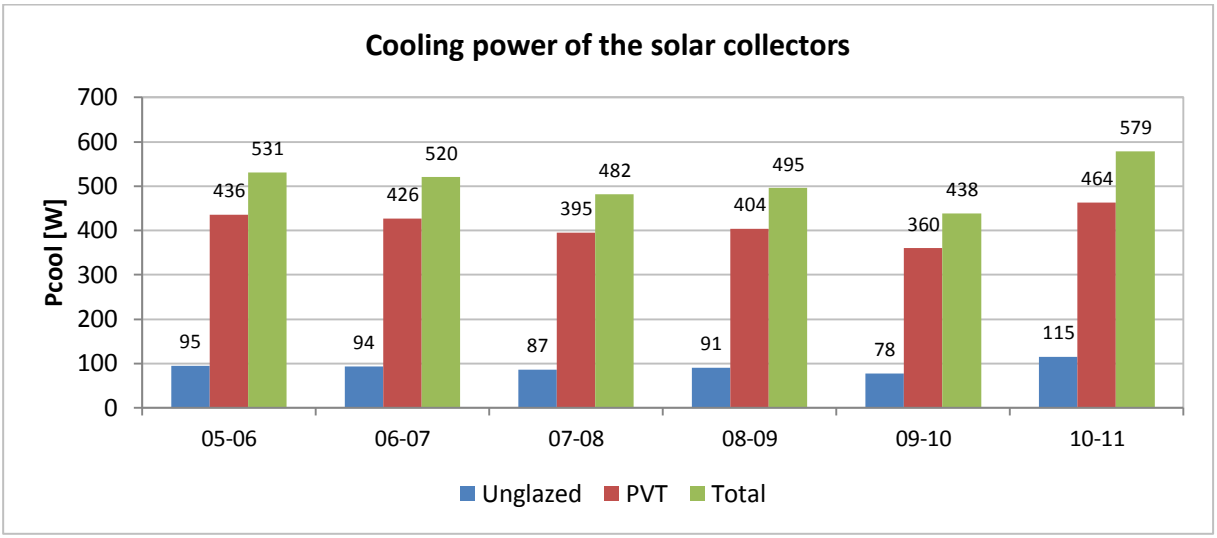

Figure 5.44 – Average specific cooling power provided by the two types of collectors

The significant gap between the cooling power provided by the PV-T panels and the unglazed collector is partially due to the difference of the emitting surface area, which was 60% bigger for the PV-T. Hence, the specific cooling power per unit area has been considered in Figure 5.45 in order to adequately compare the performances of the two different kinds of collector.

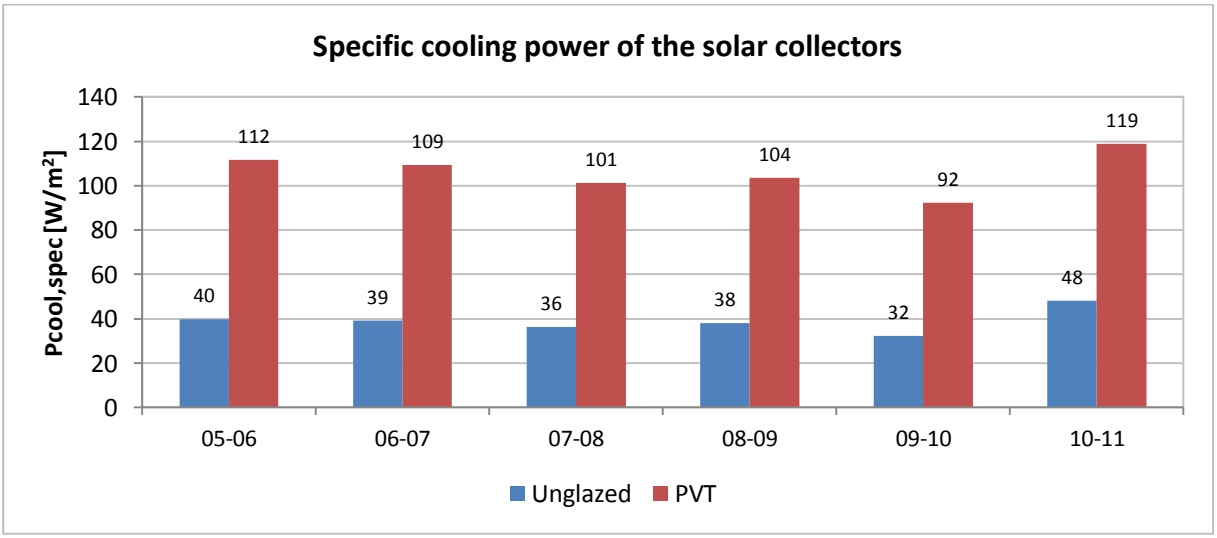

Figure 5.45 – Comparison between the specific cooling powers provided by the two types of collectors

The cooling output per unit area produced by the unglazed collector is significantly lower than the one provided by the PV-T panels, even though the same flow rate per unit area was implemented in the two branches of the solar circuit. The rate between the two values (in the mentioned order) ranges between 35% and 40%. This

tendency is opposite to what expected, since the surface of the unglazed collector has higher emissivity than the PV-T panels, thus leading to higher radiative heat exchange with the sky; furthermore, the absence of the glass cover should result in higher convective heat losses compared to the PV-T collectors.

The limited performance of the unglazed collector could be ascribed to the high thermal resistance existing between the fluid and the external environment. Indeed, the pipes of the internal loop were made of polyvinyl chloride, which has a low thermal conductivity (0.19 W/m K [33]) compared to the one of metals. Contrarily, low thermal resistance was present between the fluid and the top surface of the PV-T collectors since the internal pipes and the absorber plate were metallic (probably made of copper).
This consideration is confirmed by the difference between the top surface temperatures of the two types of collector, which are illustrated in Figure 5.46 and Figure 5.47 for the nights between 7th and 8th and between 10th and 11th of March, respectively. The external air temperature is reported as well.

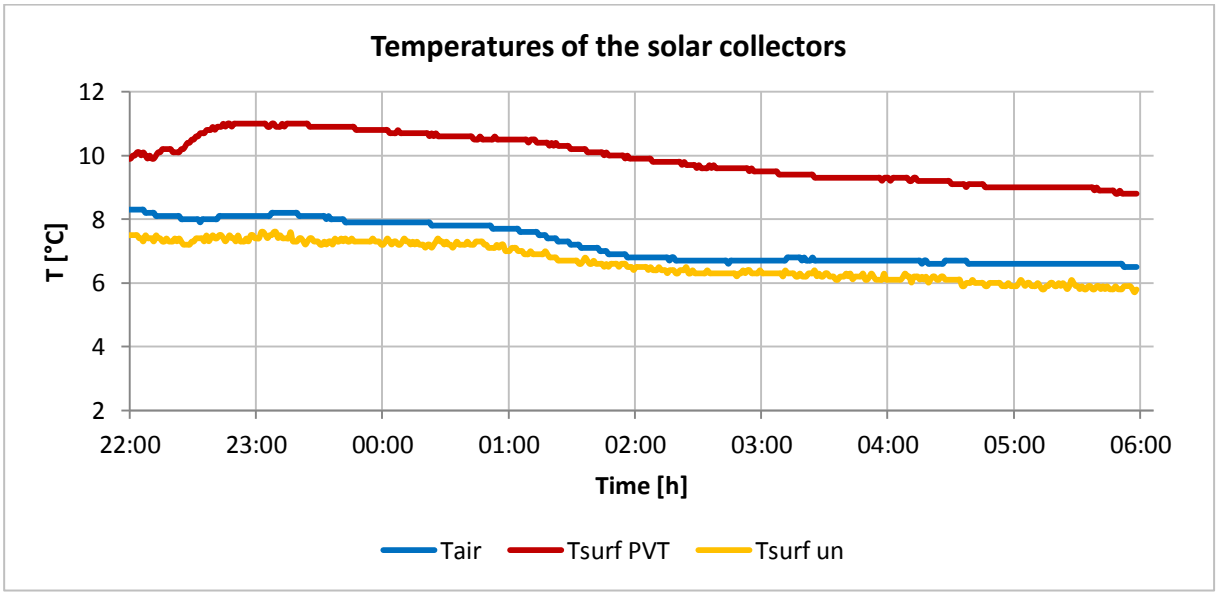

Figure 5.46 – Temperatures of the solar collectors during the night between 7th and 8th of March

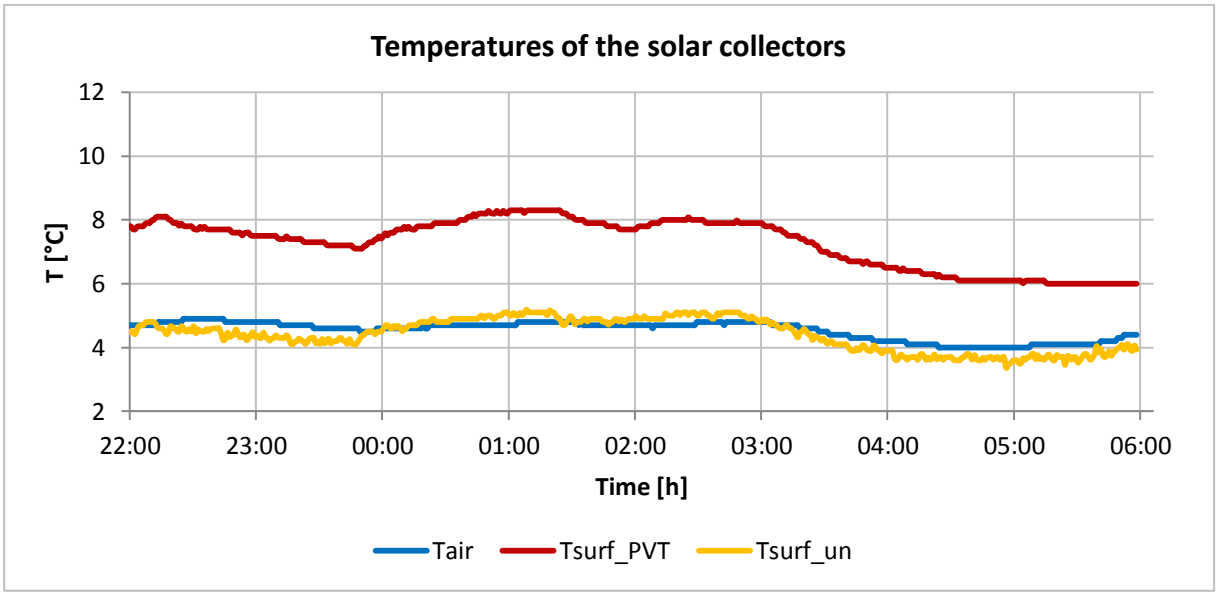

Figure 5.47 – Temperatures of the solar collectors during the night between 10th and 11th of March

It can be noticed that the surface temperature of the unglazed collector is always very close to the one of the external environment (sometimes it is even lower than the air temperature) while a gap between 2 °C and 3 °C exists between the latter value and the surface temperature of the PV-T panels. This difference may be due to the diverse thermal resistance existing between surface and fluid for the two kinds of collector. As regards to the PV-T, the high conductivity of the pipe walls of the internal loop allows a good heat transfer from the fluid to the external environment and therefore the surface temperature of the panel is heated by the thermal energy coming from the fluid. The opposite consideration can be made for the unglazed collector: the water temperature does not affect directly the surface temperature because of the high thermal resistance of the pipe walls of the internal hydraulic loop.

The variability of the cooling output performed along the two nights considered is mainly attributable to the variation of the external weather conditions and mostly to the air temperature and the effective sky temperature. It can be noticed that the air temperature was lower in the second night, thus leading to higher convective heat losses. Furthermore, the ambient temperature affects the effective sky temperature: lower values of the first parameter lead to lower sky temperatures and consequently to an enhancement of the radiative heat exchange, other conditions (cloud cover, relative humidity etc.) being equal. This aspect is studied in depth in Appendix 12.1.3.

5.4 Comments and conclusions

The system fulfilled its main aim during the whole experimental period, assuring the complete discharge of the phase changing material inside the suspended ceiling during the night.

Due to the thermal conditions implemented for the indoor space during the experimental study, no conclusions can be drawn about the performances of the PCM panels in terms of improvement of the indoor comfort. The internal gains affecting a real office room and a proper solar load profile should be considered in order to evaluate the real potential of the PCM technology.

The average cooling power produced by the nighttime cooling process varied between 438 W and 579 W. The PV-T technology showed a good potential, providing a cooling output between 90 and 120 W/m^2. Much lower performances were observed for the unglazed flat plate collector, whose specific cooling power output was between 30 and 50 W/m^2.

As expected, the chiller was never utilized because the cooling production of the solar collectors was enough to keep the temperature at the middle of the CWT always below of 17 °C, which was the threshold for the activation of the ancillary cooling system. However, the system needs to be tested under less advantageous climatic conditions, such as during the summer, when the cooling demand is at maximum levels and the availability from the natural environment is expected to be lower, due to the higher temperatures of the air and the sky.

Some improvements should be carried out to increase the performance of the system. The most important modification concerns the manner used to perform the switch from the cooling to the heating mode and vice versa. As it was said, the pump of the solar circuit and the one in the intermediate loop were operating 24 hours a day, even when neither cooling load was provided to the CWT nor heat power was supplied to the HWT. This aspect leads to two drawbacks: firstly, electrical energy is supplied to the pumps even if no useful effect is performed; secondly, since priority was given to the cooling mode, cooling power is supplied to the HWT for some time period after the 3-way valve switches to the heating mode. Both these defects can be removed by implementing an additional control on the 3-way valve and by controlling the pump of the intermediate circuit (P2). The 3-way valve should be switched to the heating mode only when the temperature of the fluid exiting the solar collectors is higher than the water temperature at the middle of HWT[19], in order to ensure that heating is supplied to the reservoir. When no useful effect is generated, pump P2 has to be turned off.
The mentioned modifications will be implemented in the simulation model studied in chapter 7.

[19] As for the cooling mode, a dead band has to be implemented to take into account the heat losses of the fluid circulating inside the pipes.

6 Simulation model: description and validation

In this chapter the potential of the system combining phase changing materials with night sky radiant cooling is analysed through computer simulations. The software TRNSYS 17 has been used for the purpose.

6.1 Description of the simulation tool TRNSYS 17

TRNSYS 17 (TRaNsient SYstem Simulation program) is an environment for the transient simulation of systems, including multi-zone buildings, with a modular structure. Due to its flexibility, it has become a reference among engineers and researchers around the world to validate new energy concepts, from simple domestic hot water systems to the design and simulation of buildings and their equipment, including control strategies, occupant behavior and alternative energy systems (wind, solar, photovoltaic, hydrogen systems) [34].

TRNSYS consists of a suite of programs: the TRNSYS Simulation Studio, the simulation engine and its executable, the Building input data visual interface (TRNBuild), and the Editor (TRNEditor) used to create stand-alone redistributable programs.
The main visual interface is the TRNSYS Simulation Studio, used to create projects by drag-and-dropping components to the workspace, connecting them together and setting the global simulation parameters. TRNSYS offers a broad variety of standard components, called "Types", and many additional libraries are available to expand its capabilities, such as the TESS library, used in this work.
TRNBuild is the tool used to enter input data for multi-zone buildings. It allows specifying all the building structure details, as well as everything that is needed to simulate the thermal behavior of the building, such as windows optical properties, heating and cooling schedules, etc.

6.2 General description of the model

The main aim of the model was simulating the behaviour of the experimental system previously presented, trying to describe the most accurately as possible the features of the components involved and the environmental conditions which occurred when the plant was tested.

The main components involved are:

- a PV-T collector
- an unglazed flat plate collector
- a building divided into multiple thermal zones
- a heat exchanger
- 2 storage tanks
- a phase changing material wall

The outlook of the simulation model is illustrated in Figure 6.1.
A description of the components utilized, including the properties chosen for each of them, is provided below. Since not all the properties required as inputs for the TRNSYS types were available, some assumptions were made. In particular, some data were taken from technical datasheets of devices similar to the ones of the experimental setup, while reference values found in literature were used in the other cases.

6.2.1 Photovoltaic-Thermal collectors

Unglazed fin-tube PV-T solar collector Type 563 from TESS additional library was chosen to simulate the three PV-T panels used in the experimental layout. This component is intended to model an unglazed solar collector which has the dual purpose of producing electrical power from embedded photovoltaic cells and providing heat to a fluid stream flowing through tubes bonded to an absorber plate located beneath the PV cells [35].
One single component with surface equal to the overall area of the three collectors was utilized. This decision was taken because there was no interest in studying the performances of every solar collector but just the overall effect of the series was evaluated.

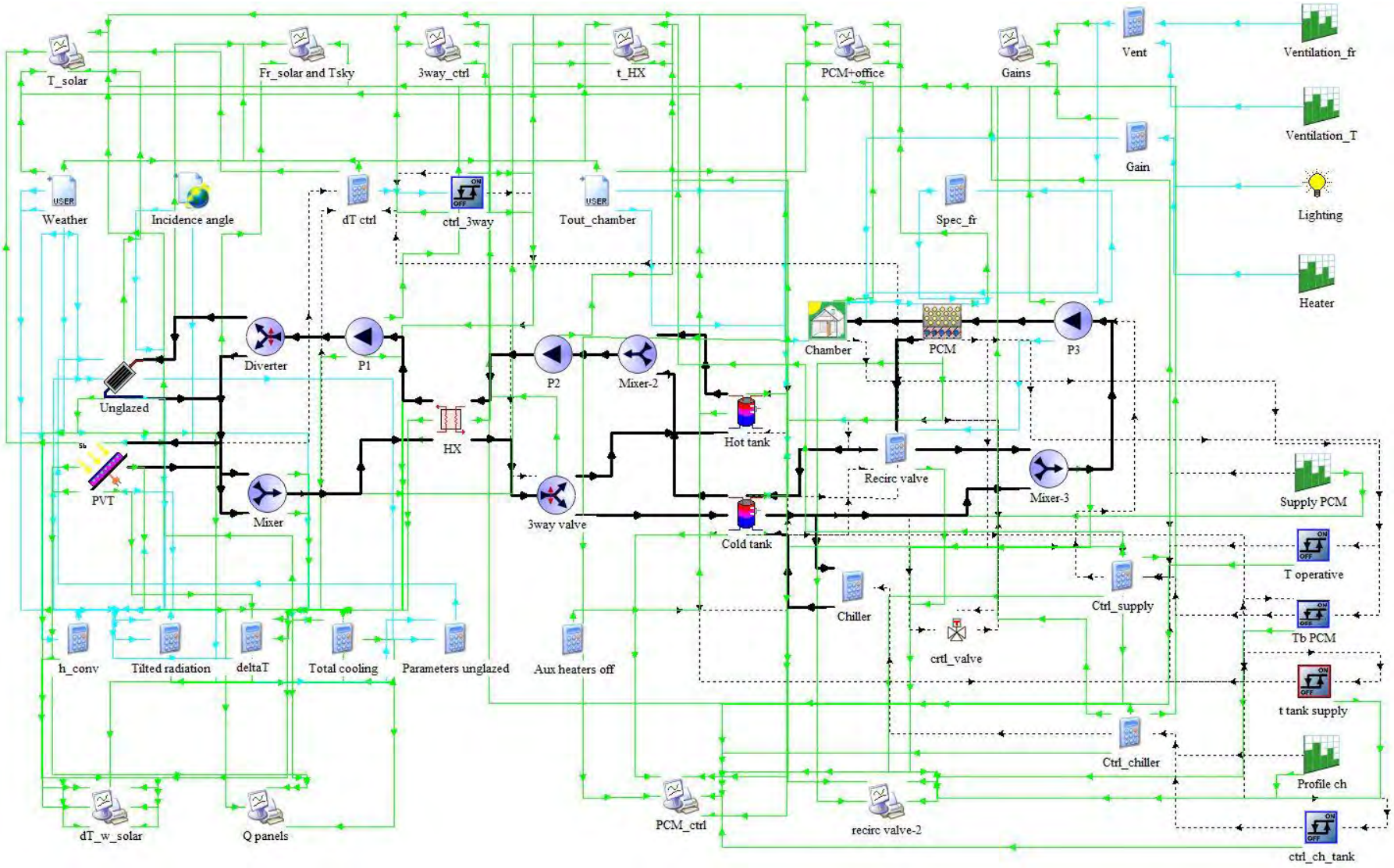

Figure 6.1 – Overview of TRNSYS simulation model

Since not all the necessary data were available from the technical datasheet, a typical water PV-T collector has been considered as reference for some of the missing characteristics [36]. Default values of Type 563 were used for the parameters which were not found in literature.

The most important properties of the PV-T collectors are listed in Table 12.1. Further details are reported in Appendix 12.1.1.

Table 6.1 – Properties of the PV-T component

Parameter	Value
Collector length [m]	1.315
Collector width [m]	2.988
Emissivity [ ]	0.89
Reflectance [ ]	0.15
PV efficiency at reference condition [ ]	0.1843
Liquid flow rate [l/h]	108
Liquid specific heat capacity [kJ/kg K]	3.35
Collector slope [°]	45
Collector azimuth [°]	0

The emissivity of the front surface was measured in a previous experiment performed on the same devices by means of a thermographic camera [22]. An average value of 0.89 was indicated in this study.

The default value of 0.15 was chosen for the reflectance.

The electrical efficiency was reported in the datasheet, referred to the standard conditions[20].

The heat carrier was assumed to be a mixture of water and ethylene glycol (40% of glycol mass fraction). A value of 3.35 kJ/kg K was found in literature as specific heat capacity of the water-glycol mixture [32].
A constant liquid flow rate of 108 l/h was implemented.

The top loss convection coefficient has been calculated iteratively in TRNSYS according to the following equation [37]:

$$h_{c,top} = 2.8 + 3 \cdot v_{wind} \qquad 0 < v_{wind} < 7\ m/s$$

6.2.2 Unglazed flat plate collector

The unglazed solar collector was modelled by *Type 559, Theoretical unglazed flat plate collector*. This component calculates itself the efficiency of the collector based on the geometry of the panel and its absorbance/emissivity [38]. The technical details of the collector are listed in Table 6.2.

Table 6.2 – Properties of the unglazed collector

Parameter	Value
Collector length [m]	2.0
Collector width [m]	1.2
Plate absorbance [ ]	0.95
Emissivity of the absorber plate [ ]	0.91
Fluid flow rate [l/h]	72
Liquid specific heat capacity [kJ/kg K]	3.35
Collector slope [°]	45
Collector azimuth [°]	0

[20] Reference solar radiation of 1000 W/m^2 and reference temperature of 25 °C.

As mentioned before, the unglazed collector used in the experiment was built of black polypropylene. The absorbance of polypropylene was found in literature to be between 0.94 and 0.95 [39]; hence, this parameter was set to 0.95.

The emissivity of the absorber plate was measured by means of a thermographic camera in a previous experiment involving the same unglazed collector considered in the present research [22]. A value of 0.91 was assessed in that occasion.

The fluid circulating through the pipes was a mixture of water and ethylene glycol, having the same properties already mentioned for the PV-T branch. A flow rate of 72 l/h was implemented.

The heat loss coefficient of back and edges and the collection efficiency factor of the unglazed collector were calculated at every time step by means of an equation block inserted in the TRNSYS model. The calculation approach for these parameters is shown in appendix 12.1.2.

6.2.3 Climatic chamber

Type 56, Multi-Zone Building was employed to simulate the climate chamber. This component models the thermal behavior of a building comprising multiple thermal zones.

The building model had floor dimensions of 5.4 x 4.2 m (surface area of 22.7 m^2) and a total height of 3 m, as it was for the experimental chamber. The internal space was constituted by two thermal zones, the first one representing the occupancy zone (2.5 m high) and the second one the space between the PCM suspended ceiling, whose characteristics are detailed in next paragraph, and the roof of the chamber (height of 0.5 m).
The layout of the simulated chamber is shown in Figure 6.2.

The walls and the roof were built of two steel sheets separated by 10 cm of mineral wood insulation. The same configuration was chosen for the slab, since no data about its structure were available.
A massless layer with surface area 18.75 m^2 was considered to simulate the PCM panels while the remaining part of the suspended ceiling was simulated by a 1.3 cm thick gypsum layer.
Further details on the building's envelope are presented in Annex 12.2.

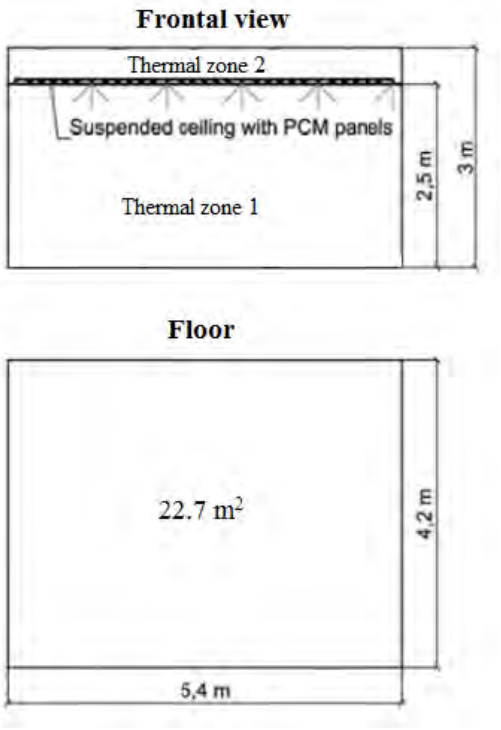

Figure 6.2 – Layout of the building model

Mechanical ventilation was considered operating from 7.30 a.m. to 6.00 p.m. with a constant flow rate of 0.2 m^3/h. Different temperatures were set for the two scenarios experimentally analysed, that are Case A and Case B.

For Case A the ventilation temperature was fixed to 30 °C from 7.30 a.m. to 9.00 a.m. and to 25.8 °C from 9.00 a.m. until 6.00 p.m. For Case B the temperature was set to 32 °C from 7.30 a.m. to 9.00 a.m. and to 27.8 °C from 9.00 a.m. until 6.00 p.m. The supplied air temperature and flow rate profiles implemented are shown in Table 6.3.

Table 6.3 – Supplied air temperature and flow rate for the considered case studies

Time interval	**CASE A**		**CASE B**	
	air temperature [°C]	air flow rate [m^3/s]	air temperature [°C]	air flow rate [m^3/s]
00.00 – 7.30	/	0	/	0
7.30 – 9.00	30	0.2	32	0.2
9.00 – 18.00	25.8	0.2	27.8	0.2
18.00 – 24.00	/	0	/	0

A heat gain of 600 W was given as input to the building model from 7.30 a.m. to 8.15 p.m. in order to simulate the use of the electrical heater.

A constant heat gain of 240 W was considered from 7.00 a.m. to 7.00 p.m. to simulate the lighting of the room. The internal heat gains in the simulation model were assumed to be 50% convective and 50% radiative gains.

6.2.4 PCM active ceiling

TRNSYS non-standard component *Type 313, Phase change materials in passive and active wall constructions* [40], was utilized to simulate the behaviour of the active ceiling included in the climatic chamber.

Due to limitations of the theoretical model implemented in the type, only one layer containing phase changing materials was allowed. Moreover, the presence of one other material was required underneath the PCM layer. For these reasons, the suspended ceiling was simulated as a double-layer structure constituted by a 5 mm thick

cardboard attached at the bottom of a 20 mm thick PCM-clayboard layer. The thermal and physical properties of the materials involved are listed in Table 6.4.

Table 6.4 – Thermal and physical properties of the PCM ceiling panels' components [7]

Material	PCM	Cardboard	Clayboard	PCM-Clayboard
Density [kg/m^3]	980	270	1300	1216.8
Melting range [°C]	21-25	-	-	-
Fusion temperature [°C]	23	-	-	-
Specific latent heat [kJ/kg]	110	-	-	-
Specific heat capacity [kJ/kgK]	-	2.1	1.0	-
Thermal conductivity [W/mK]	0.14	0.14	0.47	0.36

The thermal conductivity of the PCM-clayboard layer has been calculated as follows:

$$\lambda_{PCM-clay} = \lambda_{PCM} \cdot \varphi_{PCM} + \lambda_{clay} \cdot \varphi_{clay} \qquad \left[\frac{W}{mK}\right]$$

while the density of the composite material has been determined with the following equation:

$$\rho_{PCM-clay} = \rho_{PCM} \cdot x_{PCM} + \rho_{clay} \cdot x_{clay} \qquad \left[\frac{kg}{m^3}\right]$$

where φ and x are respectively the volume fraction and the weight fraction of the single material over the total volume and weight of the PCM-clay mixture.

An external file containing the value of the specific heat capacity of the PCM for different temperatures was linked to Type 313. As explained in paragraph 5.1.2, the present values were taken from [7] and are shown in Table 6.5. Since no data were available for the discharge process, the mentioned file was used for both the charge and discharge phases. Therefore, the hysteresis phenomenon was not taken into consideration.

Table 6.5 – Specific heat capacity of the PCM for different temperatures

T_{PCM} [°C]	<19	19	20	21	22	23	24	25	26	>26
c_p [J/kg]	1300	1300	1419	1892	2769	4686	2256	1360	1300	1300

The convection heat transfer coefficients for the ceiling's surface facing upwards (back side) and downwards (front side) were assumed constant with values of 7.7 W/m^{2}K and 5.88 W/m^{2}K, respectively [40].

The logical connections between the multi-zone building and the PCM wall component are illustrated in Figure 6.3.

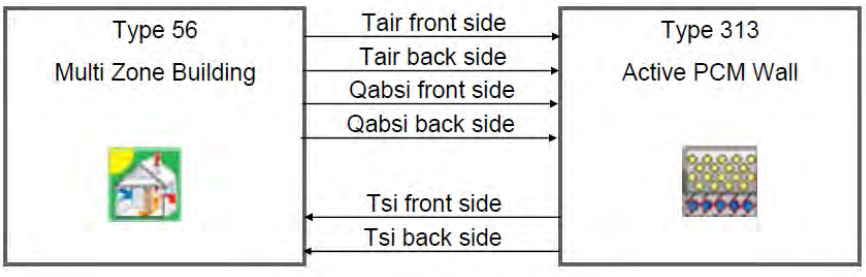

Figure 6.3 – Logical connections between the building (Type 56) and the PCM wall (Type 313)[21] *[40]*

[21] "Qabsi" is the heat flux flowing through the considered surface (incl. solar gains, radiative heat, internal radiative gains and wall gains, except longwave radiation exchange with other walls). "Tsi" is the surface temperature of the PCM ceiling.

6.2.5 Intermediate heat exchanger

Type 5b, Counter Flow Heat Exchanger was used to model the intermediate heat exchanger between the two tanks and the solar collectors.

The technical details of the heat exchanger are listed in Table 6.6.

Table 6.6 – Heat exchanger technical data

Parameter	Value
Number of plates	16
Heat exchange surface [m^2]	0.37
Heat transfer coefficient [W/K]	970.4[22]

The fluid circulating in both the source side (solar circuit) and the load side (intermediate loop) was a mixture of water and ethylene glycol (40% mass fraction).

6.2.6 Storage tanks

Storage Tank Fixed Inlets, Uniform Losses and Node Heights Type 60d was used to model the two storage tanks included in the experimental setup. This type models a stratified liquid storage tank allowing including multiple heat exchangers.

Both the tanks had a height of 1.47 m and contained 255 l of water. Two spiral heat exchangers were included in the CWT, both assumed made of copper (external diameter 18 mm, pipe thickness 1.5 mm) and with a surface area of 0.75 m^2. The HWT was provided with one heat exchanger with the same features.
The inlet and outlet of the stored water were located at the top and bottom of the tanks, respectively.

The specific heat loss coefficient was assumed to be uniform along the reservoirs' height and constant in time. A common value of 2.8 W/m^{2}K was found in literature for storage tanks in solar heating systems [41].

6.2.7 Hydraulic elements

The pumps involved in the system were modelled by *Type 3d, Single speed pump*, except for the one included in the chiller. The chiller was indeed represented by an equation block in which the supply water flow rate and temperature (set at 12 °C) were implemented.

The flow rate set for each pump is shown in Table 6.7

Table 6.7 – Pump flow rates

Subsystem	Flow rate [l/h]
Solar circuit	180
Intermediate circuit	190
Chiller circuit	150
Ceiling supply circuit	150

Type 11h Tee-piece was used to represent the juncture between the unglazed and the PV-T collectors' branches. The same component was used to model the intersection between the return water from the PCM ceiling and the water from the CWT.

[22] The heat transfer coefficient is referred to the following parameters, given in the heat exchanger technical datasheet:
- heat exchange rate: 7 kW
- hot fluid temperature range: 70 – 40 °C
- cold fluid temperature range: 35 – 60 °C

Type 11f Controlled Flow Diverter was employed to simulate the divergence of the water supplied to the solar collectors. This instance of the Type11 models a flow diverter in which a single inlet liquid stream is split into two liquid outlet streams, according to a user specified valve setting [38].
A constant control signal value of 0.6 was implemented for the supply of the solar collectors; in this way, 60% of the total flow rate was directed to the PV-T circuit while the remaining 40% was supplied to the unglazed flat plate collector.

The 3-way valve was modelled by Type 11f as well. The control signal was set to 1 when the temperature difference between the bottom[23] of the CWT and the return water from the solar collectors was above 3 °C, thus directing the entire flow rate towards the CWT. An input value of 0 was fixed for the opposite case, in such a way that all the water coming from the intermediate heat exchanger was supplied to the HWT.

Type 953 Controller for Tempering Valves from TESS additional libraries was used to describe the operation of the recirculation valve in the water supply system of the PCM ceiling. This component calculated at every time step the fraction of fluid exiting the PCM component which had to be sent to the CWT and the amount of fluid recirculated, in order to provide the set point temperature (t^*_{supply}).

6.2.8 General assumptions

In addition to the assumptions for the description of the components, some other hypothesis which is worthwhile mentioning were made:

- the heat losses (or gains) along the pipes of the circuit were not taken into consideration
- the environment surrounding the chamber was assumed to be homogeneous, so that the temperature measured by the sensor above the entrance was considered to be same in all the space around.

The model was simulated for one week for each of the case studies, with a simulation time step of 1 minute.

6.3 Inputs to the model

The data recorded by the weather station were given as input to the model, in order to compare the performances of the system under the same climatic conditions. Indeed, the cooling and heating performances of the solar collectors and therefore the temperatures of the tanks were influenced by the external weather conditions.
The weather input file contained the external air temperature, the wind velocity, the solar radiation and the sky temperature, the latter calculated with the theoretical approach described in Annex 12.1.3.

An input file simulating the conditions of the environment surrounding the chamber was implemented in the model. This text file contained the values measured by the temperature sensor located above the door of the room.

Both the weather data and the temperature outside the room were averaged over a 1 minute time step, which corresponds to the simulation time step.

6.4 Results

In the present paragraph the results of the simulation analysis are presented and discussed. A comparison with the results obtained from the experimental study is provided, in order to verify if the TRNSYS model reproduces the behaviour of the experimental setup with sufficient accuracy.

[23] The temperature at the bottom of the CWT was used instead of the one in the middle (as it was in the experiment) because the latter was not an output of the tank type.

As for paragraph 5.3, this section has been divided in two parts: the first one concerns the behaviour of the room and the PCM suspended ceiling while the other one focuses on the performances of the night sky radiant cooling process.

6.4.1 Climate chamber and PCM ceiling

Figure 6.4 and Figure 6.5 illustrate the profile of the operative temperature and the air temperature inside the chamber for Case A and B, respectively. A 24-hour interval, from 7.30 a.m. to 7.30 a.m. of the following day, is considered.

As regards to Case A, the simulation model shows good accuracy in the description of the thermal situation inside the room. The highest discrepancy between the experiment and the model occurs in the time range between 7.30 and 9.00 a.m. During this limited period of time the indoor environment was subject to a fast variation of the thermal conditions, since the air temperature increased from about 21.5 °C to 26 °C. Moreover, the electrical heater used in the experiment was blowing air with a temperature of about 50 °C, much higher than the air temperature of the room. Therefore, the assumption of homogeneous thermal environment, which is made in TRNSYS building model, cannot be considered valid. This explains the significant difference between the temperatures observed in the simulation and the ones experimentally evaluated.
After the water supply system of the suspended ceiling was turned on, the air and operative temperatures of the simulation decreased approximately with the same rate of the measured ones, reaching values of about 21 °C at the end of the night (considered at 7.00 a.m.).

In Case B, the gap between the simulation and the experiment is more pronounced. However, this is mainly due to the difficulties encountered in reaching and keeping the indoor air temperature constant at 28 °C. Indeed, it can be noticed that the air and operative temperatures which were measured were subject to unintentional but considerable fluctuations during daytime.
The same considerations made for Case A are valid for the time intervals between 7.30 a.m. and 9.00 a.m. and after 6.00 p.m.

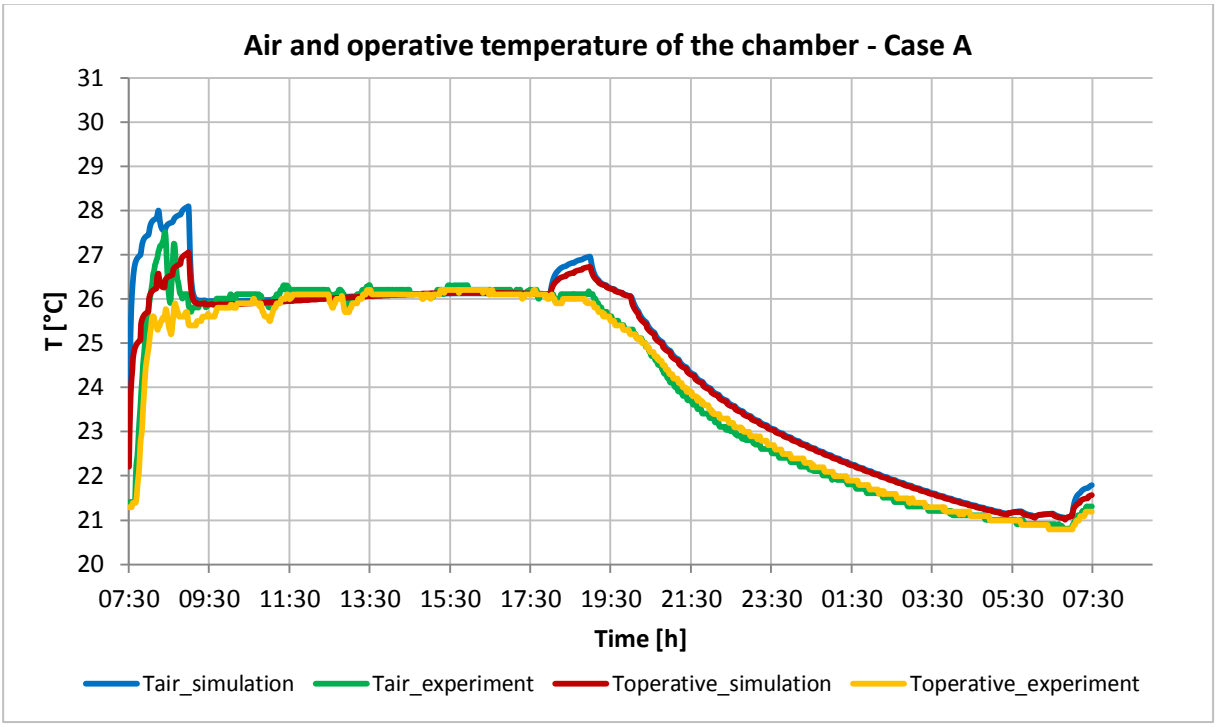

Figure 6.4 – Chamber operative and air temperature for Case A

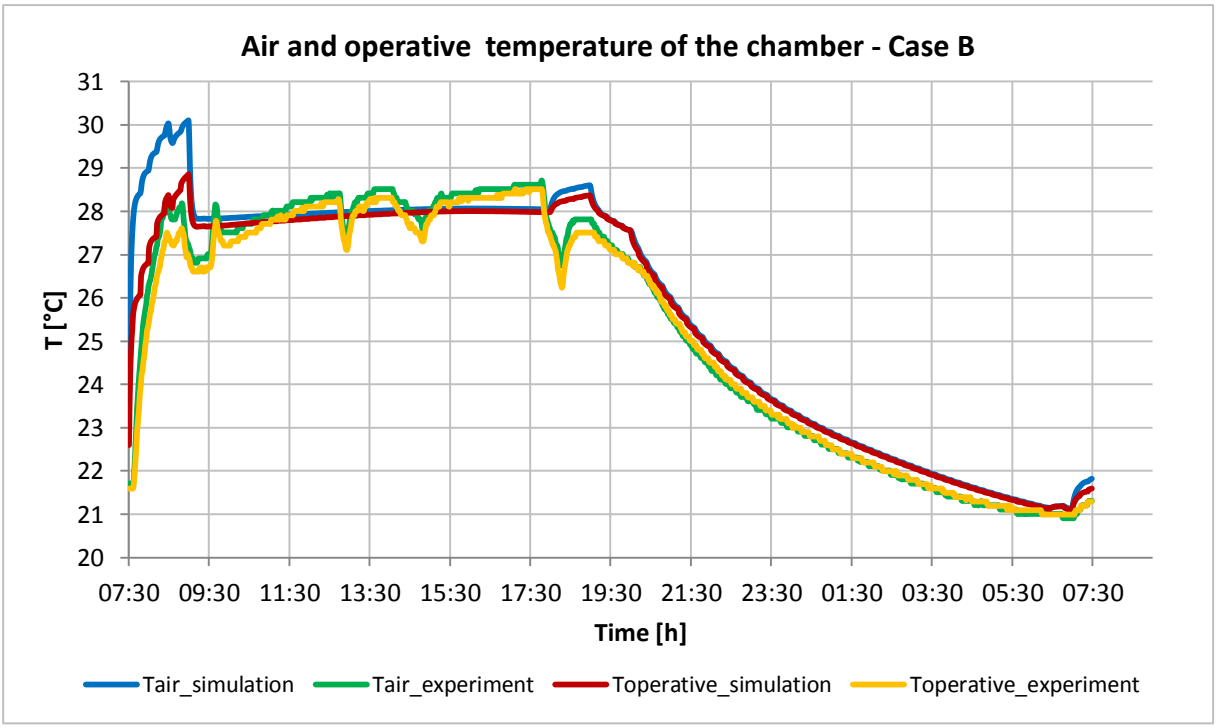

Figure 6.5 – Chamber operative and air temperature for Case B

The comparison between the experimental and simulated bottom and top surface temperatures of the ceiling panels is provided in Figure 6.6 and Figure 6.7.

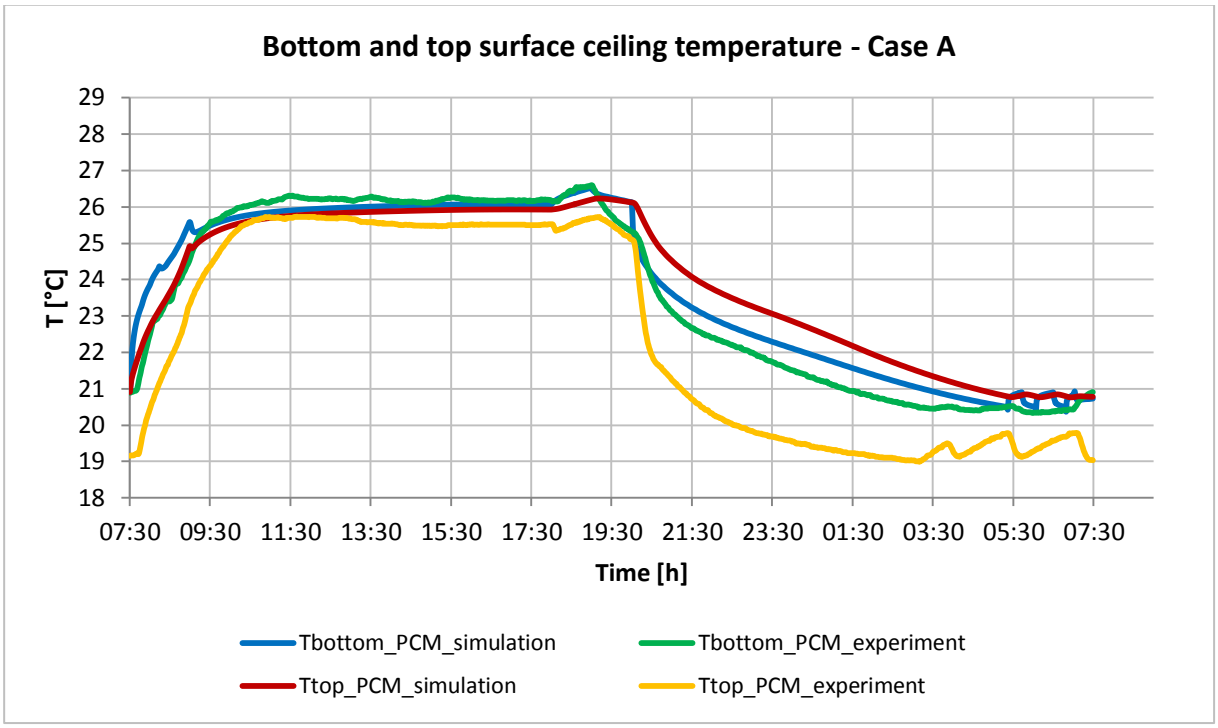

Figure 6.6 – Ceiling panels top and bottom temperature for Case A

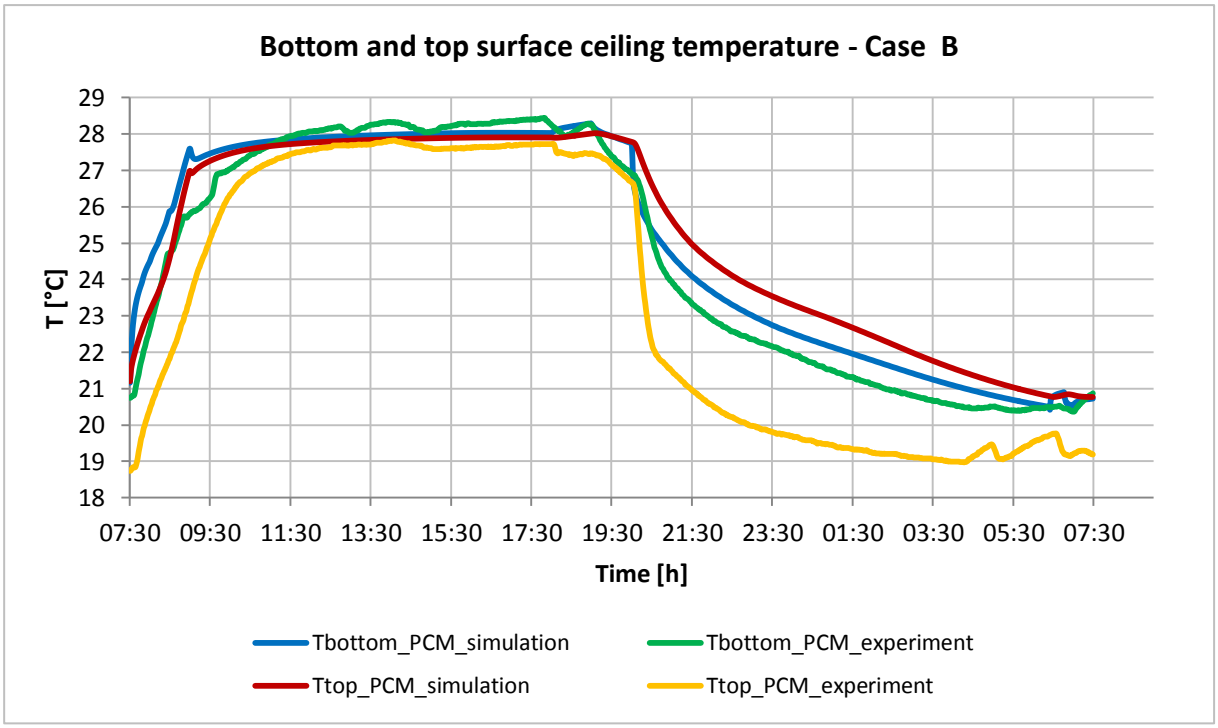

Figure 6.7 – Ceiling panels top and bottom temperature for Case B

For both cases A and B the simulation model provides a satisfactory description of the bottom surface temperature of the PCM ceiling. Indeed, taking no notice of period between 7.30 a.m. and 9.00 a.m., the difference between the measured and the simulated temperature value is always below 1 °C for both case studies. The highest gap is observed right after the water supply system started operating, that is at 8.00 p.m. The noticeable difference can be explained by the different temperature of the water circulating in the ceiling's

internal loop in this phase. Indeed, the recirculation valve needed some time to stabilize the temperature at the desired value of 18 °C, therefore this parameter oscillated between 16.5 and 18 °C in the time range between 8.00 p.m. and 8.45 p.m. This phenomenon was not contemplated in TRNSYS.
During the operation of the supply pump the bottom surface temperature dropped approximately with the same trend in the simulation and in the real case.

With regards to the top surface temperature, the divergence between the output of the model and the measured one is remarkable in both cases. This is probably due to how the structure of the PCM panels was modelled in TRNSYS. The measured top surface temperature of the panels was subject to a fast drop when water started circulating through the internal loop, because the pipes were located in the upper part of the ceiling. However, there was no possibility to specify the position of the embedded pipes in the employed PCM type and therefore the local cooling effect of the water was not correctly simulated.

Finally, the fluctuations of the surface temperatures of the panels which can be noticed after 3.00 a.m. were due to the turning on and off of the supply pump.

As a consequence of the difference of the average bottom temperature of the PCM panels, the first turning off of the water supply system in the model occurred at a different time compared to the one of the experiment. The comparison between the operational times of the ceiling's water supply system is shown in Figure 6.8 and Figure 6.9 for Case study A and B, respectively.

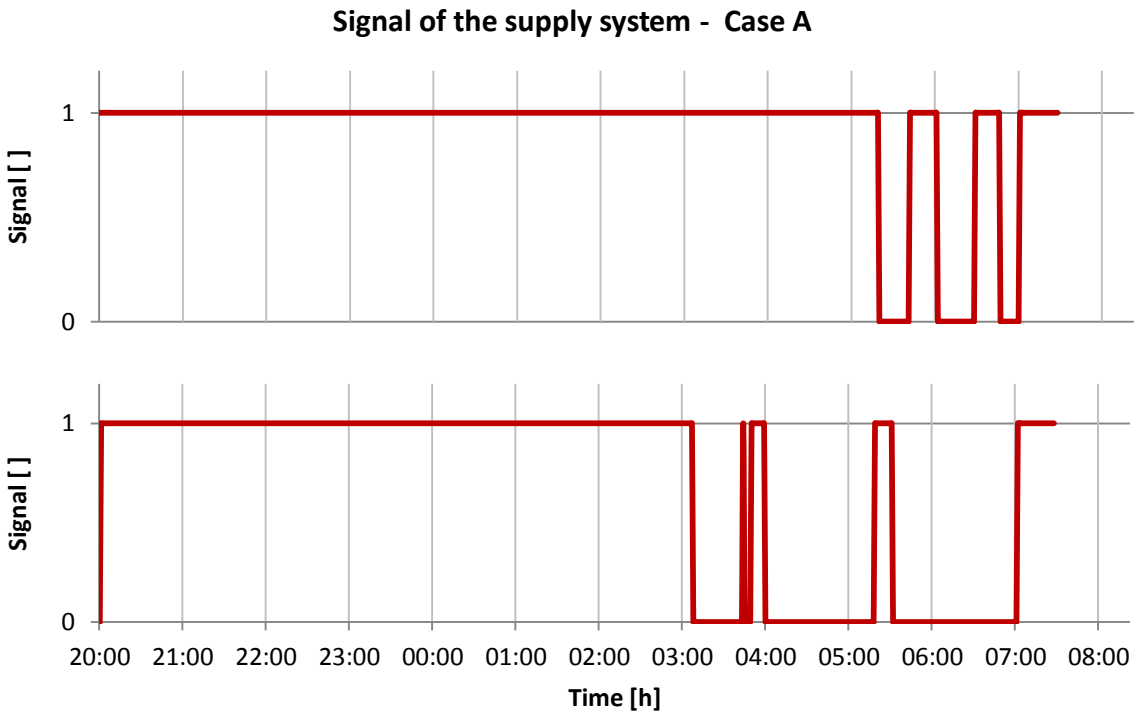

Figure 6.8 – Input signal to the pump of the water supply system in simulation model (top) and experiment (bottom) for Case A (1=ON, 0=OFF)

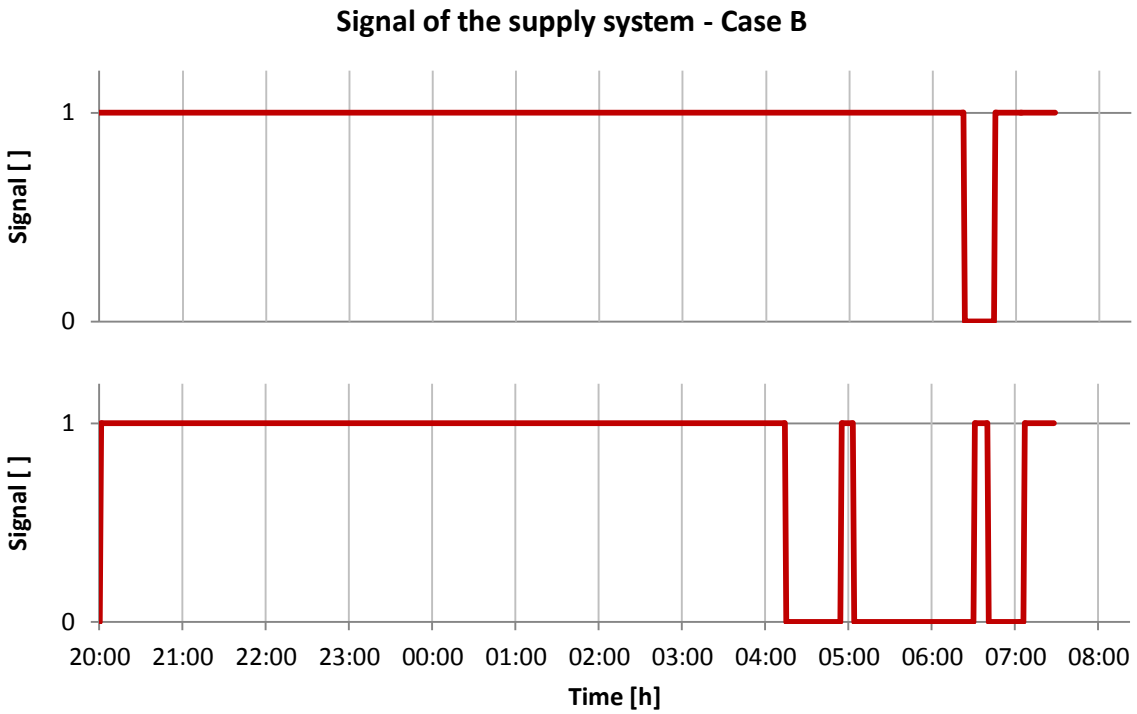

Figure 6.9 – Input signal to the pump of the water supply system in simulation model (top) and experiment (bottom) for Case B (1=ON, 0=OFF)

As regards to Case A, in the model the first turning off of the pump occurred at about 5.20 a.m., approximately 2 hours later than the time it was happening in the experiment. This difference implies higher electrical energy consumption for the simulation. The dissimilarity in the input signal profile after the first switching off is due to the different values assumed by the bottom surface temperature: a slight variation of this parameter in this phase leads to a change in the pump operational state (from ON to OFF or vice versa) since the dead band implemented for this control was limited.

In case B the same time gap between the experiment and the simulation can be observed: the pump switched off at about 4.20 a.m. in the first case while it was continuously operating until 6.30 a.m. in the simulation.

Despite of the mentioned differences in the operational mode of the water supply system, the chiller has never been employed, neither in the experiment nor in the simulation. Indeed, the water temperature in the bottom part of the CWT was always lower than 17 °C, set point value for opening the valve in the chiller hydraulic supply branch. This means that the cooling load provided to the CWT by nighttime natural cooling was always enough to completely discharge the PCM contained in the suspended ceiling.

6.4.2 Night sky radiant cooling

In this section the performances of the solar collectors during nighttime are investigated. The results obtained from the simulation model are illustrated together with the ones from the experimental study in order to provide a comparison between them. As for the experimental analysis carried out in paragraph 5.3.2, the night between 7th and 8th and the one across 10th and 11th of March were selected as representative cases and the related results are presented for the time interval between 10.00 p.m. and 6.00 a.m.

The useful specific cooling power supplied to the water/glycol mixture of the solar circuit is presented in Figure 6.10 and Figure 6.11.

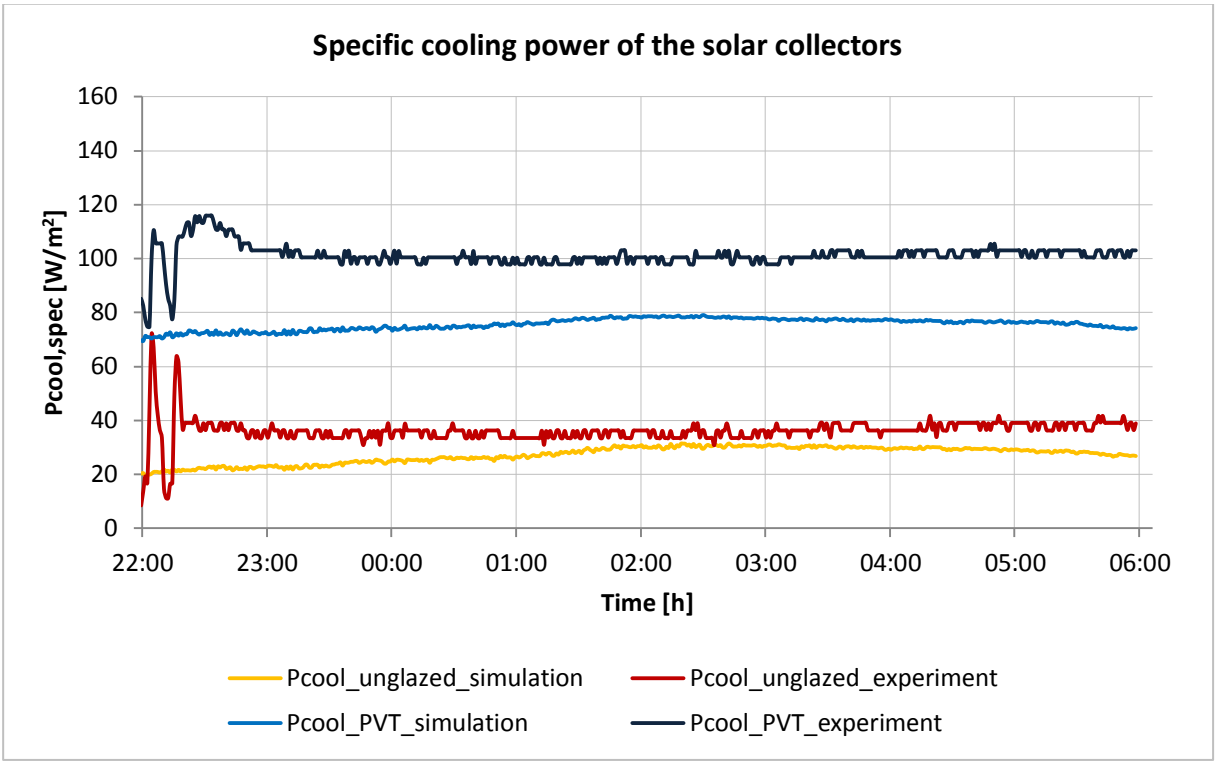

Figure 6.10 – Specific cooling power provided by the collectors in the night between 7th and 8th of March

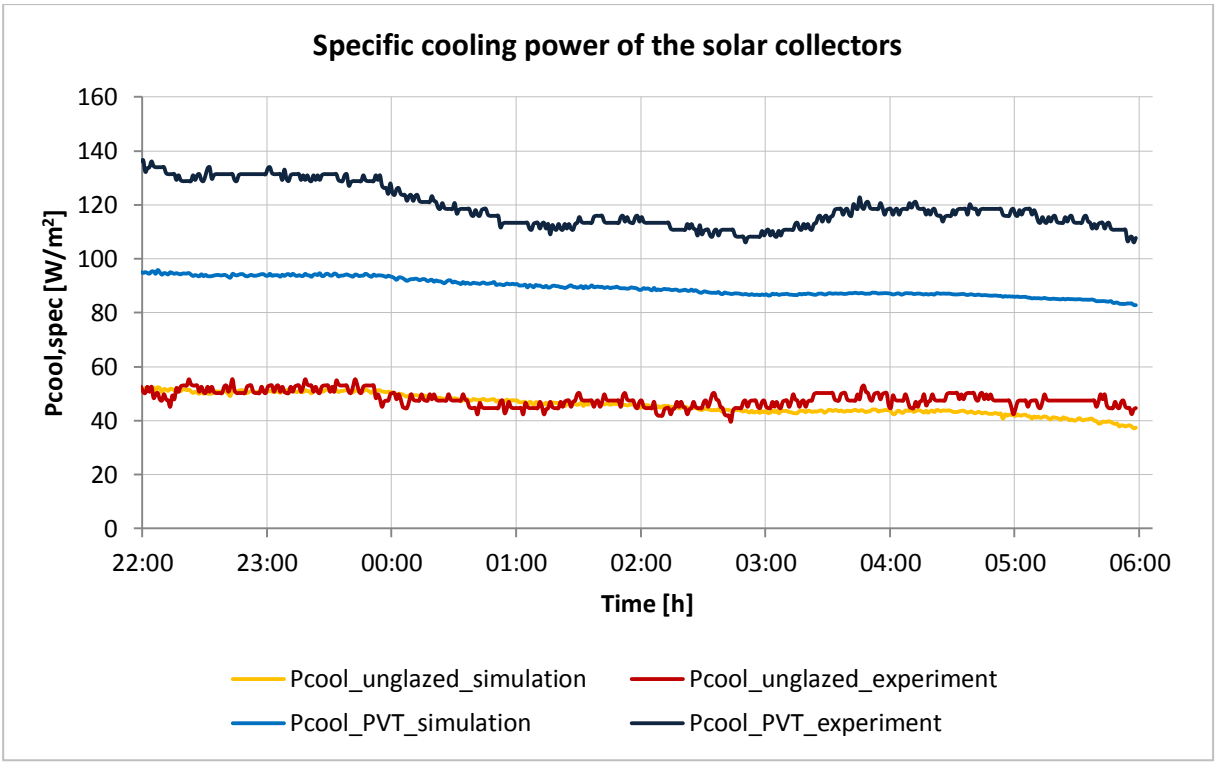

Figure 6.11 – Specific cooling power provided by the collectors in the night between 10th and 11th of March

It can be observed that for both the considered nights and for both the types of collector the simulation model tends to underestimate the cooling power produced.

As regards to the unglazed collector, omitting the time period from 10.00 p.m. to 11.00 p.m.[24], a gap ranging from 5 W/m^2 to 12 W/m^2 can be noticed between the simulation and the experimental measurements for the first considered night. The difference is significant since in relative terms it ranges from 15% to 35% of the experimental cooling power.
The accuracy of the model is significantly higher in the second night illustrated: in this case the difference with the experimental cooling load is always below 10 W/m^2, with a maximum relative gap of approximately 16%. For the present night the cooling power assessed through the simulation is slightly overestimated for some limited time periods (from 0.00 a.m. to 1.00 a.m., for example), respect to the experimental one.

The output cooling load of the PV-T collectors is underestimated by the model for both the two nights. The divergence between the experimental results and the ones from TRNSYS model ranges from 20 to 30 W/m^2 for the first night and between 20 and 40 W/m^2 in the second one. In relative terms, the underestimation of TRNSYS model is between 20% and 30% in both cases.

The representation of the nighttime cooling process given by the theoretical model is not totally satisfying since the difference respect to the experimental evaluation is not negligible, neither for the unglazed collector nor for the PV-T panels.

One reason for the observed inaccuracy could be attributed to the weather file given as input in TRNSYS and primarily to the effective sky temperature. Indeed, there was no possibility of measuring the present parameter and therefore the theoretical approach described in Appendix 12.1.3 was employed for the calculation. However, there was a considerable level of uncertainty related to the cloud cover ratio which was a required input for the calculation method, since hourly forecast values were considered. The cloud cover may have been overrated and the radiative cooling component could have been consequently underestimated.

Another factor which could explain the significant dissimilarity between the simulation and the experimental evaluated cooling power is the way the solar collectors were modelled in TRNSYS. As concerns the unglazed collector type, just few details were required as input and therefore the description was not scrupulous. On the other hand, a lot of parameters had to be specified for the PV-T component but just a few of them were available from the technical datasheet. Hence, many assumptions needed to be made, such as for the characteristics of the absorber plate and of the substrate and bond materials.

Finally, the output cooling power is influenced by the temperature of the water entering the two branches of the solar circuit, which for the most of the night-time was lower in the model than the real one, as illustrated in Figure 6.12 and Figure 6.13. Indeed, a reduction of the fluid inlet temperature leads to a lower surface temperature of the collectors and therefore to a lower temperature difference between the latter and the air temperature. As a consequence, the convective heat losses are reduced. The amount of heat exchanged through the radiative process drops as well since the temperature difference between the top surface of the collectors and the sky decreases.
The value of the inlet temperature to the solar collectors depends on many factors, such as the efficiency of the intermediate heat exchanger and the heat gains affecting the water while circulating through the pipes and inside the storage tanks. Therefore, some of the assumptions made in the TRNSYS model (such as the one of neglecting the pipes heat losses) could lead to a significant divergence respect to what happens in the real system.

[24] From 10.00 p.m. to 11.30 p.m. of the night between 7th and 8th of March the useful cooling power was subject to noticeable fluctuation due to the instability caused by the switch from the heating mode to the cooling operation.

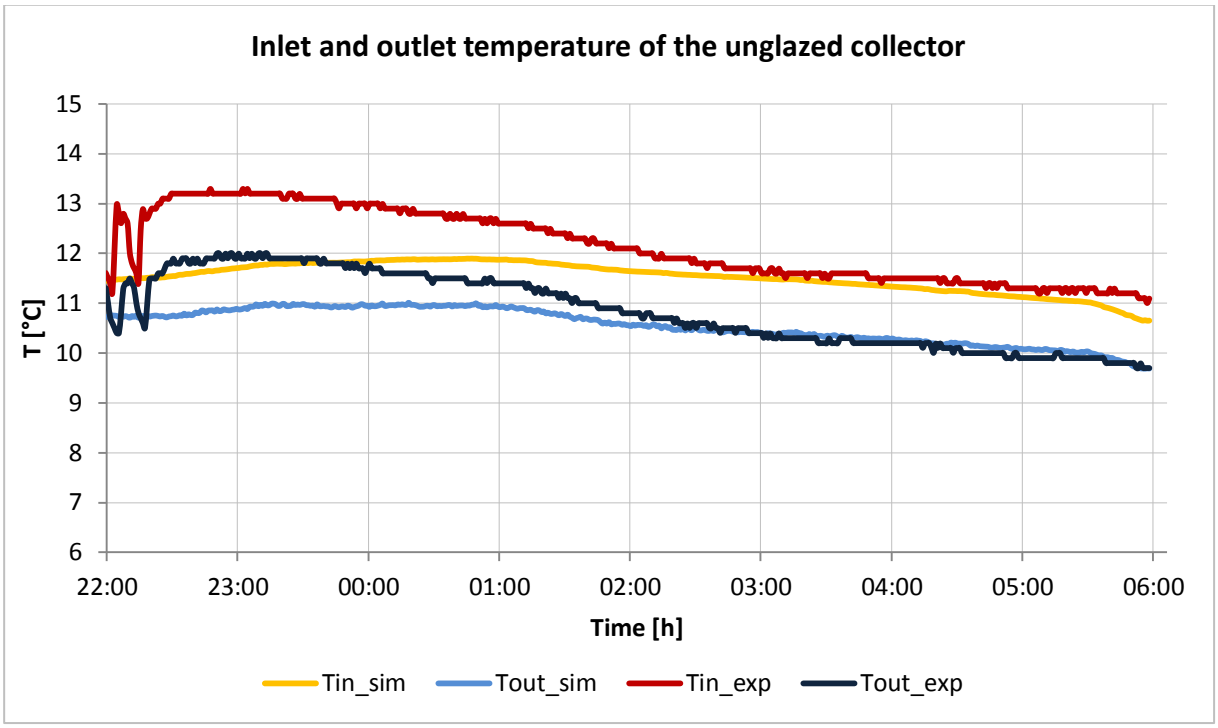

Figure 6.12 – Fluid Inlet and outlet temperature of the unglazed collector

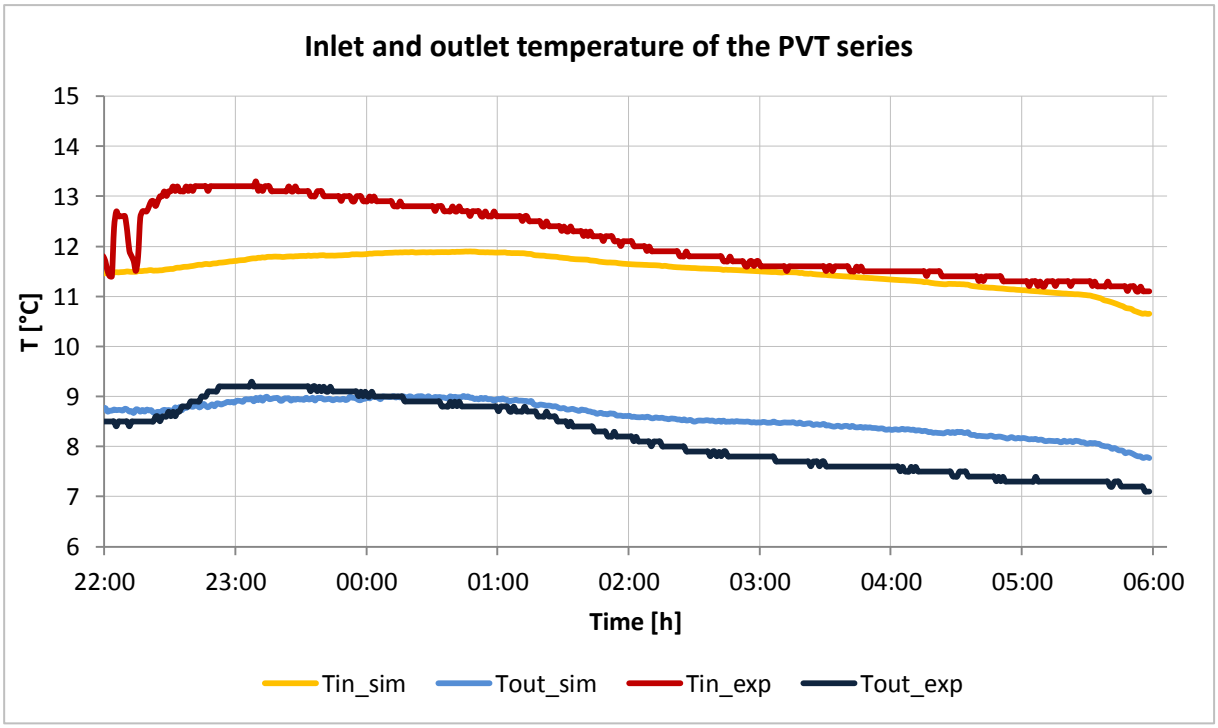

Figure 6.13 – Fluid Inlet and outlet temperature of the PV-T series

Due to the explained reasons, the overall cooling power provided by the solar collectors calculated in the model was lower than the one evaluated in the experiment. The average underestimation of the model was around the 25% of the measured power for the first night and about 20% for the second one, as can be noticed in Figure 6.14 and Figure 6.15.

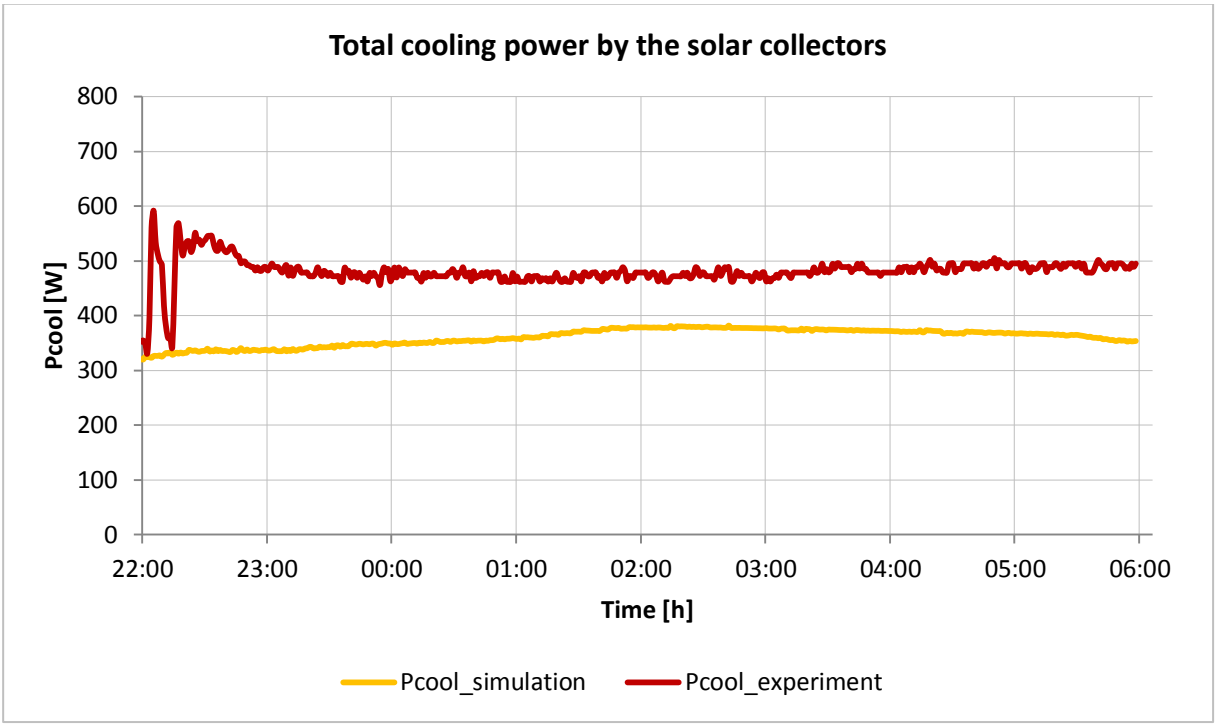

Figure 6.14 – Total cooling power by the collectors in the night between 7th and 8th of March

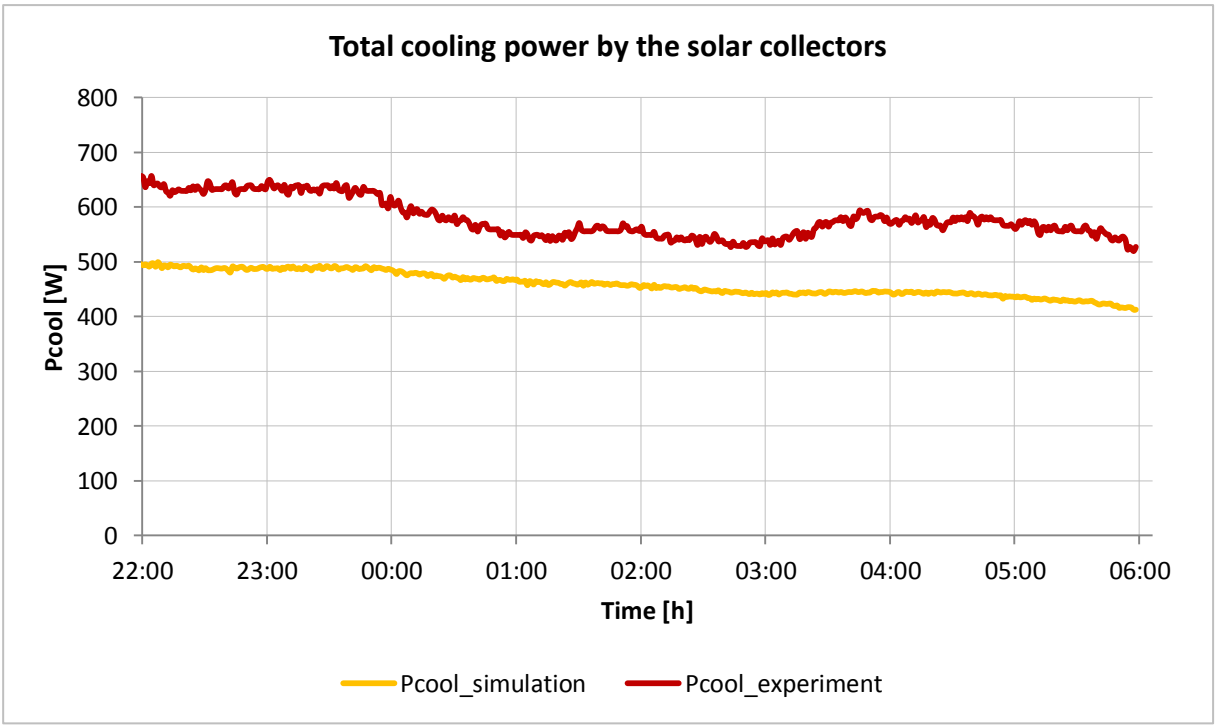

Figure 6.15 – Total cooling power by the collectors in the night between 10th and 11th of March

In order to provide a more complete comparison between the simulation model and the experimental results, the average specific cooling power of the solar collectors is shown for 6 consecutive nights, from 10.00 p.m. to 6.00 a.m. Figure 6.16 and Figure 6.17 illustrate the average specific cooling power produced by the unglazed collector and by the PV-T panels, respectively.

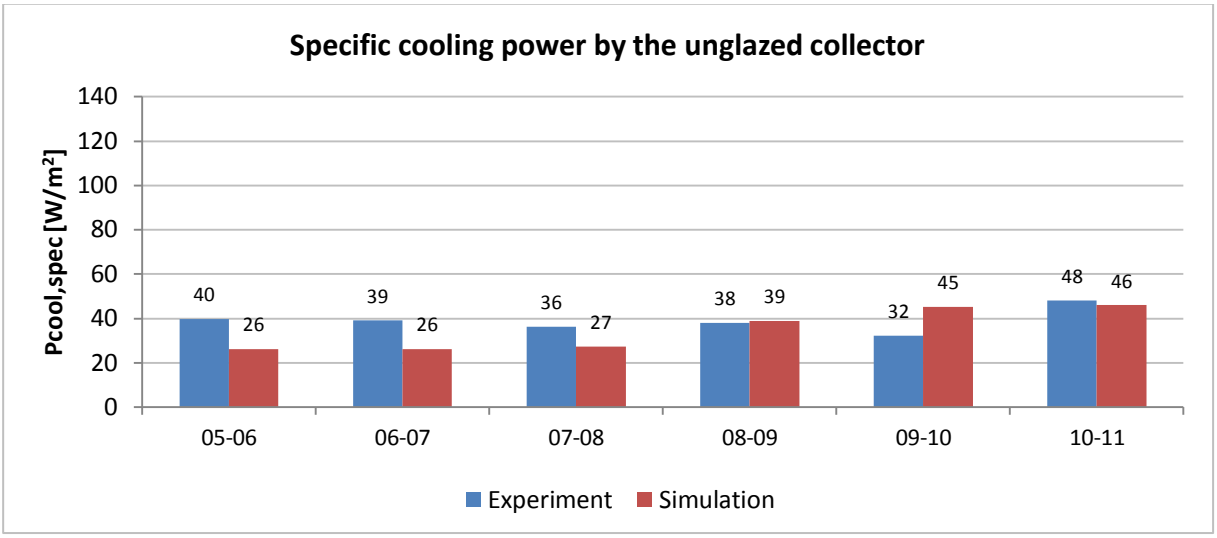

Figure 6.16 – Average nocturnal specific cooling power provided by the unglazed collector

As regards to the unglazed collector, the gap between the simulation and the experimental study varies between 35% of the experimentally evaluated cooling power for the night between 5th and 6th of March and 3% for the night across 8th and 9th of March, which was the best represented.

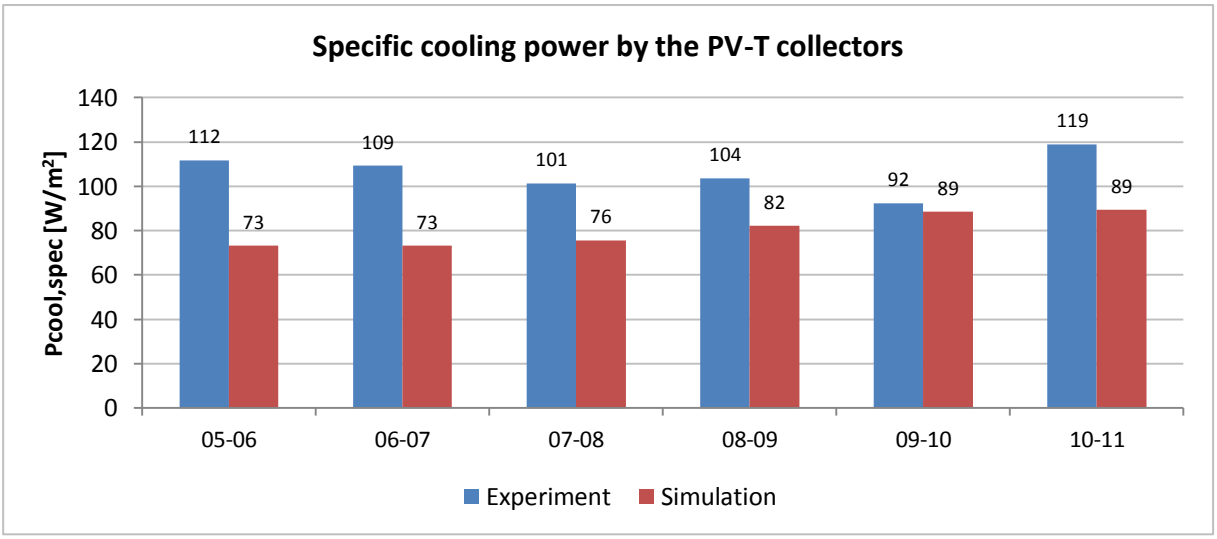

Figure 6.17 – Average nocturnal specific cooling power provided by the PV-T collectors

As concerns the PV-T series, the specific cooling output assessed through the simulation study was 65% of the experimental one for the night between 5th and 6th, while the difference between the two approaches was lower than 4% for the night across 9th and 10th of March.

The average cooling power provided by the night sky radiant cooling process is shown in Figure 6.18.

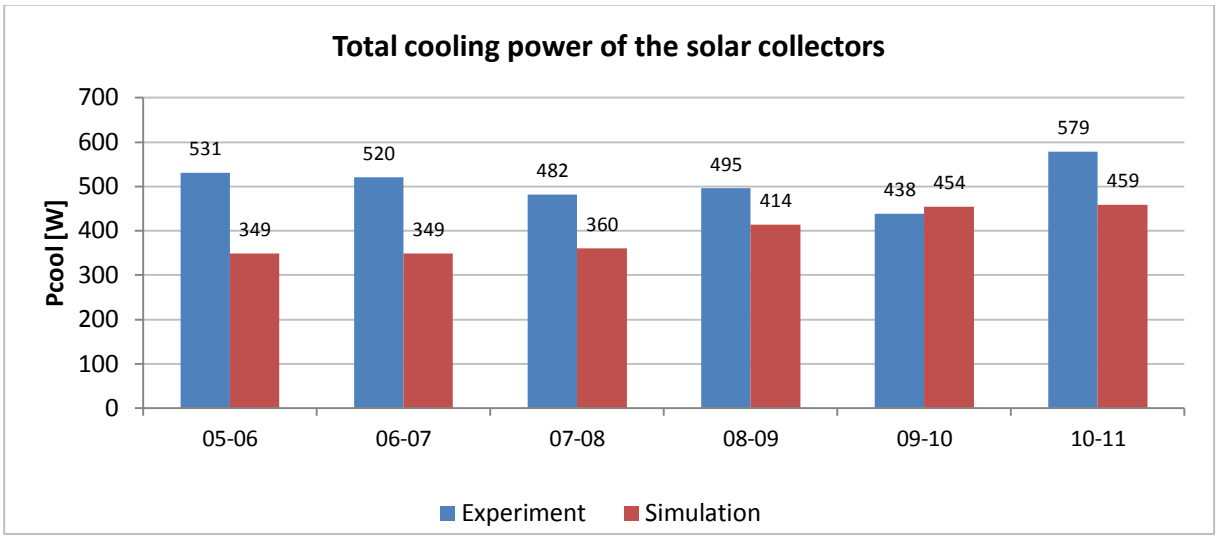

Figure 6.18 – Average nocturnal cooling output provided by the solar collectors

The inaccuracy of the theoretical model in terms of overall cooling power provided by the solar circuit ranges from less than 4% for the night of 9th of March to 34% for the night of 5th of March.

The noticeable variation of the accuracy of the simulation model along the 6 nights presented is partially due to the divergence in the operation of the 3-way valve, which affects the water temperature at the inlet of the solar circuit and therefore both the convective and the radiative components of the heat losses, as previously explained. Indeed, the inlet water temperature observed in the model was lower than the experimental one for the nights of 5th, 6th and 7th of March while the two values were close to each other for the other nights.

Finally, it is worthwhile mentioning that for the parametric study the cooling power per unit are produced by the unglazed collector was noticeably lower than the one provided by the PV-T, thus confirming the result obtained from the experimental analysis (Figure 6.19).

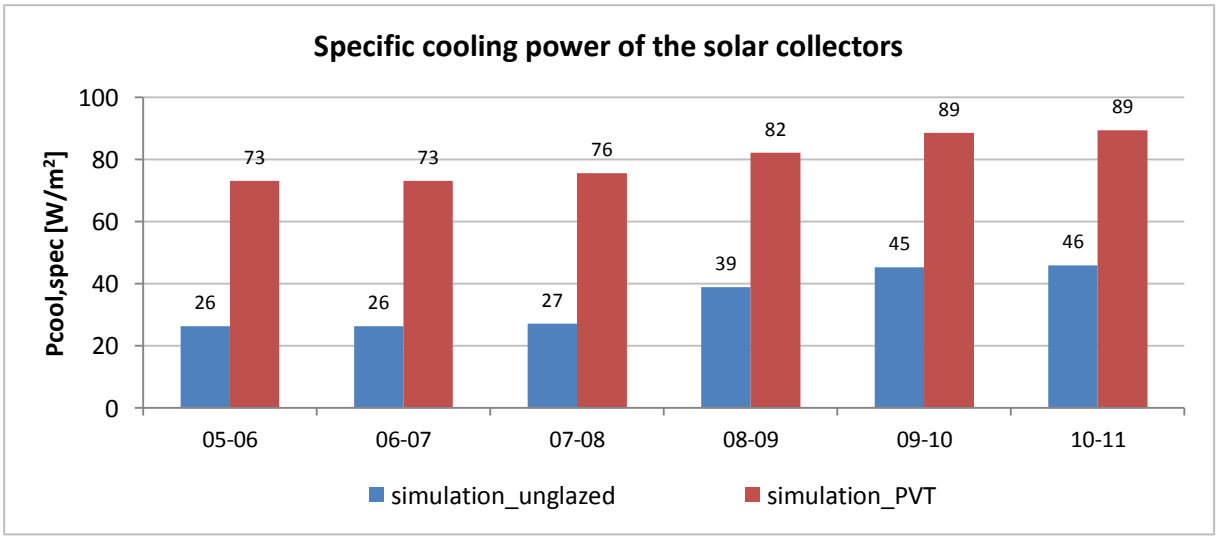

Figure 6.19 – Comparison between the specific cooling power provided by the two types of collector

The cooling power per unit of surface area produced by the unglazed collector varies from 37% to 52% of the output of the PV-T panels.

6.5 Comments and conclusions

For both case studies A and B the simulation model shows satisfactory accuracy in describing the thermal conditions existing inside the climate chamber. Indeed, the air temperature and operative temperatures of the room resulting from the model have the same trend of the measured ones. However, it has to be remarked that TRNSYS represents the indoor volume of the building type as a homogeneous air node, while the non-uniformity of the air temperature observed at different heights from the floor is not entirely negligible.

The representation of the ceiling panels' performance is only partially satisfying. The model shows sufficient accuracy in representing the thermal situation of the ceiling's surface facing the occupancy zone, since the difference between the average measured and the simulated surface temperature is always below 1 °C for both the case studies. However, not sufficient precision is exhibited in the representation of the thermal conditions of the upper part of the PCM panels. This is due to the way the active ceiling was modelled.
Finally, some differences can be noticed regarding the operation of the water supply pump: generally the time required by the model to completely discharge the PCM is longer than the one experimentally verified. This is a direct consequence of the gap between the experimental and the simulated bottom surface temperature of the active ceiling.

The simulation demonstrated that for the selected time the system was able to provide the necessary cooling load to discharge the phase change material by the beginning of the occupancy period. The temperature of the water at the middle of the CWT was always below 17 °C; therefore the chiller was never used. However, as it was pointed out for the experimental analysis, the system should be tested under less favourable climatic conditions, such as during summer time, when the natural cooling availability of the external environment is lower and the cooling demand is substantial.

As concerns to the night sky radiant cooling process, the accuracy of the model shows a considerable variability during the 6-nights-time period considered. For the unglazed collector, the gap between the simulation and the experimental study varies between 3% and 35% of the experimentally evaluated cooling power. The same discrepancy between the simulation and the experimental approaches occurs for the PV-T panels, being between 4% and 30%. The inaccuracy of the simulation model in terms of overall cooling power provided by the solar circuit, ranges from less than 4% to 34% of the experimental value.
The low fidelity showed for some of the considered nights could be explained by many factors, including the inaccuracy of the weather data given as input (especially the cloud cover factor) and the lack of information required for the detailed description of the TRNSYS components.
Finally, it has to be pointed out that a longer period should be considered in order to provide a more complete comparison between the experimental results and the ones obtained from the simulation model.

The average cooling power produced by the nighttime cooling process varies between 350 W and 460 W. As for the experimental study, the PV-T technology showed a good potential, providing a cooling power between 70 and 90 W/m^2. Significantly lower performances were exhibited by the unglazed flat plate collector, whose specific cooling output was between 26 and 46 W/m^2.

7 Simulation study

In this section the simulation model developed in TRNSYS is used to assess the performances of the system previously described, used to provide space cooling to a 2-persons office room in a multi-storey building.

The behaviour of the system is investigated under the reference summer climates of Copenhagen (56N), Milan (45N) and Athens (38N) [42]. The summer period from the 1st to the 17th of July was selected for the purpose for all the three simulations. The first week (from 1st to 7th of July) was taken as initialization period.

7.1 Description of the model

The simulation model employed for the present study is analogous to the one described in chapter 6, except for some modifications which were carried out to improve the performances of the system, adapting it to the summer weather conditions. Furthermore, the internal gains and the characteristics of the environment surrounding the room were modified in order to simulate the circumstances existing for a real office room.

Figure 7.1 shows the overall structure of the TRNSYS simulation model.

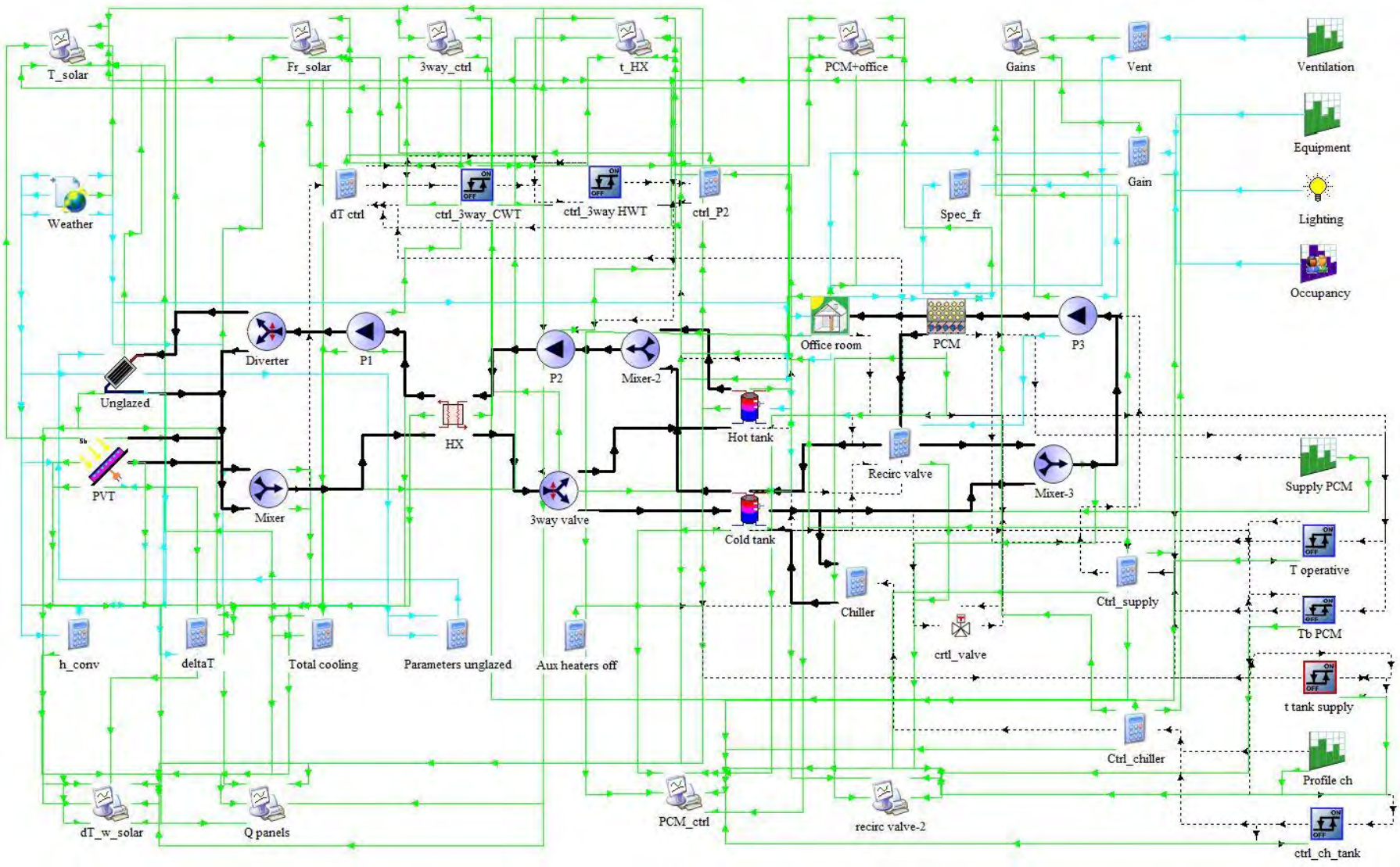

Figure 7.1 – Overview of TRNSYS simulation model

7.1.1 Office loads and structures

The modelled room comprises of two thermal zones, the first one simulating the occupancy zone and the other one representing the space between the suspended ceiling and the actual ceiling of the room. The same dimensions of the building type used in chapter 6 were implemented, as illustrated in Figure 7.2.

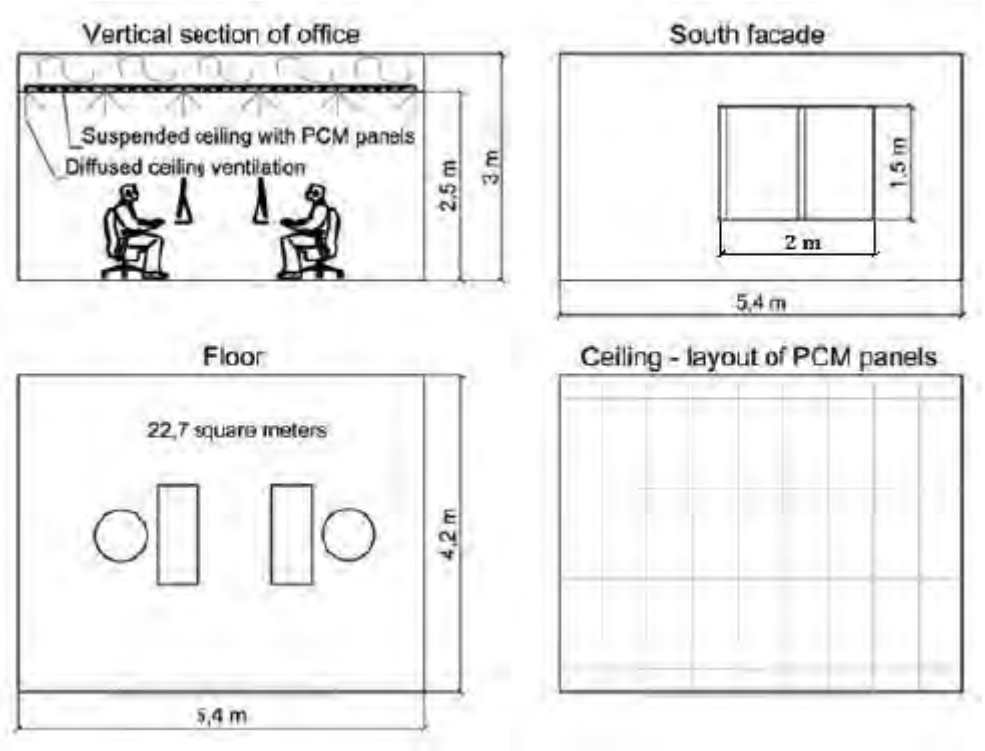

Figure 7.2 – Layout of the office room [7]

As can be noticed, a window with an overall surface are of 3 m^2 was added to façade facing south, being approximately 15% of the floor area (20% of the related façade). The size of the glazed element was chosen accordingly to the Italian praxis to guarantee sufficient lighting to the indoor space, which suggests a total glazed area equal to 1/8 (12.5%) of the floor area [43].

The requirements of the Italian standards for a new office building situated in Milan were taken as reference for selecting the structure of the window [43]. A window built of a double glass layer with Argon gap in between, having a U-value of 1.4 W/m^2K was considered, which fulfils the mentioned requirement for Milan's climate (maximum U-value of 1.77 W/m^2K).
The window was included in the wall facing south in order to consider the most critical case in terms of amount of solar gain absorbed by the room. For the same reason no shading devices were considered.

As regards to the envelope structure of the room, the south façade was mainly constituted by two layers of high density hollow bricks and an in-between insulation layer made of mineral wool with thickness of 10 cm. The present structure has been chosen in order to fulfill the U-value requirement for new conventional buildings in the intermediate climate of Milan, which fixes a maximum value of 0.33 W/m^2K [43].
The slab, the ceiling and the internal walls were built of two layers of plasterboard separated by an 8 cm thick bricks layer. Further details on the envelope's structure of the building are reported in Table 7.1 and Appendix 12.3.

Table 7.1 – Building envelope properties

Type of wall	layer	thickness [cm]	λ [W/mK]	heat capacity [kJ/kgK]	U-value [W/m^{2}K]
External wall	plasterboard	1	0.16	0.84	0.3
	bricks	6	0.4	1	
	mineral wool	10	0.04	0.8	
	bricks	6	0.4	1	
	plasterboard	2	0.16	0.84	
Internal wall	plasterboard	1	0.16	0.84	4.92
	bricks	8	0.4	1	
	plasterboard	1	0.16	0.84	

The suspended ceiling (Figure 7.3) was simulated by means of a massless layer, connected to the PCM type as explained in paragraph 6.2.4.

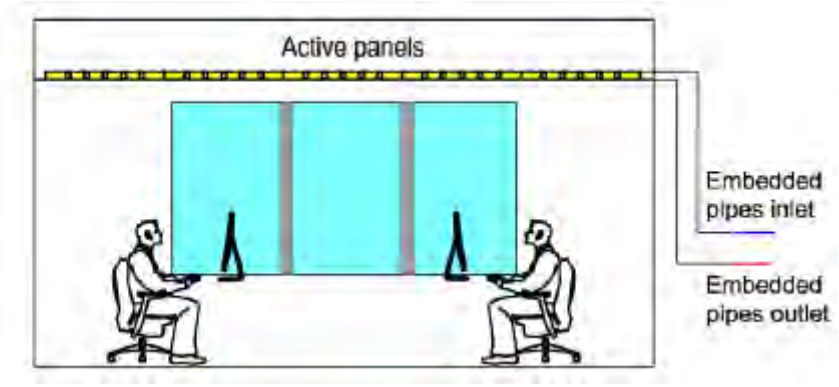

Figure 7.3 – Layout of the active ceiling loop [7]

The internal heat loads comprised of 2 occupants, lighting and equipment (Table 7.2). The loads were assumed to be 100% present during the daily occupancy hours (from 9 a.m. to 5 p.m.).

Table 7.2 – Internal heat gains [7]

Type of internal gain	Number	Heat gain per unit [W]	Overall heat gain [W]
Occupants	2	75	150
PCs	2	45	90
Monitors	2	30	60
Lighting	6 bulbs	40	240

A mechanical ventilation system operating daily from 8 a.m. to 5 p.m. was used to provide conditioned air to the indoor space. The ventilation flow rate implemented was determined according to UNI EN 15251 [44], for Category I of indoor air quality (in a low polluting office), resulting in 40 l/s (136 m^3/h, equal to 2h^{-1}). The supply temperature of the ventilation air was decided to be 18°C.
No air infiltrations were considered, since the office room is supposed to be in overpressure.

The period during which each internal heat load and the ventilation system were active is represented in Figure 7.4.

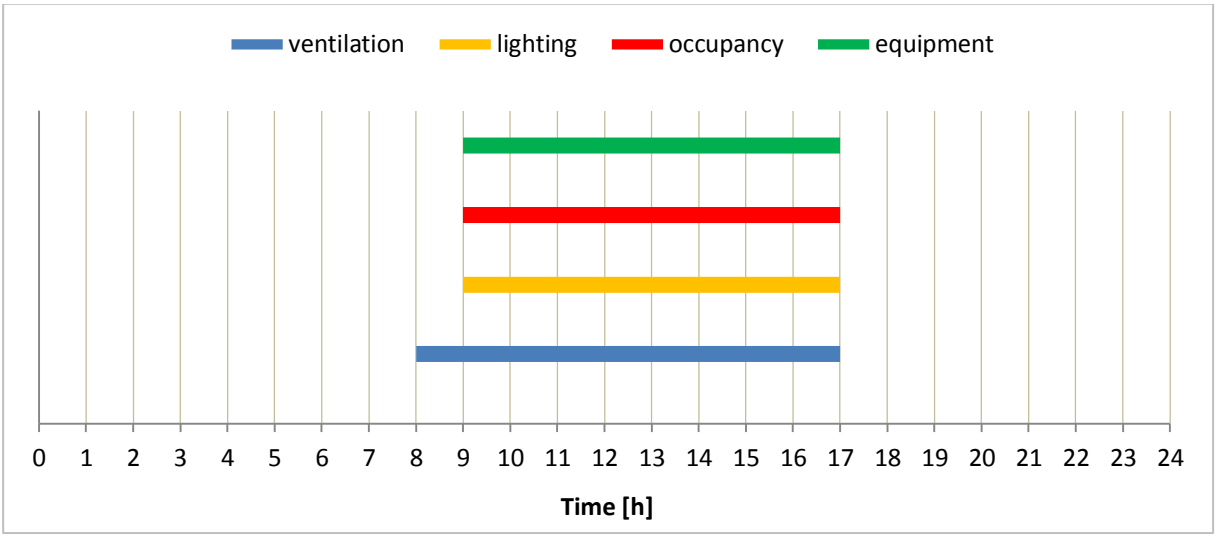

Figure 7.4 – Ventilation and internal heat loads profile for the office room

7.1.2 Flow rates and set points

Some of the flow rates of the hydraulic circuits comprised in the system were modified (respect to the ones presented in Table 6.7) with the main aim of optimizing the performance of the night sky radiant cooling process. Several combinations of flow rates and set points have been simulated in TRNSYS and a rough comparison between the different attempts has been performed. The selected flow rates are detailed in Table 7.3.

Table 7.3 – Flow rates implemented for the hydraulic circuits

Subsystem	Flow rate [l/h]
Solar circuit	100
Intermediate circuit	100
Chiller circuit	150
Ceiling's water supply circuit	150

The set points of the control system were adjusted with the same modality mentioned for the flow rates. The selected values are listed in Table 7.4.
Furthermore, an additional control was implemented for the pump of the intermediate circuit, based on the difference between the fluid temperature exiting the solar collectors and the temperature at the top of the HWT (the related set point is indicated as Δt**). This control ensured that whenever the 3-way valve was switched on the heating mode, the solar circuit was effectively supplying heating energy to the HWT. When no one of the conditions set was fulfilled, pump P2 was turned off since it was useless both for heating and cooling purposes.

Table 7.4 – Set points implemented in the model [25]

Controlled device	Parameter	Set point value [°C]
3-way valve	Δt*	2 ± 1
Pump P2	Δt**	4 ± 1
Supply system	t^*_{mt}	21 ± 1
	t^*_{o}	21 ± 0.5
	$t^*_{b\_PCM}$	20.5 ± 0.5
Recirculation valve	t^*_{supply}	18
Chiller	t^{**}_{mt}	16 ± 1

[25] The same nomenclature of Table 5.5 is employed for the set points.

Besides all the conditions described in Table 7.4, the water supply system and the chiller have to fulfil a requirement based on time. Indeed, the supply system is allowed to operate during the time interval from 8.00 p.m. to 9.00 a.m. while the chiller can be turned on only from 00.00 a.m. to 9.00 a.m. On one hand the present operational time ranges guarantee to exploit as much as possible the natural cooling process, while on the other hand they ensure the complete discharge of the PCM by the beginning of the occupancy period.

7.1.3 Weather input file

An external weather data file was given as input to the model for each of the three considered locations. The IWEC (International Weather for Energy Calculations) format was used for this purpose. This climatic file contains averaged hourly weather data derived from up to 18 consecutive recording years [45]. The following terms of the weather file were employed:

- ambient temperature
- effective sky temperature
- wind velocity
- total sky cover
- solar radiation (split in beam and diffuse components)
- ground reflectance
- solar azimuth and zenith angles

7.2 Results

In the present section the results of the simulation study for all the three considered locations are presented and discussed. The paragraph has been divided in subparagraphs based on the category of the parameter analysed. For each subparagraph the results obtained for the climates of Copenhagen, Milan and Athens are shown together in order to ensure an immediate comparison between them.

7.2.1 Office and PCM ceiling

The air temperature and the operative temperature of the office are shown together with the temperature at the bottom and top surfaces of the active ceiling in Figure 7.5, Figure 7.6 and Figure 7.7. A three-day profile is taken as reference for all the three considered locations.

In spite of what expected, the maximum air and operative temperatures inside the room occur in Copenhagen. The maximum indoor air temperature ranges from 29.8 °C for Copenhagen to 26.6 °C for Athens, while an intermediate value of approximately 27 °C is shown under Milan's climate.
However, while the temperature profiles in Athens are rather regular among the three days presented, noticeable difference is observed between the last day and the previous ones in the other two locations. During the third day represented, the maximum indoor air temperature is approximately 28 °C in Copenhagen and 25.5 °C in Milan. This difference is due to the variability of the weather conditions among the three days; indeed, the first two days were sunny whereas significant cloud cover was present during the third one.

European Standard EN ISO 7730 [46] defines a design operative temperature included in the range 24 ± 1.5 °C for office buildings (Category B of thermal environment quality).
As regards to the first two days, the operative temperature of the room is above the maximum boundary of the thermal comfort temperature range for more than 80% of the occupancy period in Copenhagen. The situation is slightly better for Milan, where although the requirement on the operative temperature is fulfilled only for 32% of the occupancy period, the gap between the actual value and the maximum temperature allowed is always below 0.8 °C. Finally, the operative temperature is comprised in the temperature interval suggested for 95% of the occupants' working hours in Athens.
Due to the lower solar heat gain, the indoor thermal comfort requirements are fulfilled for a longer duration in the third day presented, in Copenhagen and Milan. The operative temperature is comprised in the range 23-26 °C for nearly 60% of the occupancy period in the first location and for approximately 93% of the time in Milan.

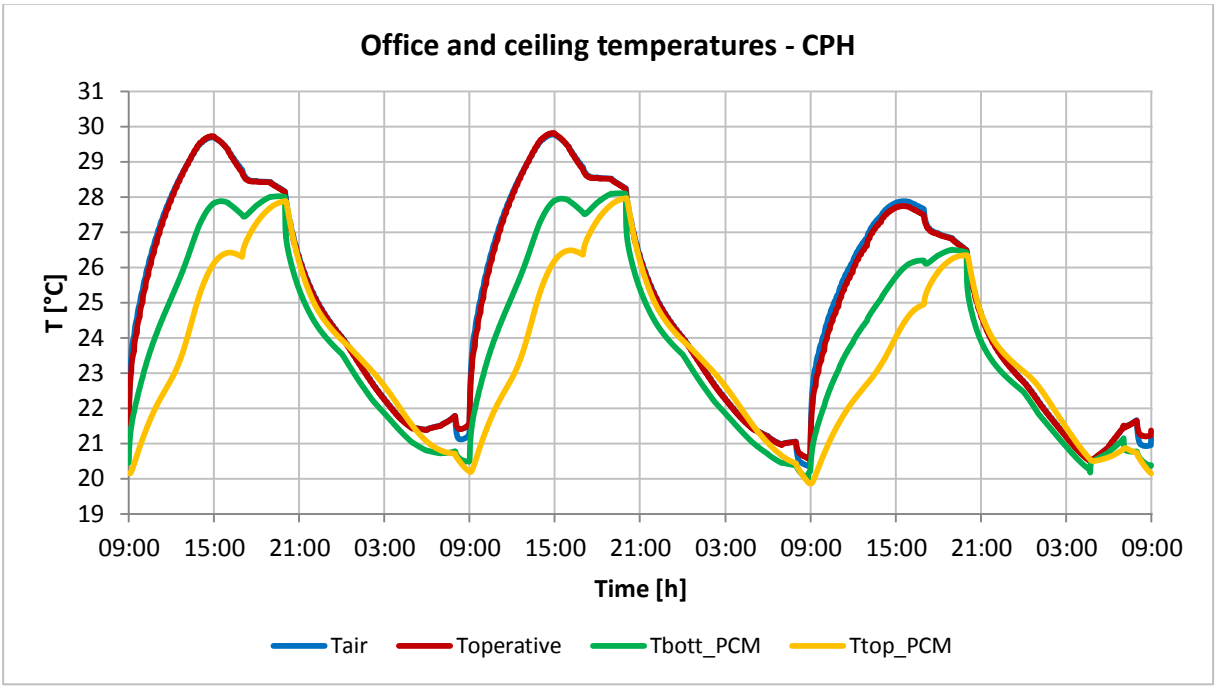

Figure 7.5 – Office and PCM ceiling temperatures for Copenhagen

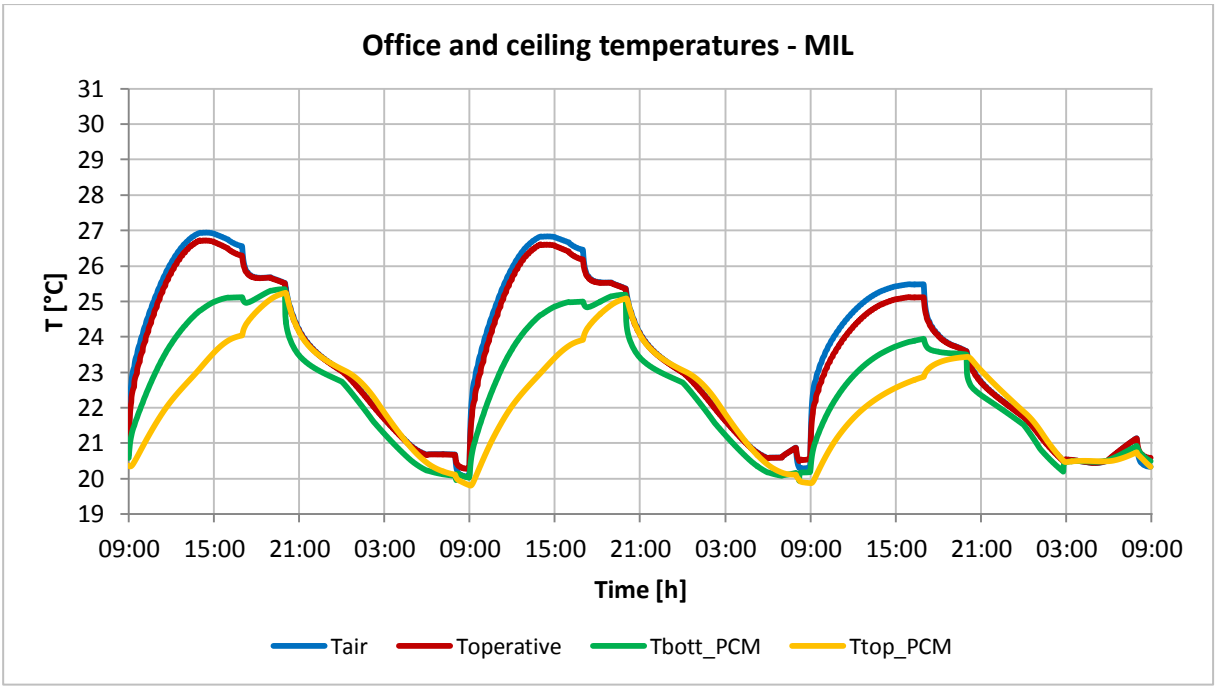

Figure 7.6 – Office and PCM ceiling temperatures for Milan

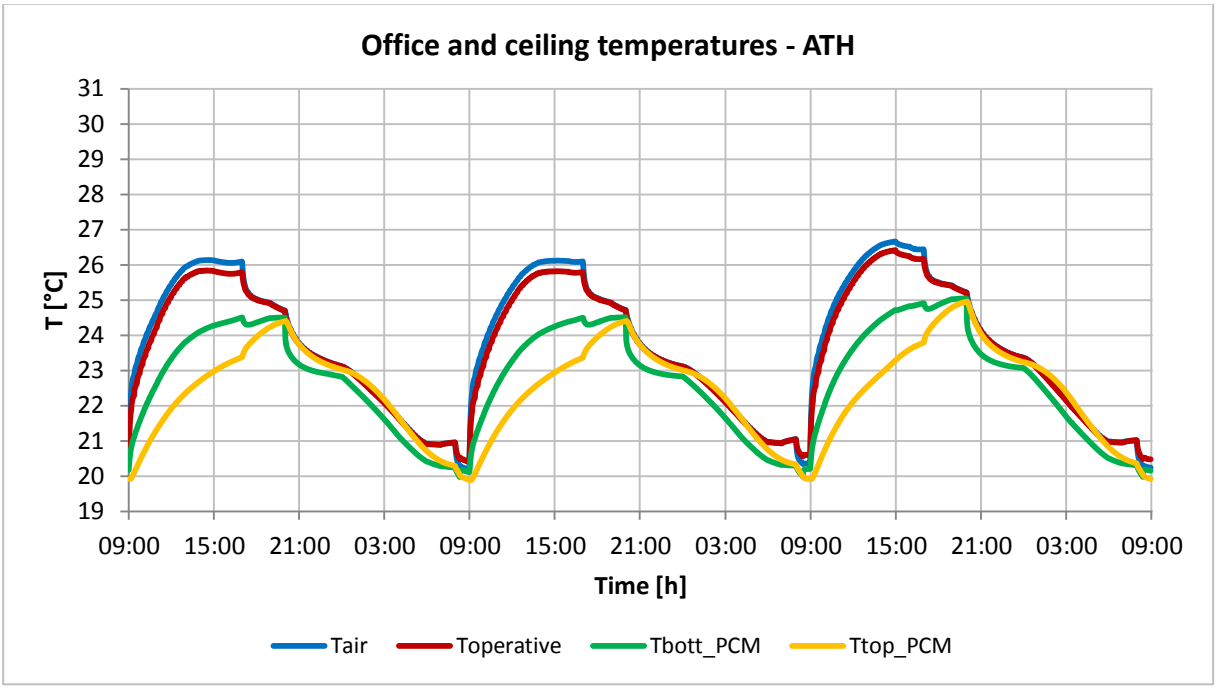

Figure 7.7 – Office and PCM ceiling temperatures for Athens

It is worthwhile remarking that the same characteristics of the envelope were implemented for the three locations. In order to perform a more realistic analysis of the indoor thermal conditions, the U-values of the window and the walls should be chosen accordingly to the requirements prescribed by national standards for the related climate conditions. Indeed, the envelope's performance in terms of insulation required for Copenhagen are stricter than for the other two cases (for example an U-value lower than 0.1 W/m^2K is required for walls of new office buildings in Denmark [47] while a maximum U-value of 0.33 W/m^2K is admitted for Milan [43]).

Since the envelope's features and the internal gains considered for the three locations are exactly the same, the difference highlighted in terms of indoor air temperature can only be ascribed to the weather conditions. In particular, since Copenhagen's external air temperature is lower than the one of Milan which in turn is lower than the one of Athens (Figure 7.8), the dissimilarity has to be due to the solar heat gain.

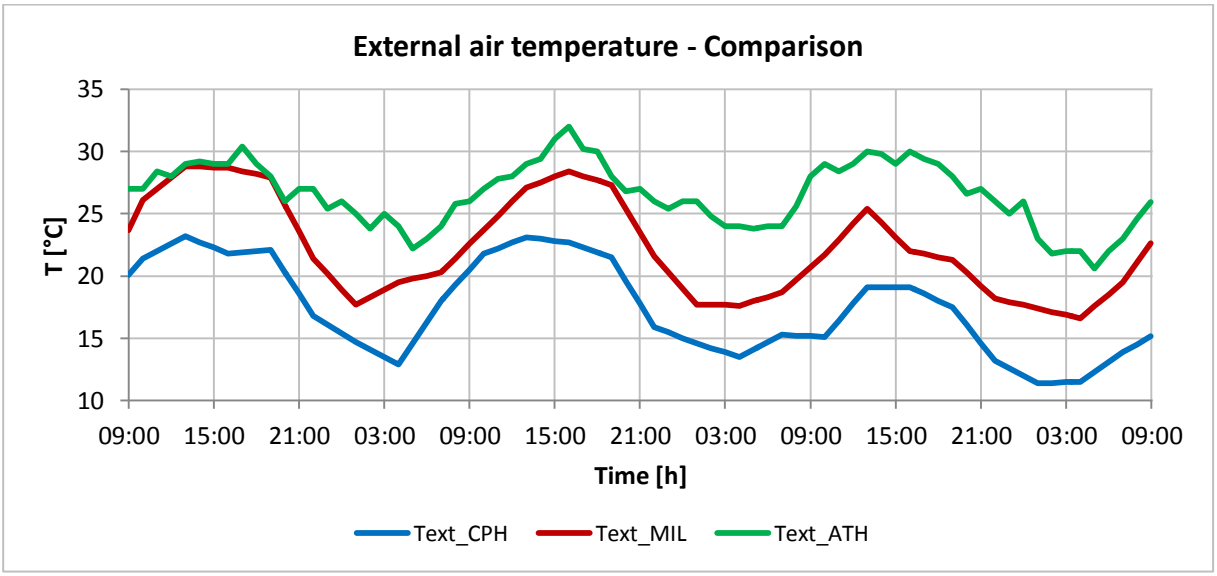

Figure 7.8 – External air temperature for the 3 considered locations

This hypothesis is confirmed by Figure 7.9, which illustrates the amount of solar radiation per square meter of the window's surface which enters the room through the glazed element. The solar load existing in Copenhagen is noticeably higher than the one observed in the other locations. This is mainly due to the fact that the average solar height increases with the latitude and so does the incident angle of the solar radiation on vertical surfaces. However, the presence of shading devices should be taken into consideration in order to provide a more realistic description of the thermal conditions of the indoor space.

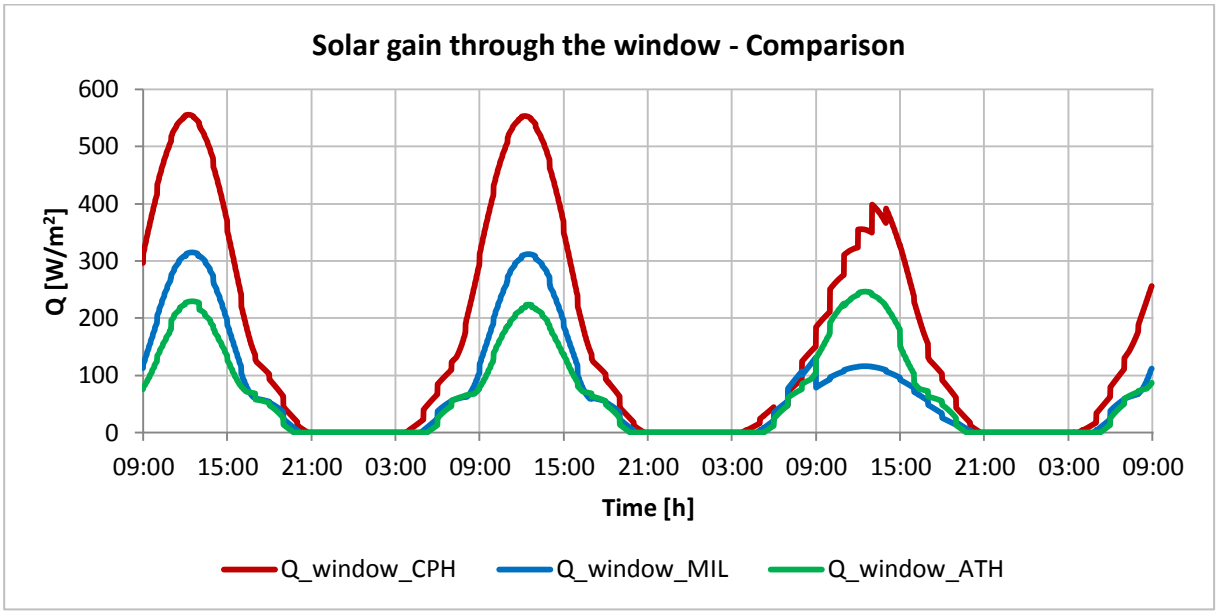

Figure 7.9 – Solar heat gain entering the window for the 3considered locations

It can be also noticed that the solar heat gain occurring in Copenhagen and Milan during the last of the three days represented is considerably lower than the previous two days. In fact, in the mentioned locations, the sky was partially overcast during the last day, while clear sky conditions existed during the previous ones. This explains the significant variation of the temperature profiles of the room and the active ceiling among the three days, which was pointed out previously. Lower variability of the indoor and ceiling temperatures was observed for Athens' case because the solar gain profile is rather regular among the three days in this location.

Consequently to the different indoor thermal conditions observed for the three case studies, the performance of the active ceiling is subject to a consistent variation from one case to another: as concerns to the first two days illustrated, the PCM reaches the fully charged state[26] around 1.30 p.m. in Copenhagen (Figure 7.5) and approximately at 6.30 p.m. under Milan's weather conditions (Figure 7.6), while the charging phase is not completed during daytime in Athens' case (Figure 7.7).
The behaviour of the PCM changes if a cloudy day is taken into consideration: during the third day illustrated the top surface temperature of the active ceiling rises above 25 °C at 5.00 p.m. in Copenhagen, whereas the PCM is never melted completely in Milan.

As regards to the discharge phase, for all three case studies it can be noticed that the water supply system of the ceiling's circuit ensured the complete solidification of the phase changing material, which occurs when the bottom surface temperature of the ceiling drops below 21 °C. The completion of the discharge process occurs at different times in the three case studies: during the first two days it happens at approximately 5.00 a.m. in Copenhagen, at 3.30 a.m. in Milan and approximately at 4.00 a.m. in Athens. Due to the lower amount of heat absorbed during daytime, the discharge phase is accomplished earlier during the third day considered in Copenhagen and Milan (at 3.00 a.m. and at 1.45 a.m., respectively).

[26] The phase change material is supposed to be totally melted when the temperature of the top surface of the suspended ceiling rises above 25 °C, which is the higher boundary of the melting range of the PCM

This difference between the three locations can be explained by the different solar heat gain during daytime and by the diverse profile of the supplied water temperature. In fact, the supply temperature rises above the set value of 18 °C if the cooling load provided by the nighttime cooling process is not sufficient to maintain the temperature of the CWT below this value. Once the chiller is activated, the temperature inside the reservoir drops quickly and the water supply temperature is kept approximately constant at 18 °C by the recirculation valve.

The supply and return water temperatures of the PCM ceiling's circuit are illustrated for the first night in Figure 7.10, Figure 7.11 and Figure 7.12, together with the temperature of the water at the bottom of the CWT.

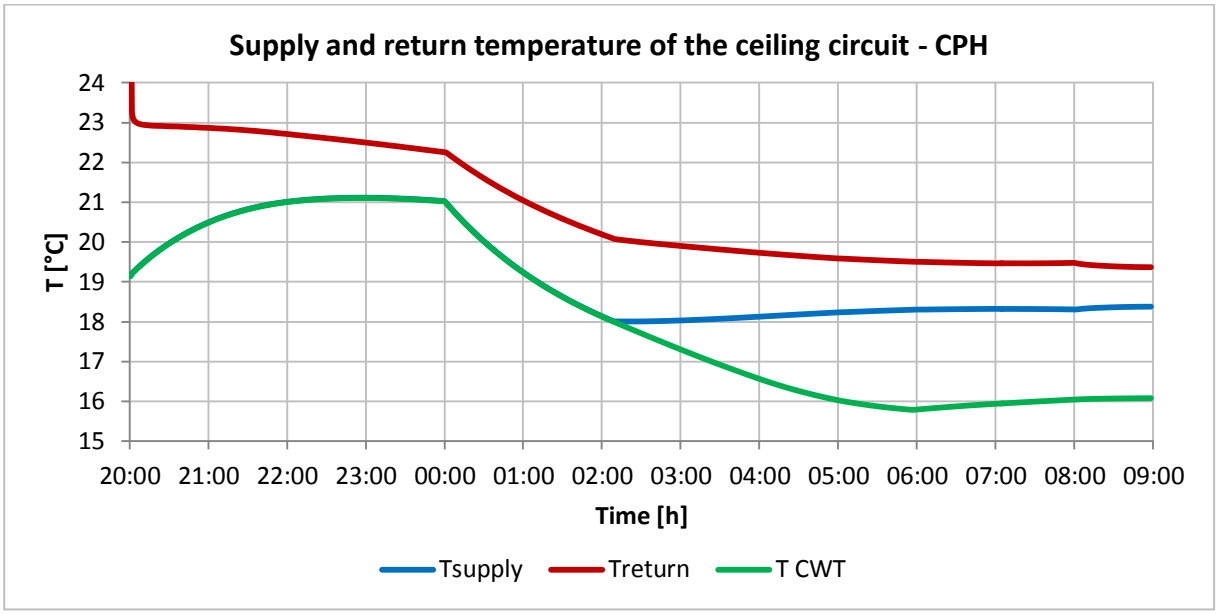

Figure 7.10 – Temperature of inlet and outlet water flows of the recirculation valve for Copenhagen

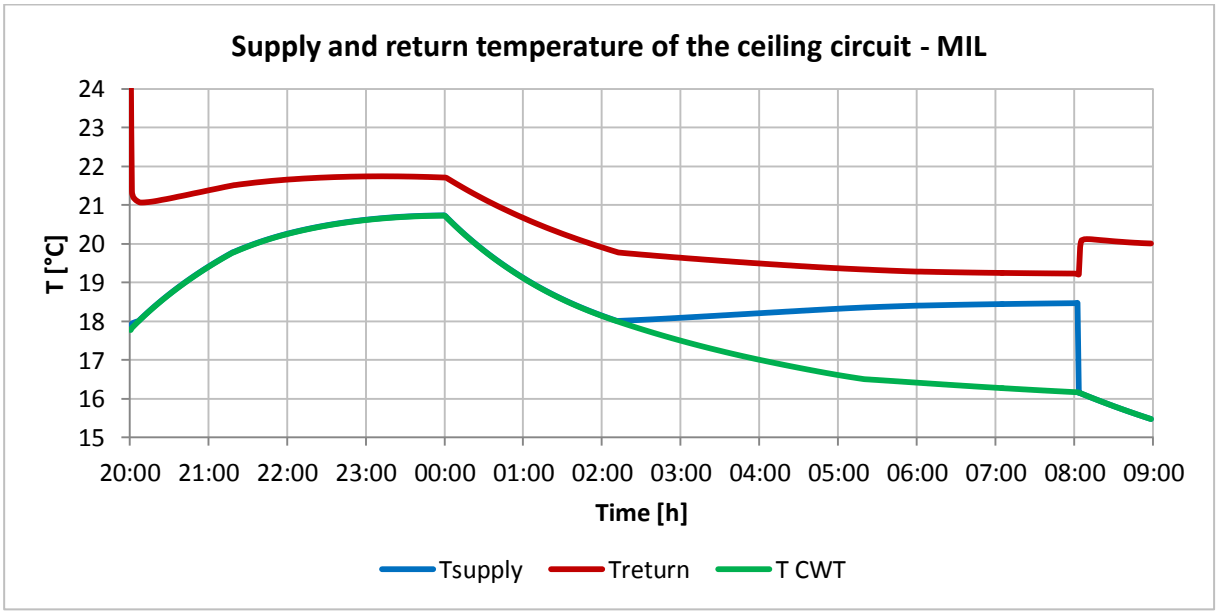

Figure 7.11 – Temperature of inlet and outlet water flows of the recirculation valve for Milan[27]

[27] The sudden variation of the supply and return water temperature happening at 8.00 a.m. is due to the turning off of the supply water pump. The same consideration is valid for the next graph.

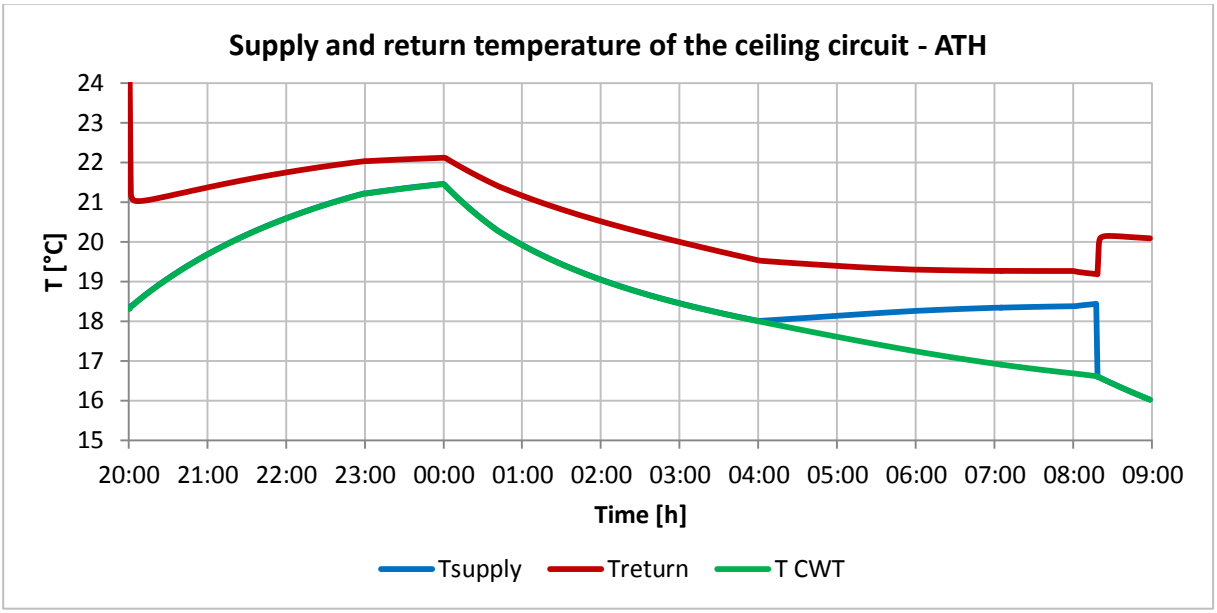

Figure 7.12 – Temperature of inlet and outlet water flows of the recirculation valve for Athens

It can be noticed that the average supply temperature for Athens' case is considerably higher than the one of the other two cases, thus explaining the low rate at which the temperature of the PCM decreases during the night.

7.2.2 Night sky radiant cooling

In the present section the performances of night sky radiant cooling are investigated, focusing mainly on the cooling power provided. The subdivision of the total cooling potential between radiative and convective contributions will be pointed out as well.

7.2.2.1 Cooling power

The cooling power per unit of surface area produced by the solar collectors during nighttime is illustrated in Figure 7.13, Figure 7.14 and Figure 7.15 for Copenhagen, Milan and Athens' climate conditions, respectively. A clear sky night is taken as reference for all the three locations and the time interval from 8.00 p.m. to 6.00 a.m. is considered. The time of sunrise and sunset is listed in Table 7.5 for each of the three reference nights.

Table 7.5 – Time of civil sunrise and sunset for the considered day in the 3 locations

Location	Civil sunrise	Civil sunset	Night length[28]
Copenhagen	3.42 a.m.	10.46 p.m.	4 h 56 min
Milan	5.07 a.m.	9.49 p.m.	7 h 18 min
Athens	5.41 a.m.	9.20 p.m.	8 h 21 min

[28] The night length is the time between civil sunset and civil sunrise of the following day

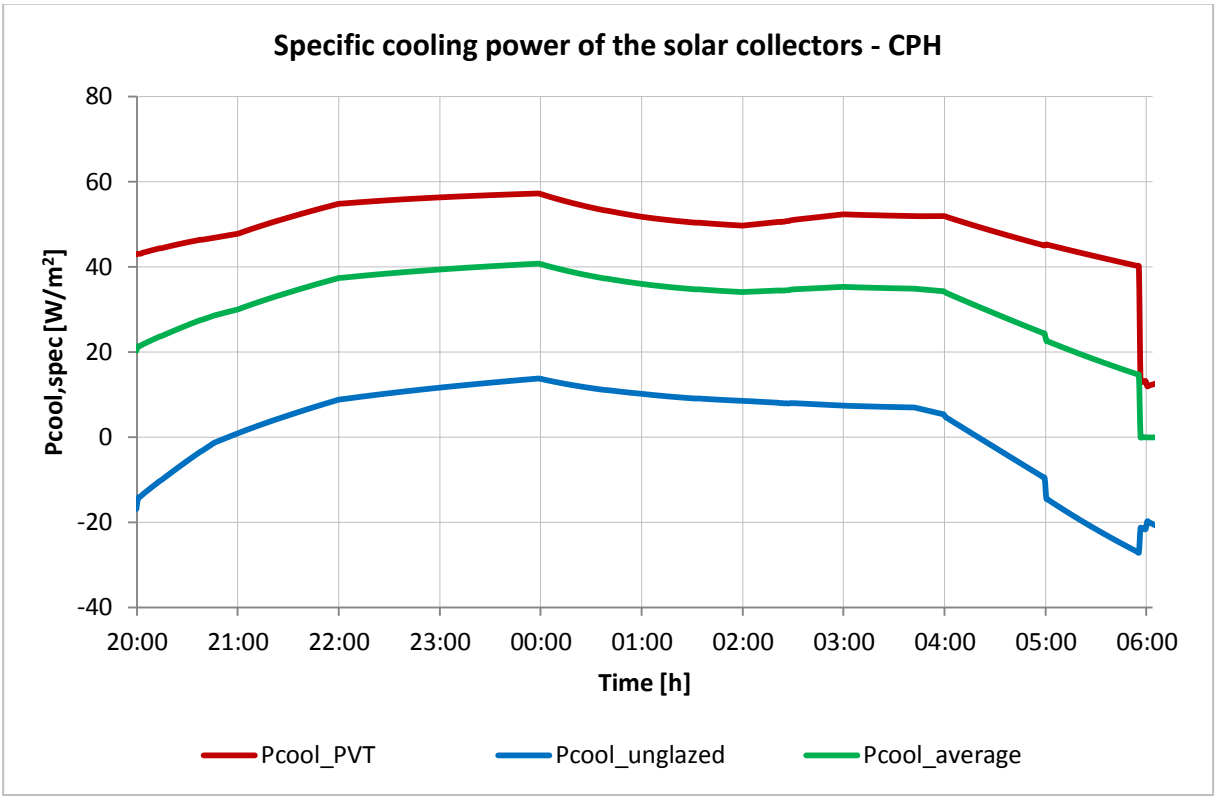

Figure 7.13 – Specific cooling power provided by nighttime radiative cooling in Copenhagen

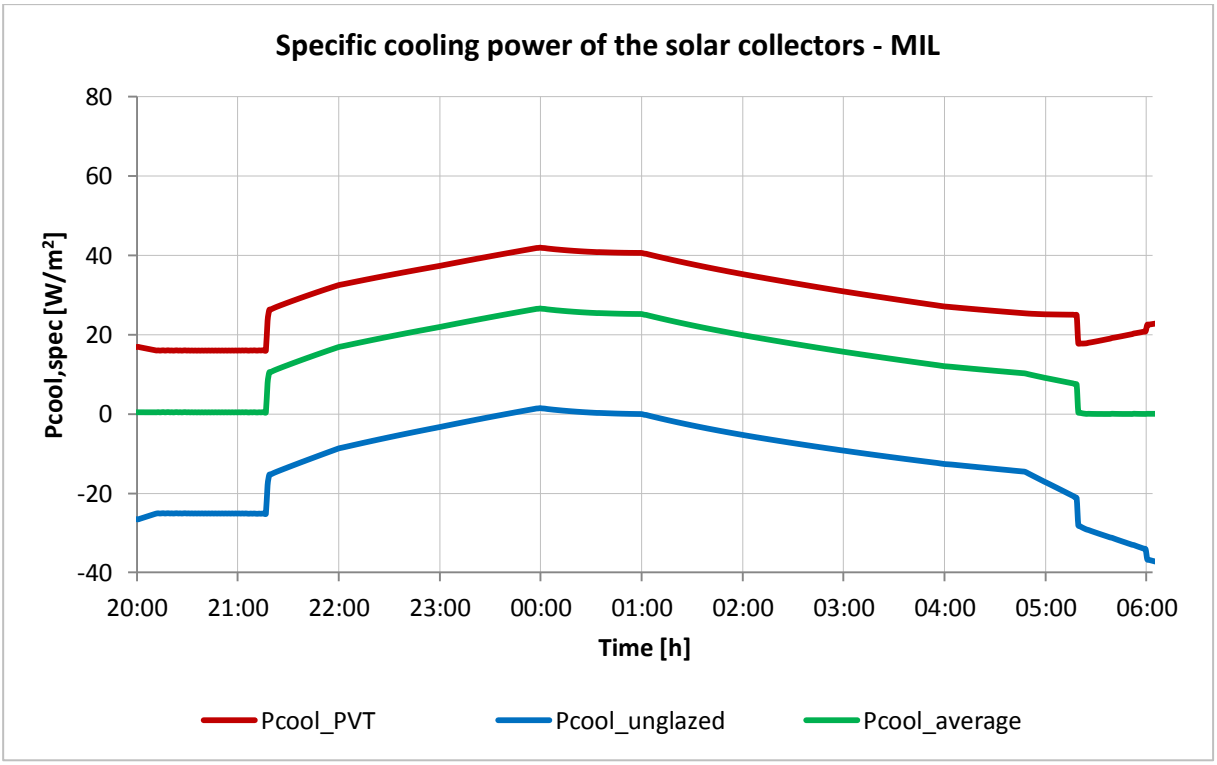

Figure 7.14 – Specific cooling power provided by nighttime radiative cooling in Milan

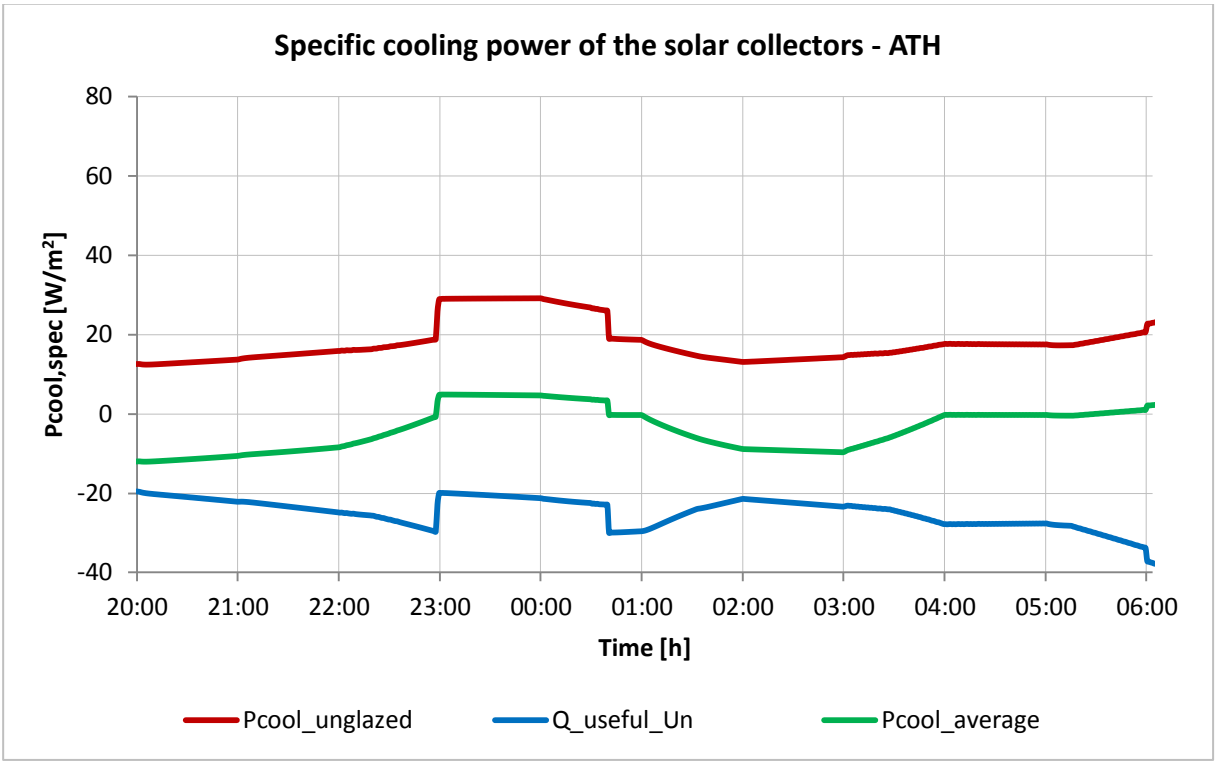

Figure 7.15 – Specific cooling power provided by nighttime radiative cooling in Athens

As expected, Copenhagen's climate shows the best potential in terms of cooling power provided by night sky cooling process. Indeed, the average cooling power[29] produced by the solar collectors varies between 27 and 42 W/m^2 during the time range between sunset and sunrise of the following day. Lower cooling load is produced in Milan, where it ranges from 10 to 27 W/m^2. Finally, limited potential is exhibited under Athens' weather conditions, where the useful cooling power gained by the circulating fluid is always below 11 W/m^2.

The significant gap in terms of performances of the nighttime cooling process in the three locations has to be attributed to the different weather conditions and primarily to the external air temperature, the effective sky temperature and the wind velocity.
As can be noticed in Figure 7.16, Figure 7.17 and Figure 7.18, the nocturnal outdoor air temperature in Copenhagen is prominently lower than the one observed for the other two locations: its value ranges from 13 °C to 20 °C in Copenhagen, from 18 °C to 26 °C in Milan and from 22 °C to 27 °C in Athens. As a consequence, the convective contribution to the cooling load is significantly higher under Copenhagen's summer climate. In fact, convective heat gains instead of heat losses occur in Milan and Athens for the unglazed collector, since for most of the nighttime its mean plate temperature is lower than the one of the air.
A significant difference between the sky temperatures in the three locations can also be noticed: the present parameter varies between -5 °C and 2 °C in Copenhagen, between 4 °C and 10 °C in Milan and from 8 °C to 13 °C during Athens' summer night. Therefore, higher radiative heat exchange is supposed to occur in Denmark, while limited radiative heat losses should exist in Athens. An intermediate situation has to be expected under Milan's weather conditions.
Finally, different wind velocity profiles can be observed for the three locations during the considered night, as illustrated in Figure 7.19: a constant wind speed of 2.1 m/s is present Copenhagen, while the wind velocity profile is less regular in Milan and Athens, with an average value of 0.6 m/s and 1.3 m/s, respectively. As a consequence, the average convective heat exchange coefficient is higher in Copenhagen, thus leading to higher convective heat exchange. Contrarily, the convection contribution to the heat exchange is limited in Milan.

Further investigation on the subdivision between radiative and convective cooling contributions will be carried out later in the text.

[29] The average specific cooling power is the ratio between the overall cooling power provided by nighttime cooling process (expressed in W) and the total surface area of the solar collectors (6.3 m^2).

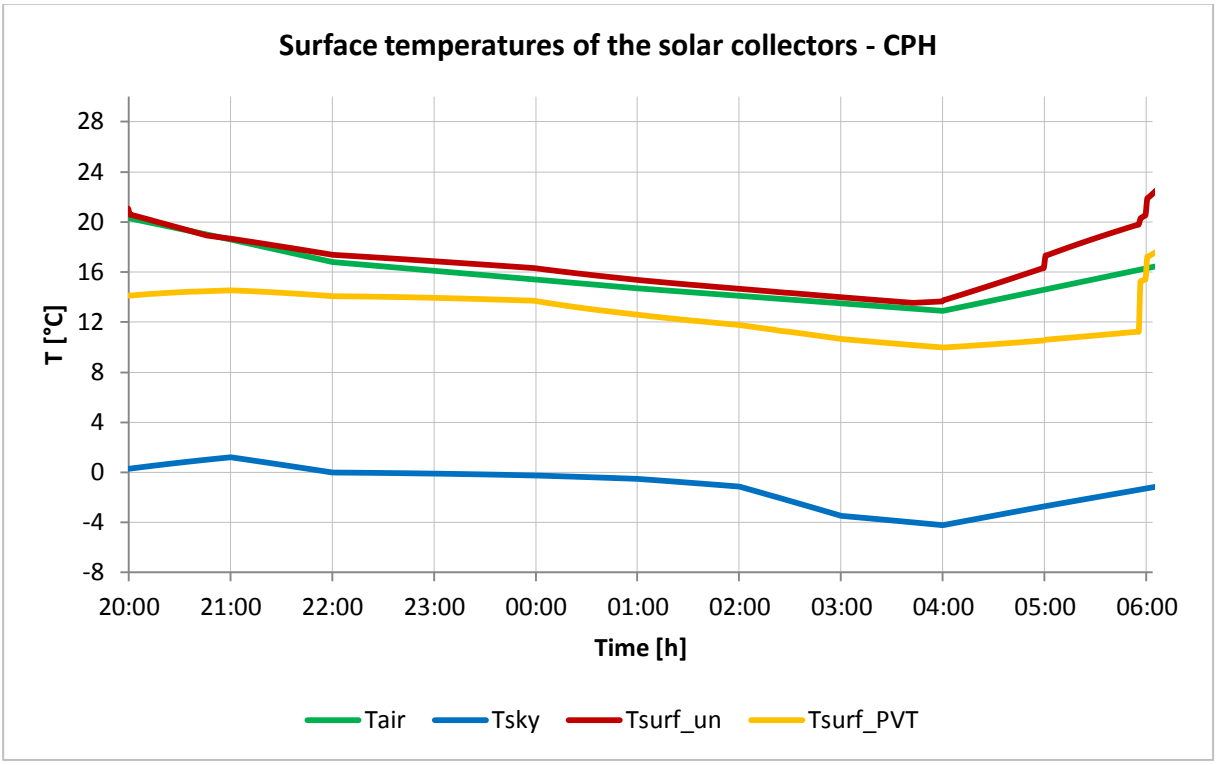

Figure 7.16 – Surface temperatures of the solar collectors in Copenhagen

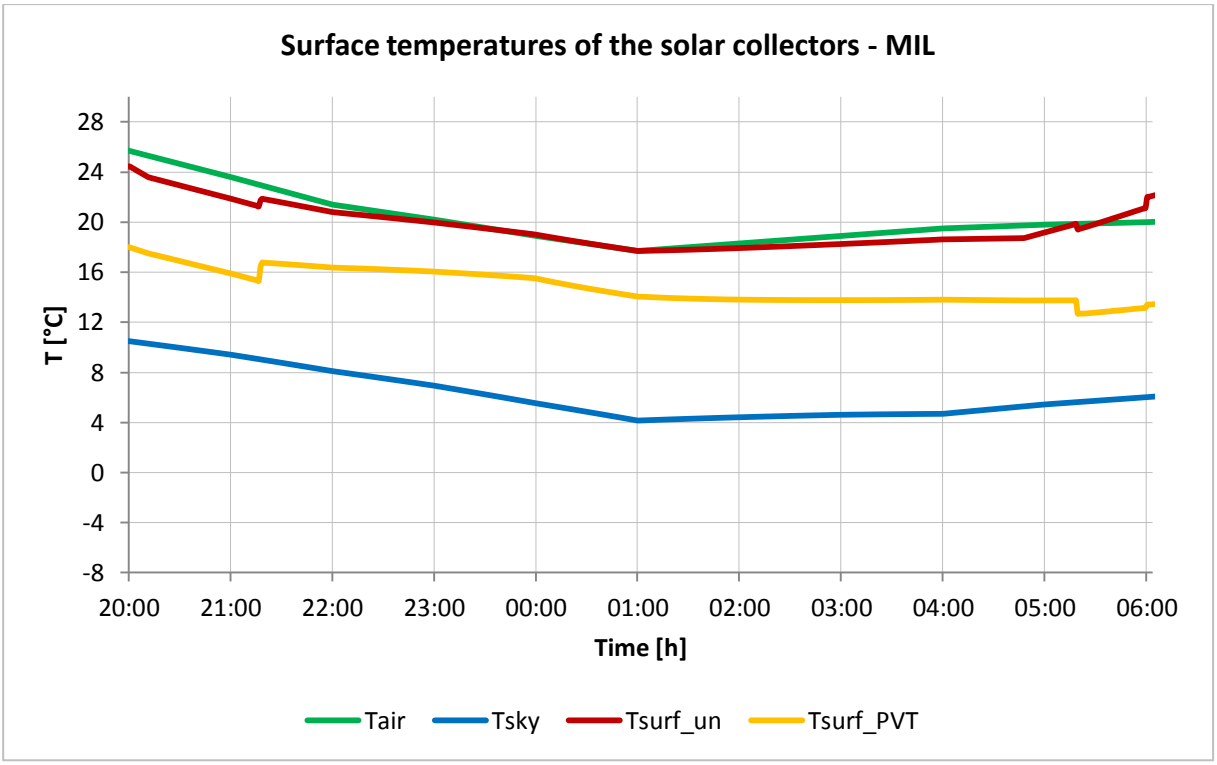

Figure 7.17 – Surface temperatures of the solar collectors in Milan

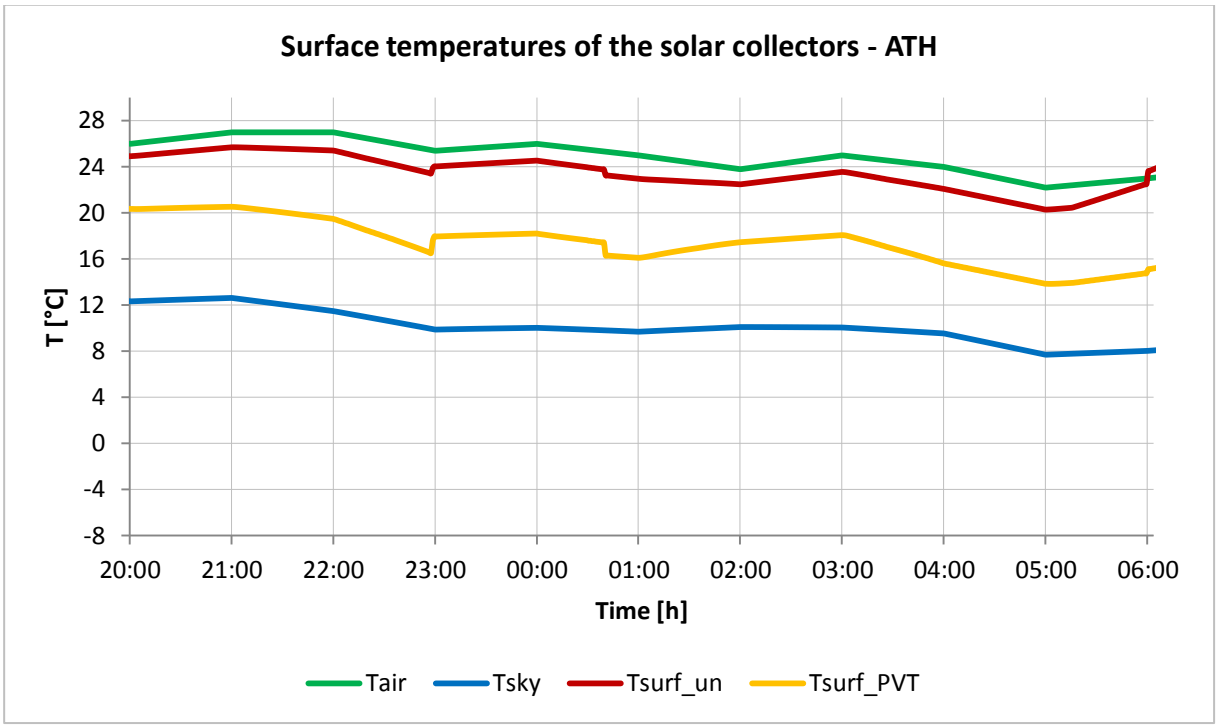

Figure 7.18 – Surface temperatures of the solar collectors in Athens

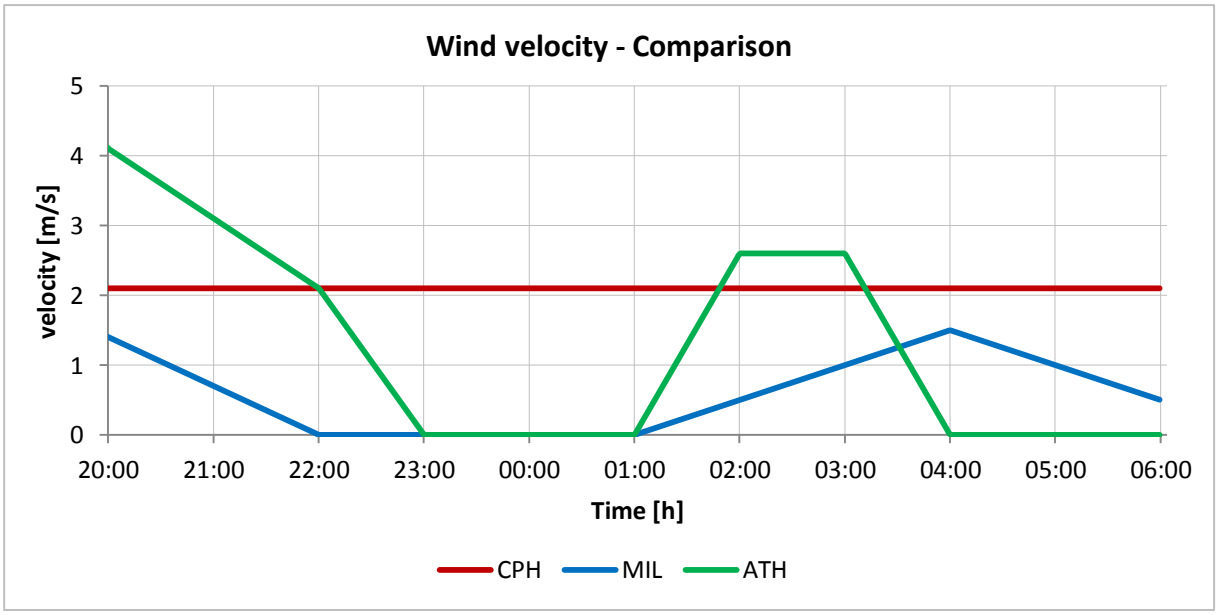

Figure 7.19 – Comparison of the wind velocity in the 3 locations

It is worthwhile pointing out that for all the three locations the output specific cooling load from the unglazed collector is significantly lower than the one provided by the PV-T panels. In fact, in Milan and Athens' case, the cooling output of the unglazed collector is negative during the whole night, thus meaning that heating is provided to the fluid instead of cooling. Hence, the overall performances of nighttime radiative cooling process would be improved by removing the present collector or by substituting it with another PV-T panel.

As mentioned in paragraph 5.3.2, the limited performances of the unglazed solar collector could be ascribed to the high thermal resistance existing between the fluid and the external environment. Indeed, the pipes of the internal loop were made of polyvinyl chloride, which has a low thermal conductivity (0.19 W/m K [33])

compared to the one of metals. Low thermal resistance was present instead between the fluid and the top surface of the PV-T collectors since the internal pipes and the absorber plate were made of copper.
The effect of the different thermal resistance is highlighted in Figure 7.16, Figure 7.17 and Figure 7.18, where the mean surface temperature of the collectors is illustrated. It is evident that the surface temperature of the unglazed collector is close to the one of the external air while a substantial difference exists between the latter and the top surface temperature of the PV-T panels, which is closer to the mean fluid temperature of the heat carrier.

Finally, further information on the performance of nighttime cooling process can be obtained by analyzing the position assumed by the 3-way valve during the night, since the present device is responsible of activating the cooling mode of the solar circuit. Figure 7.20 shows the input control signal to the valve: a value of 1 means that the cooling operation is active while when the input signal is 0 the solar circuit is either operating in the heating mode or it is not working, pursuant to what described in paragraph 7.1.2. It can be noticed that while in Copenhagen and Milan's case studies the system is able to provide cooling to the CWT during almost all the night, in Athens the cooling mode is active only for a short time (less than 2 hours). This difference is due to the cooling output provided by the solar collectors, which is limited under Athens' climate conditions, as previously pointed out.

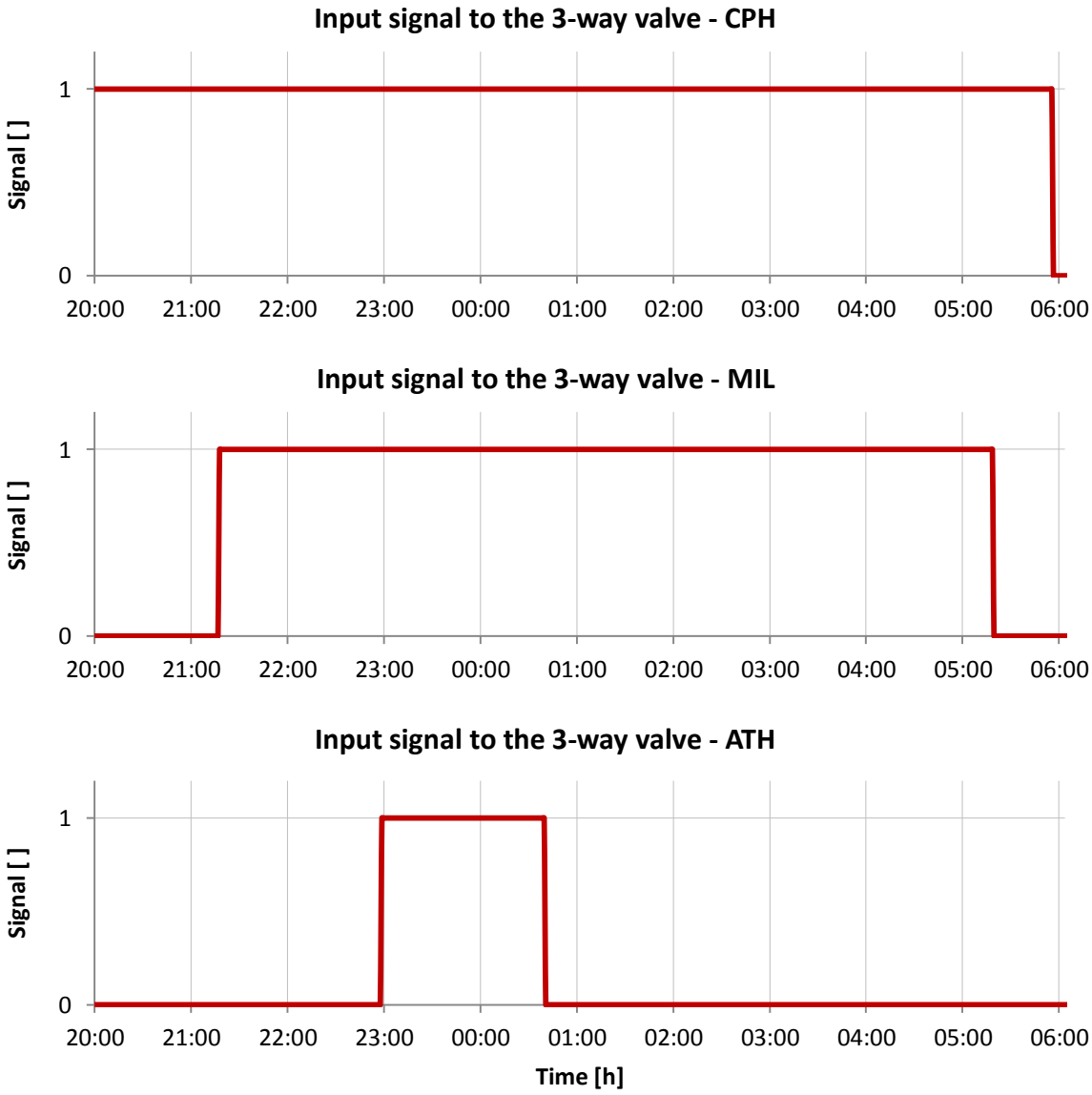

Figure 7.20 – Input signal to the 3-way valve (1=cooling mode)

In order to provide a more complete comparison between the performances of night sky radiant cooling process under the considered climate conditions, the average specific cooling power of the solar collectors is shown for 7 consecutive nights, from 10.00 p.m. to 6.00 a.m.

As can be noticed from Figure 7.21, the contribution of the unglazed collector to the total cooling load produced by the solar circuit is positive (except for one night) only under Copenhagen's climate, although it is scarce (average of 5 W/m^2). For Milan and Athens' case studies, the unglazed collector generally heats the circulating fluid, thus reducing the overall cooling effect of the nighttime radiative cooling process.

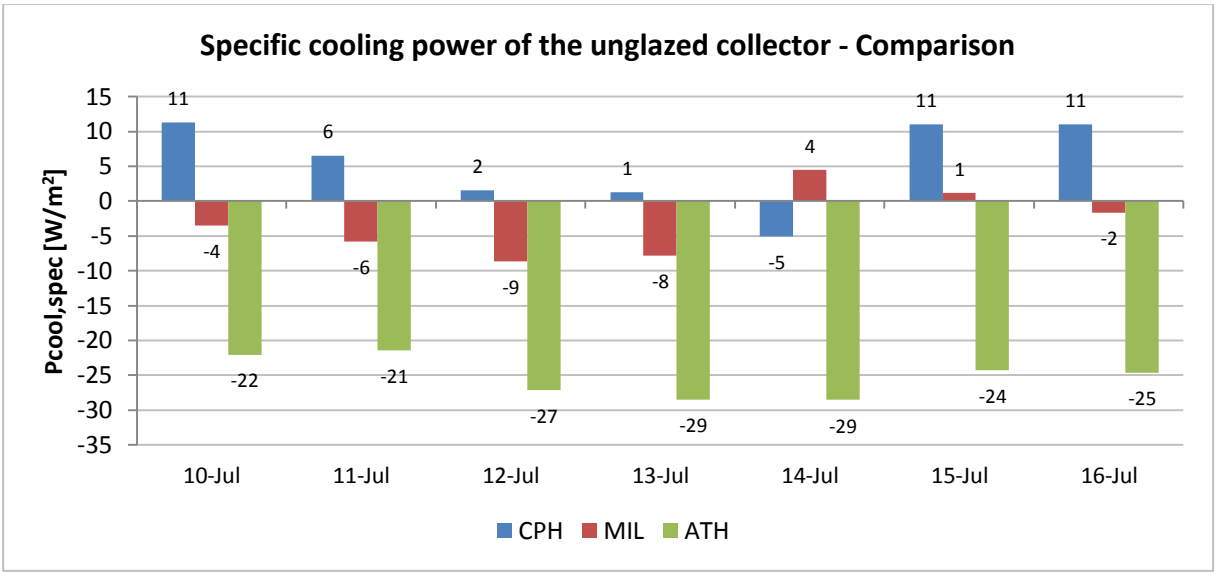

Figure 7.21 – Comparison of the specific cooling power of the unglazed collector in the 3 locations

Figure 7.22 illustrates the average specific cooling power produced by the PV-T panels. Contrarily to what resulted for the night previously investigated, the average cooling load provided to the heat carrier in Copenhagen and Milan is similar, being the average 32 W/m^2 for the first case and 33 W/m^2 for the Italian city. However, it is confirmed that the performance of the PV-T collectors is noticeably lower in Athens, where an average specific cooling power of 18 W/m^2 is calculated.

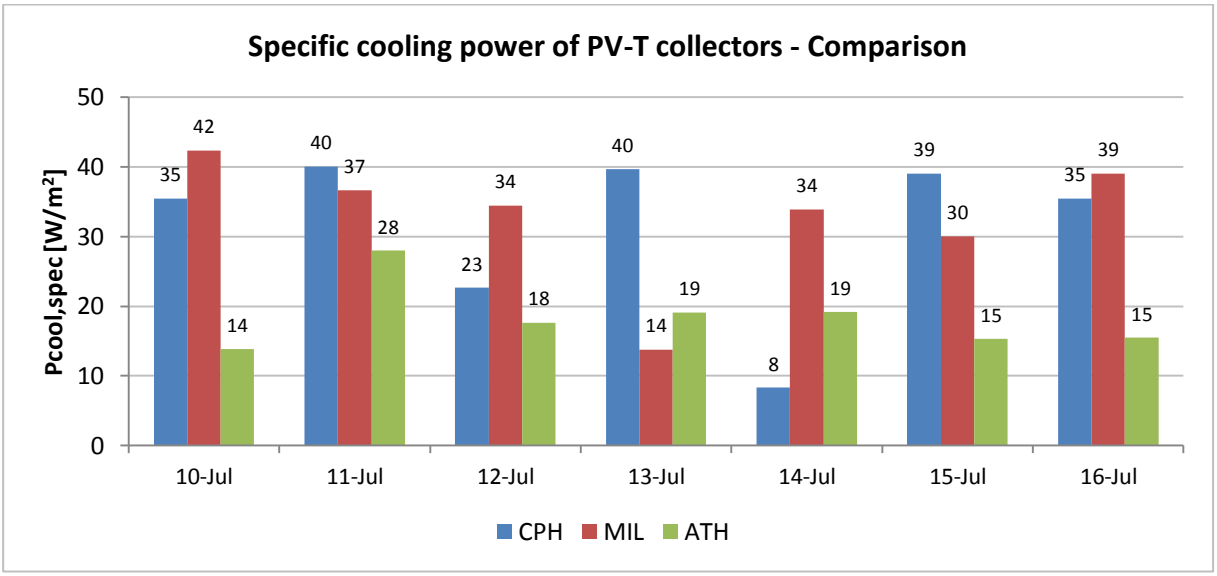

Figure 7.22 – Comparison of the specific cooling power of the PV-T collectors in the 3 locations

Finally, Figure 7.23 shows the overall average cooling power produced by the solar circuit. As noticed for the PV-T panels, Copenhagen and Milan show similar potential, with an average cooling output of 137 W in the first location and a value around 122 W in the second case. Due to the substantial heating effect of the unglazed collector, the overall cooling power produced in Athens is derisory (average of 12 W).

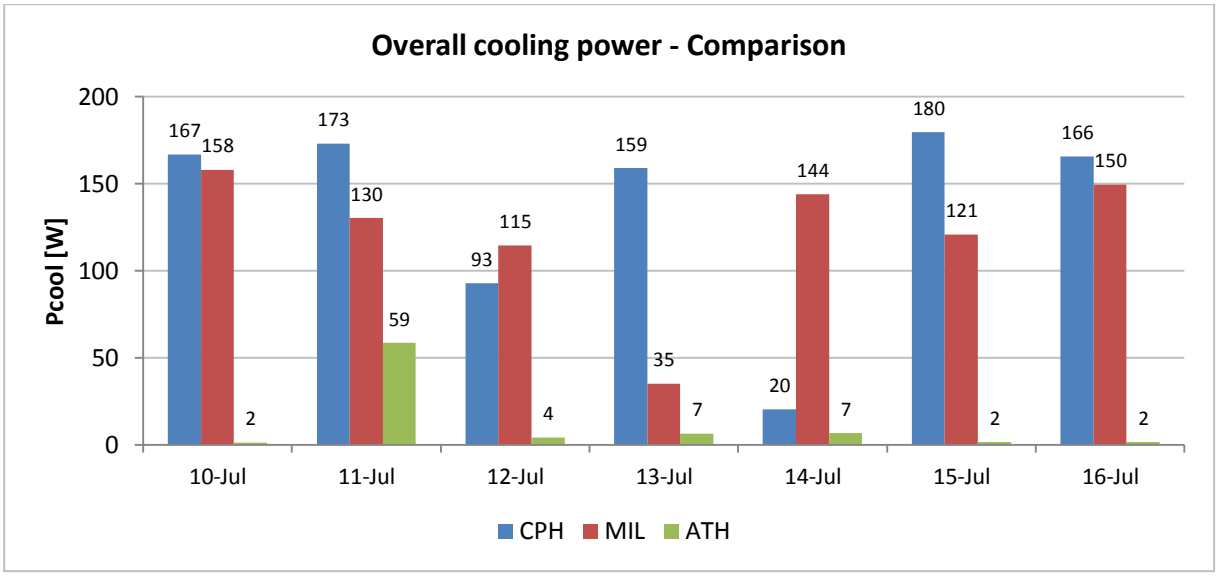

Figure 7.23 – Comparison of the overall cooling power in the 3 locations

The low cooling production (compared to the weekly average) highlighted for the nights of 12th and 14th of July in Copenhagen is due to the considerable cloud cover of the sky, whose average percentage value was 70% in the first night and 85% in the second one. The same reason underlies the limited cooling production during the night of 13th of July in Milan, being the average cloud cover percentage around 87%. The present consideration verifies what mentioned in paragraph 3.3, where the influence of the cloud cover on the radiative heat exchange was pointed out.

As it was mentioned previously, the cooling performances of the solar circuit in Milan and Athens could be improved by removing the unglazed collector or by substituting it with a PV-T collector of the same type of the other three employed.

7.2.2.2 Average cooling energy

The main purpose of night sky radiant cooling process is cooling the water stored inside the CWT, which is used to discharge the PCM contained in the suspended ceiling. Therefore, it is interesting to compare the cooling energy provided to the CWT by the solar collectors with the one supplied by the auxiliary chiller. The comparison is presented for one week in Figure 7.24, for each of the considered locations. The time interval from 8.00 p.m. to 9.00 a.m. is contemplated.

For all three locations, the amount of energy supplied to the CWT by the nocturnal cooling technology among the seven considered nights is comparable, apart from some isolated incidents. An average cooling load around 2 kWh can be observed for Copenhagen, covering between 35% and 57% of the cooling demand of the CWT. Lower potential is obtained under Milan's weather conditions, where the night sky radiant cooling process produces an average energy of 1.5 kWh, with a relative amount varying between 25% and 40% of the total cooling load. Finally, the contribution of natural cooling in Athens appears to be negligible.

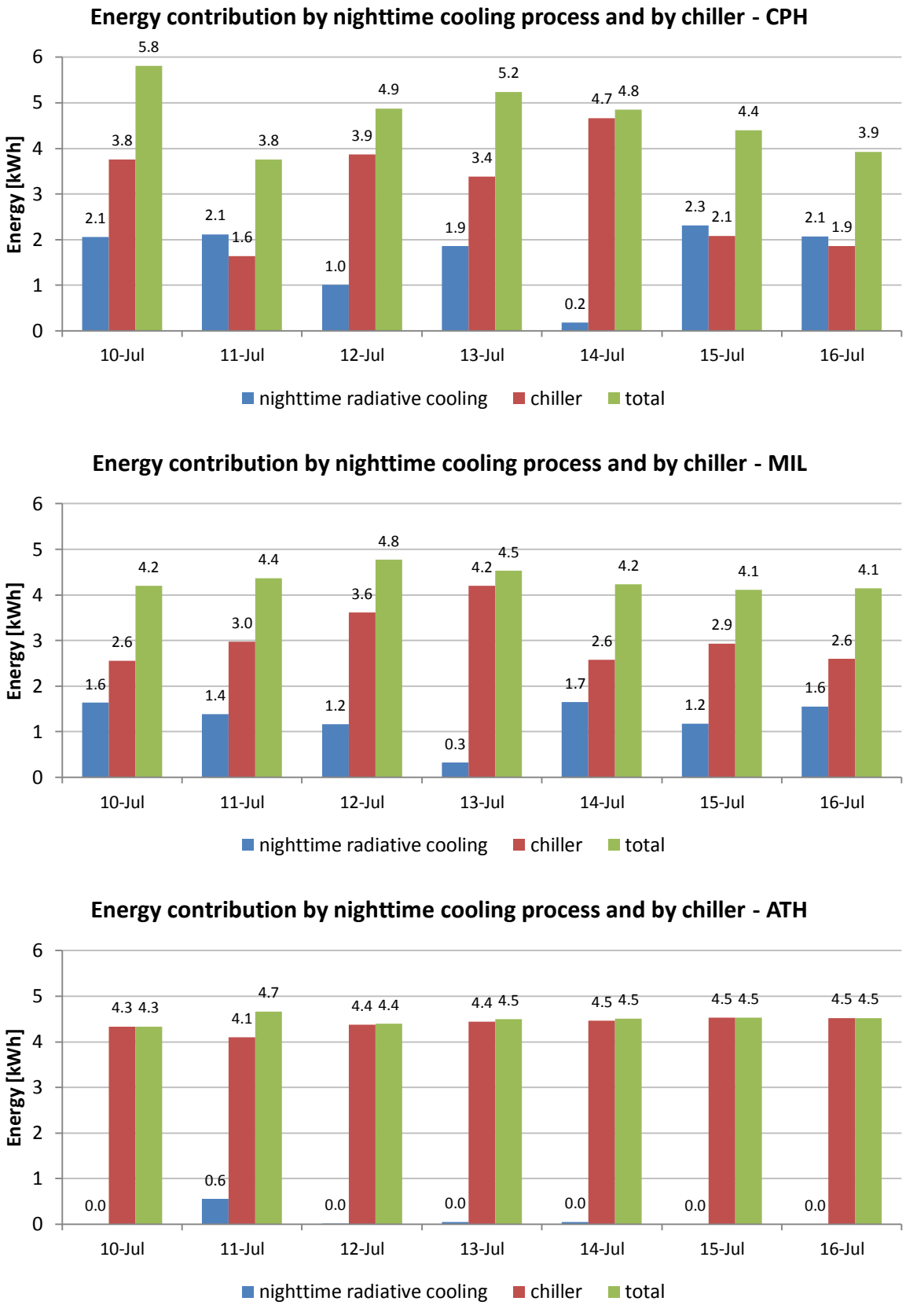

Figure 7.24 – Cooling energy provided to the CWT by nighttime cooling process and by the chiller

The variation of the overall cooling load required by the CWT among the presented week in Copenhagen is noteworthy. Indeed, this value ranges from 3.8 kWh for the night of 11th of July to 5.8 kWh for the 10th of July (53% higher). This considerable difference could be explained by the high variability of the cloud cover during the considered period, which affects the amount of incident solar radiation passing through the window and consequently the solar heat gain absorbed by the office room. Indeed, the sky was almost totally overcast during the 11th of July while no clouds were present during daytime of the 10th of July.
The gap between the different nights is much lower for the cases of Milan and Athens, since the amount of clouds covering the sky was generally limited.

In order to provide a direct comparison between the three locations, the subdivision of the overall cooling energy provided to the CWT between the contributions of night sky radiant cooling and chiller during the 7-nights-period considered is illustrated in Figure 7.25.

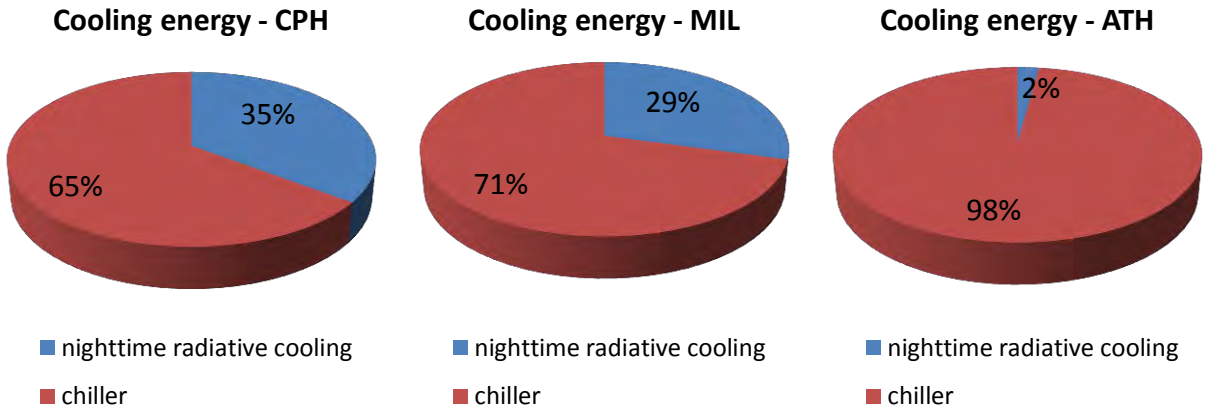

Figure 7.25 – Average cooling energy provided to the CWT by nighttime cooling process and by the chiller

As highlighted above in the text, the night sky radiant cooling technology exhibits high potential under Copenhagen's climate, covering 35% of the cooling demand of the CWT. High potential is shown in Milan's case as well, where the natural cooling process provides almost 30% of the required energy. Finally, the contribution given by the solar collectors in Athens is paltry since the 98% of the cooling energy is given by the chiller.

7.2.2.3 Radiative and convective contributions

Interesting information can be deduced by analysing the subdivision of the overall cooling power provided by the solar collectors into radiative and convective contributions. The present comparison is illustrated for the PV-T collectors[30] in Figure 7.26. The data were calculated over the time interval from 10.00 p.m. to 6 a.m. of every night.

For all three cases, the value concerning the convective heat exchange is negative for every night taken into consideration, this meaning that convective heat gains occur instead of heat losses. This phenomenon is logical since the external air temperature is always higher than the collectors' surface temperature. The overall cooling power is therefore entirely provided by the radiative part of the heat exchange process. This consideration justifies the names of "night sky radiant cooling" and "nighttime radiative cooling" assigned in literature to this technology.

The convective heat gains occurring in Copenhagen and Milan are comparable (the average value is 5 W/m^2 in the first case and about 4 W/m^2 in the second one) while a considerably higher value is observed for Athens' case (17 W/m^2). This gap can be explained considering that the average external air temperature in Athens is significantly higher than for the other two locations.

[30] The TRNSYS type employed to model the unglazed collector does not separate the two components of the heat exchange.

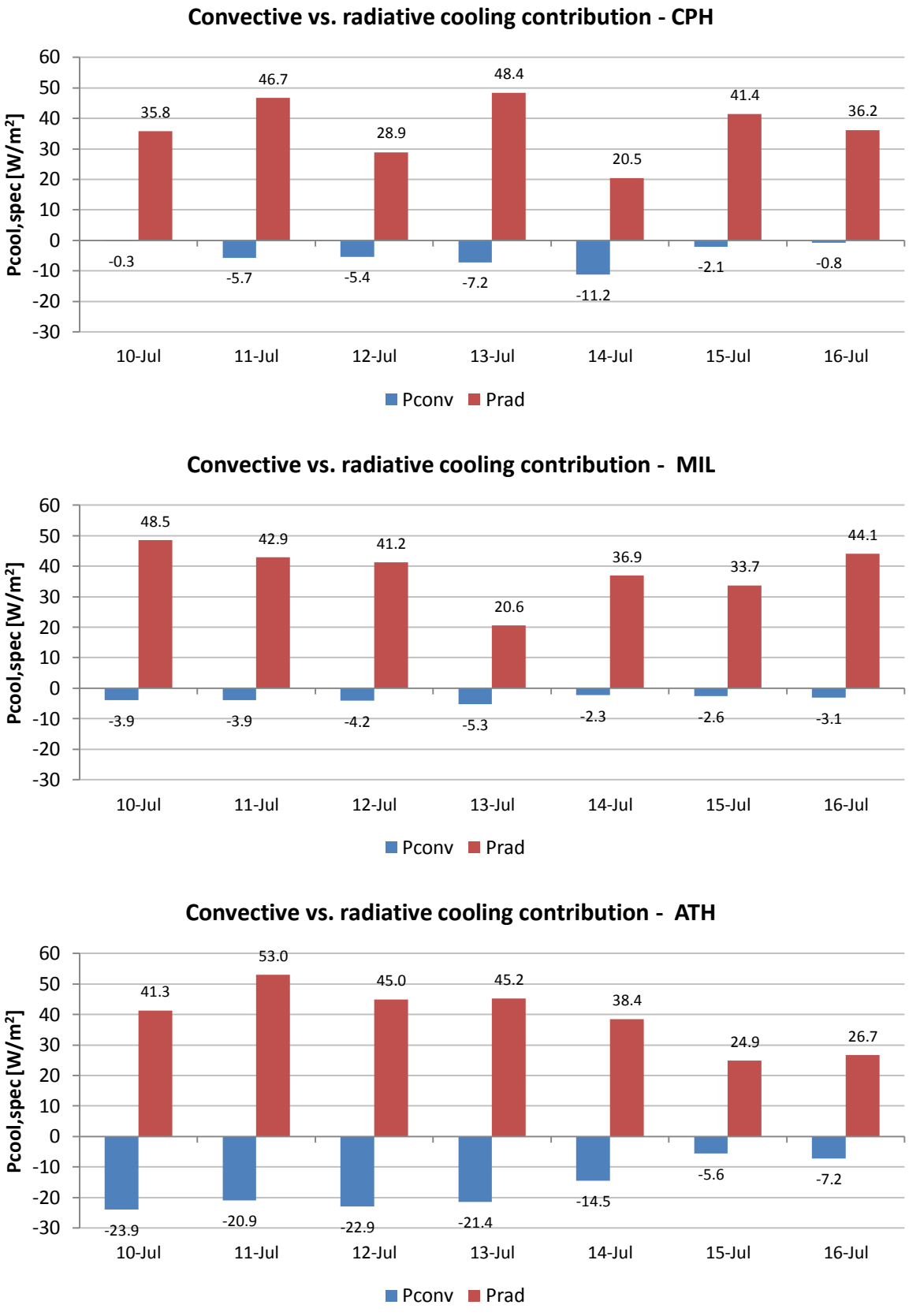

Figure 7.26 – Convective and radiative cooling contributions of the PV-T solar collectors

As regards to the radiative component of the heat exchange, the difference between the three locations is negligible: the average nocturnal radiative loss corresponds to 37 W/m^2 in Copenhagen, 38 W/m^2 in Milan and 39 W/m^2 in Athens. The reduction of the radiation heat exchange caused by the higher average cloud cover observed in Copenhagen is probably counteracted by the lower sky temperature existing in this location, compared to the other two.

7.3 Comments and conclusions

The indoor thermal comfort requirement is not fulfilled under Copenhagen and Milan's climate conditions, being the operative temperature outside the suggested range for most of the occupancy hours during sunny days. Furthermore, the phase changing material contained in the suspended ceiling reaches the fully charged state some hours before the end of the occupancy period in Copenhagen and Milan, thus suggesting that higher thermal capacity is needed to improve the thermal quality of the indoor environment. The enhancement of the thermal capacity can be pursued by increasing the area covered by PCM panels or employing a PCM with higher latent heat.
As concerns to Athens' case, the operative temperature is comprised in the temperature interval suggested for almost the entire occupancy period. Moreover, the PCM charging phase is not completed during daytime; hence, the surface of the suspended ceiling covered by PCM panels could be slightly reduced.
However, the presence of shading devices and the effective structure of the building's envelope for each location should be implemented in the model to provide a more realistic investigation of the indoor thermal conditions.

In all the three considered locations the system provides the cooling energy required to ensure the complete discharge of the phase changing material inside the suspended ceiling by the beginning of the occupancy period. The present consideration indicates that the supply system was well designed and that the set points of the control system were properly selected. Nevertheless, further analysis should be carried out in order to optimize the operation of the system, setting customized operating conditions (such as flow rates and working time intervals of pumps and valves) for each of the three considered locations.

As regards to the performance of night sky radiant cooling process, several conclusions can be drawn.
Firstly, this technology shows similar potential in Copenhagen and Milan in terms of cooling production, with an average value of 140 W and 120 W, respectively. Contrarily, the overall cooling power produced in Athens is scarce, due to the substantial heat load provided by the unglazed collector.
However, in all three locations the cooling load produced per unit area of the collectors is considerably higher if only the output of the PV-T collectors is taken into account: an average cooling power of 30 W/m^2 is ascertained for Copenhagen and Milan, while a value of about 20 W/m^2 is verified under Athens' climate. These values are lower than what found in literature for similar applications under analogous climate conditions (cooling power between 30 W/m^2 and 60 W/m^2 in Copenhagen [22] and between 40 and 45 W/m^2 in Madrid [14]). However, the mean temperature of the water flowing through the solar collectors was considerably higher in these studies, thus resulting in greater radiative and convective heat losses.

In terms of cooling energy supplied to the cold water tank, the night sky radiant cooling technology exhibits high potential under Copenhagen's climate, covering 35% of the cooling demand. Good potential is shown in Milan's case as well, where the natural cooling process provides nearly 30% of the required energy. Contrarily, the contribution given by the solar collectors in Athens is negligible and the cooling load is almost entirely provided by the chiller.
The fraction of cooling demand satisfied by the night sky radiant cooling process could be enhanced by raising the surface area of the solar collectors. However, the available area for the installation of solar collectors could represent a limiting factor, since several office rooms like the one considered are generally comprised in an office building.

Finally, for all of the three considered locations, it has been highlighted that the cooling power from the solar collectors is completely provided by the radiative heat exchange process, thus justifying the names of "night sky radiant cooling" conferred to this technology. An approximate value of 40 W/m^2 of radiative heat losses has been assessed for all three investigated cases.

8 Final comments and conclusions

The experimental study proved that the considered system fulfilled its main aim during winter, ensuring the complete discharge of the phase changing material embedded in the suspended ceiling during the night. The energy supplied by the night sky radiant process to the cold water tank was enough for the purpose, so that the ancillary chiller has never been utilized.

The average cooling power produced by the night sky radiant cooling process varied between 440 W and 580 W. The PV-T technology showed a good potential, providing a cooling output between 90 and 120 W/m^2. Much lower performances were observed for the unglazed flat plate collector, whose specific cooling output was between 30 and 50 W/m^2.

Due to some constraints on the thermal conditions implemented for the indoor space during the experiment, no considerations can be performed about the performances of the PCM panels in terms of improvement of the indoor comfort.

The simulation model developed with the software TRNSYS exhibited satisfactory accuracy in describing the thermal conditions inside the climate chamber and the behaviour of the phase changing material contained in the suspended ceiling. The representation of night sky radiant cooling process was in general less precise; the gap between the results of the simulation and the experimental study, in terms of overall cooling power provided by the solar circuit, ranged from less than 4% to 34% of the experimental value. The low fidelity showed for some of the considered nights could be explained by the inaccuracy of the weather data given as input and the lack of information required for the detailed description of the TRNSYS components.

The coupling between phase changing materials and night sky radiant cooling shows good potential in Copenhagen and Milan, since a significant portion of the energy required to discharge the PCM (35% and 30% respectively) is covered by the nocturnal cooling output of the solar collectors, even under the non-advantageous summer weather conditions. Contrarily, limited potential is expressed by the integration of the two technologies under warmer climates, such as the one of Athens; this is because the average external air temperature is noticeably higher than the mean fluid temperature, thus resulting in significant convective heat gains which contrast the radiative cooling effect. Better performance could be achieved in Southern Europe during fall or spring, where more advantageous weather conditions (such as lower air temperature and lower effective sky temperature) are expected. However, the cooling demand existing during these seasons is lower than the one of summertime.

The average cooling power per unit area provided by the PV-T collectors ranges between 30 and 35 W/m^2 in Copenhagen and Milan, whereas a value of approximately 20 W/m^2 is achieved under Athens' climate conditions. The nocturnal cooling output of the unglazed solar collector is negligible for the first two locations while a considerable heating effect is observed in Athens.

One important outcome consists in the subdivision of the overall cooling power provided by the solar collectors between convective and radiative components. It has been highlighted that in all the three reference locations only the radiative heat exchange contributes to the cooling effect during summertime, thus justifying the name "night sky radiant cooling" assigned to the considered technology; the convective part of the heat exchange process tends instead to reduce the cooling effect, due to the high external air temperatures.

Further experimental analysis should be carried out to assess the performances of the system during Spring and Summer and verify if the theoretical model built describes the behaviour of the system with sufficient accuracy under these weather conditions. Moreover, the energy consumption of the pumps has to be taken into account in order to provide a more complete analysis of the energy saving potential of the present application compared to conventional cooling technologies, such as refrigeration cycles.

Finally, the economic feasibility of the system needs to be studied in detail in order to evaluate the effective commercial potential of the application. On one hand, the night sky radiant cooling technology allows to increase the utilization factor of the solar collectors, which are supposed to be already installed for conventional water heating purposes (and possibly for electricity production). Indeed, their useful effect is extended to night-time. On the other hand, some components need to be added to the circuit just to perform the cooling operation, such as the cold water tank, the 3-way valve and most importantly the PCM panels, thus leading to additional capital investment. Furthermore, the complexity of the control system cannot be neglected.

9 Bibliography

[1] "The 2020 climate and energy package." [Online]. Available: http://ec.europa.eu/clima/policies. [Accessed: 15-Oct-2014].

[2] Y. Saheb, "Policy Pathway: Modernising Building Energy Codes." International Energy Agency, 2013.

[3] M. De Carli, "Energy and Buildings, course lectures." Università degli Studi di Padova, Padova, 2014.

[4] A. Sharma, V. V. Tyagi, C. R. Chen, and D. Buddhi, "Review on thermal energy storage with phase change materials and applications," *Renewable and Sustainable Energy Reviews*, vol. 13, no. 2, pp. 318–345, Feb. 2009.

[5] L. F. Cabeza, C. Castellón, M. Nogués, M. Medrano, R. Leppers, and O. Zubillaga, "Use of microencapsulated PCM in concrete walls for energy savings," *Energy and Buildings*, vol. 39, pp. 113–119, 2007.

[6] BASF Micronal, "Micronal PCM Brochure," 2015. [Online]. Available: http://www.micronal.de. [Accessed: 20-Oct-2014].

[7] G. Krasimirov Pavlov, "Building Thermal Energy Storage," Technical University of Denmark, 2014.

[8] H. Mehling and L. F. Cabeza, *Heat and cold storage with PCM: an up to date introduction into basics and applications*. Berlin: Springer Science & Business Media, 2008, pp. 11–55.

[9] D. W. Hawes, D. Feldman, and D. Banu, "Latent heat storage in building materials," *Energy and Buildings*, vol. 20. pp. 77–86, 1993.

[10] D. A. Neeper, "Thermal dynamics of wallboard with latent heat storage," *Solar Energy*, vol. 68, pp. 393–403, 2000.

[11] X. Jin, X. Xu, X. Zhang, and Y. Yin, "Determination of the PCM melting temperature range using DSC," *Thermochimica Acta*, vol. 595, pp. 17–21, Nov. 2014.

[12] F. Kuznik and J. Virgone, "Experimental assessment of a phase change material for wall building use," *Applied Energy*, vol. 86, pp. 2038–2046, 2009.

[13] S. Scalat, D. Banu, D. Hawes, J. Paris, F. Haghighat, and D. Feldman, "Full scale thermal testing of latent heat storage in wallboard," *Solar Energy Materials and Solar Cells*, vol. 44, pp. 49–61, 1996.

[14] U. Eicker and A. Dalibard, "Photovoltaic-thermal collectors for night radiative cooling of buildings," *Solar Energy*, vol. 85, pp. 1322–1335, 2011.

[15] M. G. Meir, J. B. Rekstad, and O. M. Løvvik, "A study of a polymer-based radiative cooling system," *Solar Energy*, vol. 73, no. 6, pp. 403–417, 2003.

[16] E. Hosseinzadeh and H. Taherian, "An Experimental and Analytical Study of a Radiative Cooling System with Unglazed Flat Plate Collectors," *International Journal of Green Energy*, vol. 9, pp. 766–779, 2012.

[17] Y. Etzion and E. Erell, "A hybrid radiative-convective cooling system for hot-arid zones," *Clean and Safe Energy Forever*, 1990.

[18] M. Santamouris and D. Asimakopoulos, *Passive Cooling of Buildings*. New York: Earthscan, 2013.

[19] Urban Omnibus, "Clip-on Architecture: Reforesting cities." [Online]. Available: http://urbanomnibus.net/2010/01/clip-on-architecture-reforesting-cities/. [Accessed: 25-Oct-2014].

[20] Archinspire, "Shallow pond roof innovative cooling system design." [Online]. Available: http://archinspire.org/wp-content/uploads/2010/04/. [Accessed: 25-Oct-2014].

[21] G. Mihalakakou, A. Ferrante, and J. O. Lewis, "The cooling potential of a metallic nocturnal radiator," *Energy and Buildings*, vol. 28. pp. 251–256, 1998.

[22] L. Gennari and P. Thibault, "Conditioning of a Plus-energy House using Solar Systems for both Production of Heating and Nighttime Radiative Cooling," Technical University of Denmark, 2014.

[23] Southface, "How solar thermal works." [Online]. Available: http://www.southface.org/learning-center/library/solar-resources. [Accessed: 03-Nov-2014].

[24] Solimpeks, "Solimpeks PV-T Datasheet." [Online]. Available: http://solimpeks.com.au/. [Accessed: 05-Nov-2014].

[25] M. Skrupskelis and O. B. Kazanci, "Solar Sustainable Heating, Cooling and Ventilation of a Net Zero Energy House," Technical University of Denmark, 2012.

[26] M. Mochizuki, T. Nguyen, K. Mashiko, Y. Saito, T. Nguyen, and V. Wuttijumnong, "A Review of Heat Pipe Application Including New Opportunities," *Frontiers in Heat Pipes*, vol. 2, no. 1, Mar. 2011.

[27] S. Zhang and J. Niu, "Cooling performance of nocturnal radiative cooling combined with microencapsulated phase change material (MPCM) slurry storage," *Energy and Buildings*, vol. 54, pp. 122–130, 2012.

[28] W. Lin, Z. Ma, M. I. Sohel, and P. Cooper, "Development and evaluation of a ceiling ventilation system enhanced by solar photovoltaic thermal collectors and phase change materials," *Energy Conversion and Management*, vol. 88, pp. 218–230, Dec. 2014.

[29] E. Bourdakis, "Experimental evaluation of chilled ceiling panels with microencapsulated PCM for energy efficient cooling of office spaces - Special Project Report," Kongens Lyngby, Denmark, 2013.

[30] *EN ISO 7726: Ergonomics of the thermal environment. Instruments for measuring physical quantities*. 2001.

[31] ASHRAE, "ASHRAE Psychrometric chart." [Online]. Available: www.ashrae.org. [Accessed: 15-Jan-2015].

[32] W. Stoecker, *Industrial Refrigeration Handbook*. New York: McGraw-Hill, 1998.

[33] "Thermal Conductivity of some common Materials and Gases." [Online]. Available: http://www.engineeringtoolbox.com/. [Accessed: 12-Mar-2015].

[34] Solar Energy Laboratory University of Wisconsin-Madison, GmbH - TRANSSOLAR Energietechnik, CSTB - Centre Scientifique et Technique du Bâtiment, and TESS – Thermal Energy Systems Specialists, "TRNSYS 17 Manual - Getting Started," *Simulation*, vol. 1. 2009.

[35] TESS – Thermal Energy Systems, "TESS Component Libraries, General Description." pp. 1–76.

[36] A. Ibrahim, M. Y. Othman, M. H. Ruslan, S. Mat, and K. Sopian, "Recent advances in flat plate photovoltaic/thermal (PV/T) solar collectors," *Renewable and Sustainable Energy Reviews*, vol. 15, no. 1, pp. 352–365, 2011.

[37] O. Rejeb, H. Dhaou, and A. Jemni, "Parameters effect analysis of a photovoltaic thermal collector: Case study for climatic conditions of Monastir, Tunisia," *Energy Conversion and Management*, vol. 89, pp. 409–419, 2015.

[38] Solar Energy Laboratory University of Wisconsin-Madison, TRANSSOLAR Energietechnik GmbH, CSTB – Centre Scientifique et Technique du Bâtimen, and T. – T. E. S. Specialists, "TRNSYS 17 - Standard component library overview." 2009.

[39] M. Kurzböck, G. M. Wallner, and R. W. Lang, "Black pigmented polypropylene materials for solar absorbers," *Energy Procedia*, vol. 30, no. 2011, pp. 438–445, 2012.

[40] A. Dentel and W. Stephan, "Thermal Comfort in Rooms with active PCM Constructions," in *Proceedings of the 8th International Conference on System Simulation in Buildings*, 2010, pp. 1–16.

[41] S. Furbo, "Hot water tanks for solar heating systems," Kongens Lyngby, Denmark, 2004.

[42] F. Causone, S. P. Corgnati, M. Filippi, and B. W. Olesen, "Solar radiation and cooling load calculation for radiant systems: Definition and evaluation of the Direct Solar Load," *Energy and Buildings*, vol. 42, pp. 305–314, 2010.

[43] S. Ferrari and V. Zanotto, "Office Buildings Cooling Need in the Italian Climatic Context: Assessing the Performances of Typical Envelopes," *Energy Procedia*, vol. 30, pp. 1099–1109, 2012.

[44] *UNI EN 15251: Indoor environmental input parameters for design and assessment of energy performance of buildingsaddressing indoor air quality, thermal environment, lighting and acoustics*. 2006.

[45] U.S. Department of Energy, "EnergyPlus Energy Simulation Software - Weather Data Sources." [Online]. Available: energy.gov/buildings/energyplus. [Accessed: 25-Mar-2015].

[46] *EN ISO 7730: Ergonomics of the thermal environment - Analytical determination and interpretation of thermal comfort using calculation of the PMV and PPD indices and local thermal comfort criteria*. 2005.

[47] E. J. de P. Hansen, *Guidelines on Building Regulations 2010*, 2nd ed. Danish Building Research Institute, Aalborg University, 2012.

[48] "Conducibilità termica." [Online]. Available: http://www.poliuretano.it/isolamento_poliuretano. [Accessed: 14-Feb-2015].

[49] *UNI EN ISO 6946, Componenti ed elementi per edilizia, Resistenza termica e trasmittanza termica, Metodo di calcolo*, no. 0. 2008.

[50] J. Fan, "Solar Collector Theory and Efficiency." Kogens Lyngby, 2012.

[51] J. A. Duffie and W. A. Beckman, *Solar Engineering of Thermal Processes: Fourth Edition*. 2013.

[52] T. Anderson, M. Duke, and J. Carson, "Performance of an unglazed solar collector for radiant cooling," *Australian solar cooling interest group*, 2013.

[53] O. Gliah, B. Kruczek, S. G. Etemad, and J. Thibault, “The effective sky temperature: an enigmatic concept,” *Heat and Mass Transfer*, vol. 47, no. 9, pp. 1171–1180, Mar. 2011.

[54] D. Pandey, “Effects of atmospheric emissivity on clear sky temperatures,” *Atmospheric Environment*, vol. 29, no. 16, pp. 2201 – 2204, 1995.

[55] Jeppesen Sanderson Inc., *Guided Flight Discovery Privat Pilot Manual*. Englewood, Colorado, 2004.

10 List of figures

11 List of tables

12 Appendices

12.1 TRNSYS component's parameters

12.1.1 PV-T parameters

Table 12.1 – Properties of the PV-T component

Parameter	Value
Collector length [m]	1.315
Collector width [m]	2.988
Absorber plate thickness [m]	0.001
Thermal conductivity of the absorber [W/mK]	380
Number of tubes [ ]	15
Tube diameter [m]	0.018
Bond width [m]	0.01
Bond thickness [m]	0.001
Bond thermal conductivity [W/mK]	380
Resistance of substrate material [m^2K/W]	0.01
Resistance of back material [m^2K/W]	2.8
U-value of roof material [W/m^2K]	25
Fluid specific heat [kJ/kgK]	3.35
Reflectance [ ]	0.15
Emissivity [ ]	0.89
PV cell reference temperature [°C]	25
PV cell reference radiation [W/m^2]	1000
PV efficiency at reference condition [ ]	0.1843
Collector slope [°]	45
Collector azimuth [°]	0
Fluid heat transfer coefficient	350

The width shown in the previous table is the sum of the widths of the 3 collectors, while the length (vertical dimension) is the same for each of them.

The absorber plate was assumed to be made of copper with a thickness of 1 mm. A thermal conductivity of 380 W/mK was taken for copper.

The bond layer between the tube and the absorber plate was assumed to be copper with a thickness of 1 mm and a width of 1 cm. These dimensions were the ones already implemented in the standard type 563.

The default value of 0.01 m^2K/W was taken as resistance of substrate material.

The thermal resistance of the back material was calculated considering a polyurethane insulation layer (thermal conductivity 0.025 W/mK [48]) with a thickness of 7 cm, as it was in the experimental setup.

The heat carrier was assumed to be a mixture of water and ethylene glycol (40% of glycol mass fraction). A value of 3.35 kJ/kgK was found in literature as specific heat capacity of the water-glycol mixture [32].

As described previously, in the experimental layout the PV-T panels were not adhering to the horizontal roof of the building but they were mounted on a wooden support structure with a tilt angle of 45°. Hence, the reciprocal of the external thermal surface resistance of a flat surface was taken as U-value of the air roof material. A value of 0.04 m^2K/W is indicated for the mentioned thermal resistance in standard UNI EN ISO 6946-2008 [49].

The default value of 0.15 was considered for the reflectance.

The emissivity of the front surface was measured in a previous experiment performed on the same panels by means of a thermographic camera [22]. An average value of 0.89 was indicated in this study.

The electrical efficiency was reported in the datasheet, referred to the standard conditions reported.

The slope and the azimuth angle of the collectors were set to 45° and 0° (the front surface was facing South), respectively.

Default values of the component were used for the efficiency modifier coefficients, both for temperature and radiation.

The heat transfer coefficient between the tubes and the collector fluid was calculated to be 350 W/m^{2}K. The calculation approach used was taken from [50].

12.1.2 Unglazed collector: efficiency factor and heat loss coefficients

The collector efficiency factor (F') describes how well the absorber/tube transports the energy from the outside of the tube into the solar collector fluid. An efficiency factor of 1 means that the heat resistance from the outside of the tube into the solar collector fluid is zero or the heat loss from the absorber/tube is zero.

The "path" of the solar radiation from the absorber plate to the fluid flowing inside the tubes is illustrated in Figure 12.1.

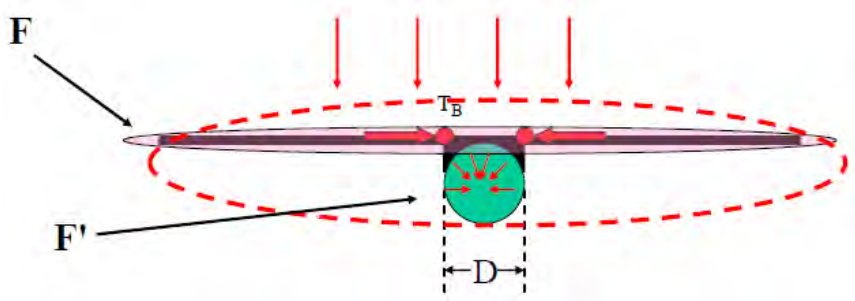

Figure 12.1 – Schematic representation of the heat transfer from the absorber plate to the fluid [50]:

The collector efficiency factor has been calculated according to the following equation [51]:

$$F' = \frac{1/U_L}{W \cdot \left[\frac{1}{U_L \cdot [D + (W - D) \cdot F]} + \frac{1}{\pi \cdot D_i \cdot h_{fi}}\right]}$$

where:

- U_L is the overall heat loss coefficient of the collector, expressed in W/(m^{2}K)
- W is the pipe spacing (m), as illustrated in Figure 12.2
- D and D_i are respectively the external and the internal diameter of one tube (m)
- F is the fin efficiency
- h_{fi} is the heat transfer coefficient between the wall and the tube wall, in W/(m^{2}K).

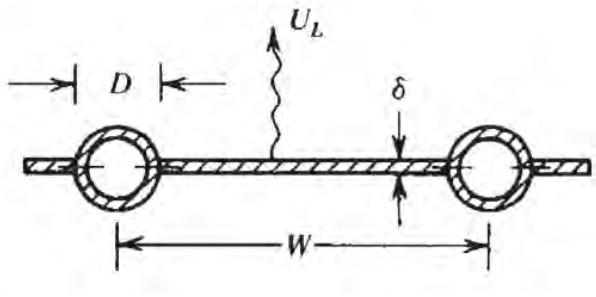

Figure 12.2 – Section of the unglazed collector [51]

The fin factor describes how well the fin transports the absorbed solar energy from the fin to the tube containing the fluid. A fin factor of 1 means that all the absorbed solar energy is transported to the tube.
The efficiency of straight fins is calculated as follows [51]:

$$F = \frac{\tanh[m\,(W-D)/2]}{m\,(W-D)/2}$$

with:

$$m = \sqrt{\frac{U_L}{k\,\delta}}$$

k and δ being respectively the thermal conductivity (in W/mK) and the thickness of the plate between the tubes (in m).

The total heat loss coefficient U_L is the sum of the heat transfer coefficient of bottom (U_b), top (U_{top}) and edges (U_e) of the solar collector:

$$U_L = U_b + U_t + U_e$$

According to [51], the bottom losses can be approximated to:

$$U_L = \frac{\lambda_{ins}}{L_{ins}}$$

λ_{ins} and L_{ins} being the thermal conductivity and the thickness of the insulation placed at the bottom of the collector. The convective and radiative contribution to the bottom losses can usually be neglected, given the much higher resistance of the insulation.

For a well-designed system, the edge loss should be small so that it is not necessary to predict it with great accuracy. The edges losses can therefore be estimated by assuming one-dimensional sideways heat flow around the perimeter of the collector, as follows [51]:

$$U_{edge} = \frac{\lambda_{edge}}{L_{edge}}$$

The convective and radiative contributions to the edge loss can be ignored for the same reason mentioned for the bottom loss.
The edge loss coefficient should then be referred to the collector area A_c [51]:

$$U_e = U_{edge} \cdot \frac{A_{edge}}{A_c}$$

where A_{edge} is the heat transfer surface of the edges.

The top thermal loss coefficient is the sum of the convection (h_c) and the radiation (h_r) heat transfer coefficient on the top surface of the collector [51]:

$$U_t = h_{c,top} + h_{r,top}$$

The convective heat transfer coefficient has been estimated according to [37]:

$$h_{c,top} = 2.8 + 3\, v_{wind}$$

while the radiative coefficient has been evaluated by means of the function [52]:

$$h_r = \sigma \cdot \varepsilon_p \cdot (T_{pm}^2 + T_{sky}^2) \cdot (T_{pm} + T_{sky})$$

where:

- σ is the Stefan-Boltzmann constant (5.670373×10^{-8} W m^{-2} K^{-4})
- ε_p is the collector plate emissivity
- T_{pm} is the mean collector plate temperature
- T_{sky} is the sky temperature.

12.1.3 Sky temperature: theoretical calculation

Since the effective sky temperature was neither measured by the weather station nor present in any meteorological database for the location were the experiment took place, an algorithm based on the available data was implemented to calculate this parameter.

The sky temperature can be calculated as follows [53]:

$$T_{sky} = \varepsilon_{sky}^{1/4} * T_{amb}$$

where:

- T_{sky} is the temperature of the sky, expressed in K
- ε_{sky} is the sky emissivity
- T_{amb} is the ambient temperature, in K.

Different methods to evaluate the atmospheric emissivity under clear sky conditions ε_0 can be found in literature, each of them leading to a different mathematical correlation [22] [53] [54]. Some of them are presented in Table 12.2, where p_v, T_{amb} and T_{dp} are the partial water vapour pressure (in mbar), the external air temperature (in °C) and the dew point temperature (in °C), respectively.

Table 12.2 – Correlations for the calculation of cloudless sky emissivity

Emissivity Correlation	**Author**
$\varepsilon_0 = 0.21 + 0.22\, ln\, p_v$	Elsasser (1942)
$\varepsilon_0 = 0.8004 + 0.00396\, T_{dp}$	Bliss (1961)
$\varepsilon_0 = 0.0552\, T_{amb}$	Swinbank (1963)
$\varepsilon_0 = 0.787 + 0.0028\, T_{dp}$	Clark and Allen (1978)
$\varepsilon_0 = 0.770 + 0.0061\, T_{dp}$	Berdahl and Fromberg (1982)
$\varepsilon_0 = 0.770 + 0.0038\, T_{dp}$	Berger et al. (1984)
$\varepsilon_0 = 0.711 + 0.0056\, T_{dp} + 0.000073\, T_{dp}^2$	Martin and Berdahl (1984)

The equation proposed by Martin and Berdahl was chosen since it is the only one interpolating the experimental data with a non-linear equation, thus allowing probably to a more detailed description of the phenomena. The dew point temperature T_{dp} is recorded by the weather station.

The presence of clouds increases the atmospheric absorbance and hence the emittance. Hence, the emissivity of an overcast sky is higher than the one of a clear sky. An empirical adjustment of the chosen cloudless model is introduced to estimate the sky emissivity under overcast conditions [15]. If clouds are present, the emissivity is a function of the fractional cloud cover, the cloud emittance and the temperature difference between the surface and the cloud base, according to the following equation:

$$\varepsilon_{sky} = \varepsilon_0 + (1 - \varepsilon_0)\, \varepsilon_c\, n\, e^{-Z_c/Z^*}$$

where:

- ε_c is the hemispherical cloud emissivity
- n is the fractional cloud amount of the sky covered by "non-transparent" clouds and its value varies between 0 and 1
- Z_c is the cloud base height, expressed in km
- Z^* is a reference value fixed to 8.2 km.

The hemispherical cloud emissivity ε_c can be approximated to 1 for low and medium high clouds (height below 4 km) and to 0.15 for clouds height above 11 km, while it has to be calculated according to the following equation if the height is between 4 and 11 km:

$$\varepsilon_c = 0.74 - 0.084\,(Z_c - 4)$$

The value of n is calculated as follows:

$$n = \frac{N}{8}$$

where N is the cloud cover factor, varying between 0 for a clear sky and 8 when the sky is completely overcast.

Since no meteorological stations sufficiently close to the location of the experiment were recording the value of the cloud cover factor, hourly forecasts of the fractional cloud amount of the sky (n) were considered. The cloud cover data were taken from a weather station located approximately 1 km South-East from the site of the experiment. Every hourly value was selected 5 minutes before the related hour started, in order to achieve the most accurate prediction possible.

The cloud base height Z_c can be calculated as a function of the air temperature and the dew point temperature measured on the earth's surface, as expressed in the following correlation [55]:

$$Z_{c,feet} = \frac{T_{air,°F} - T_{dp,°F}}{4.4} * 1000$$

where $Z_{c,feet}$ is the approximated cloud base height in thousands of feet, while $T_{air,°F}$ and $T_{dp,°F}$ are the air temperature and the dew point temperature expressed in Fahrenheit, respectively.
This equation derives from a consideration regarding the cloud formation process. Indeed, clouds often form at the altitude where the air rising in a convective current equals the dew point temperature. When lifted, unsaturated air cools at about 5.4 °F per 1000 feet while the dew point temperature decreases at about 1 °F per 1000 feet. Therefore, the air temperature and the dew point converge with a rate of 4.4 °F every 1000 feet.
The conversion between feet and km has been implemented in order to obtain the cloud base height expressed in km (1000 feet = 304.80 m).

12.2 Envelope characteristics of the climate chamber simulated in TRNSYS

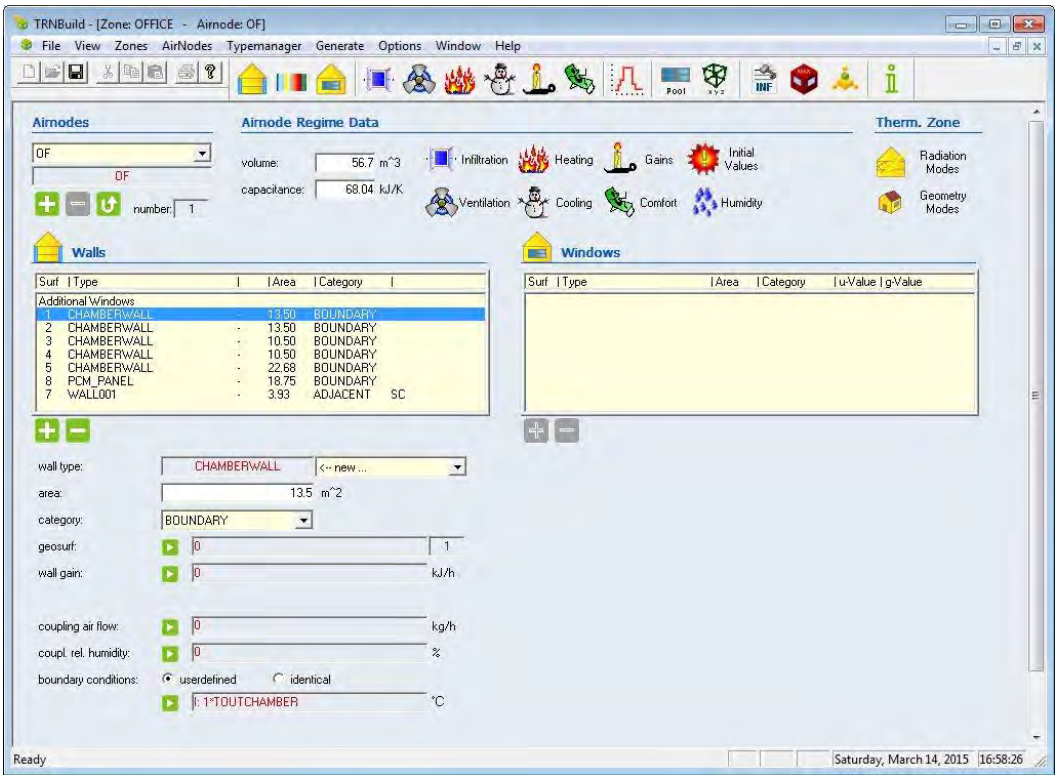

Figure 12.3 – Overview of the occupancy zone of TRNSYS building model

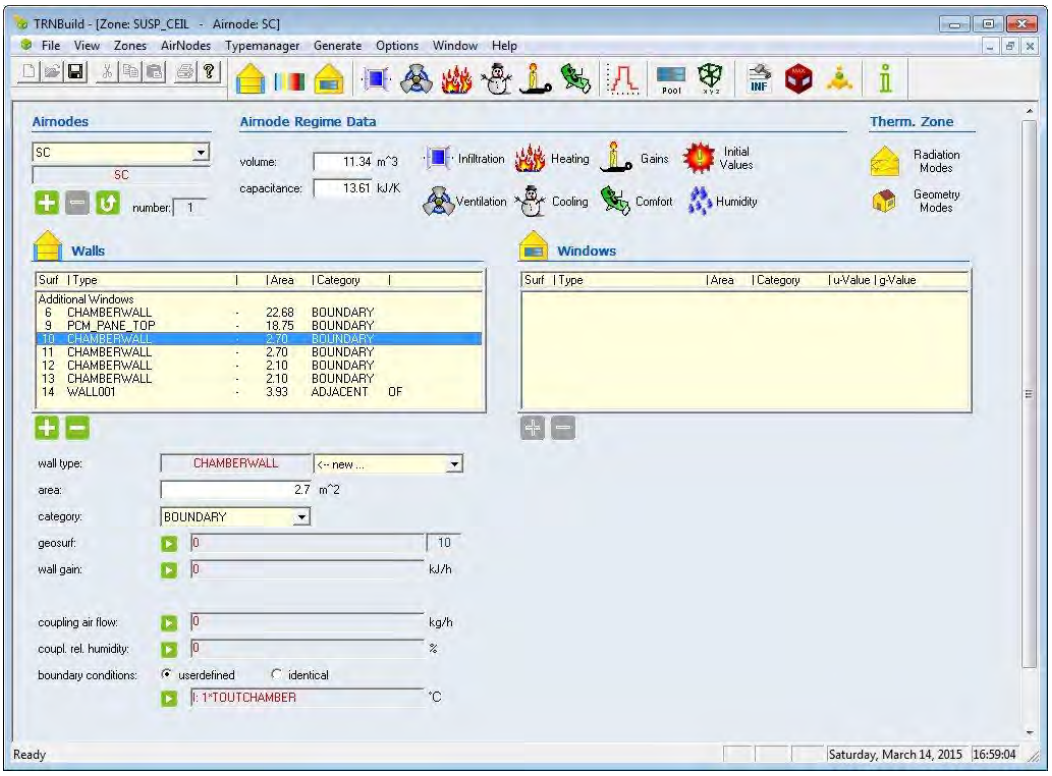

Figure 12.4 – Overview of the zone above the suspended ceiling of TRNSYS building model

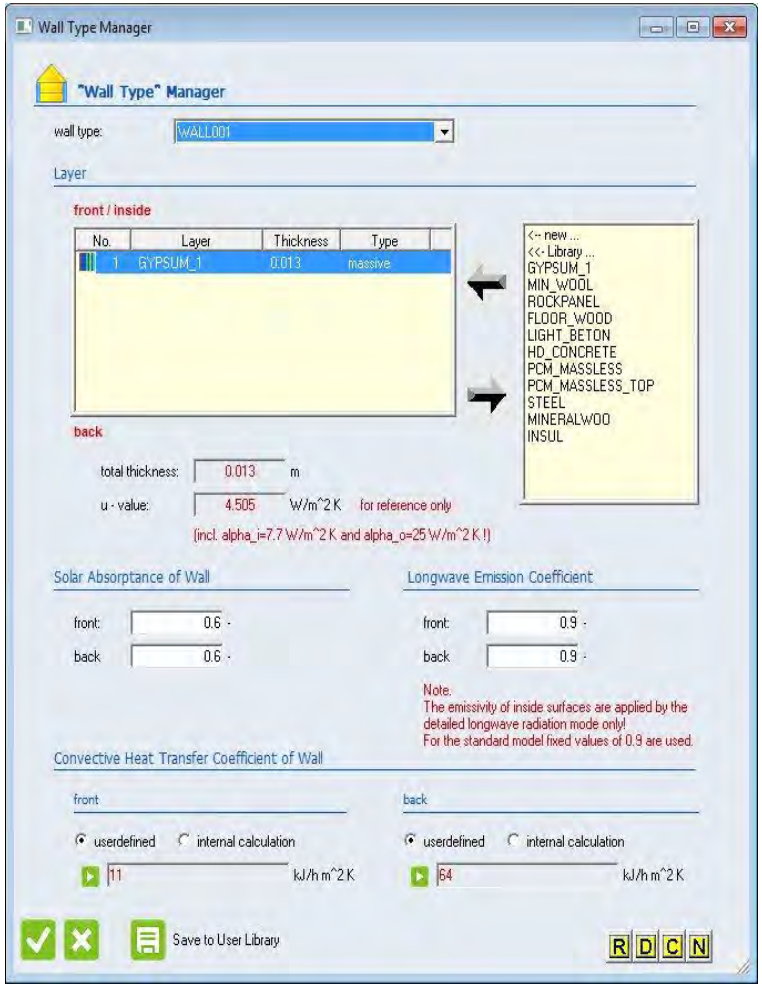

Figure 12.6 – Parameters of the ceiling gypsum panels

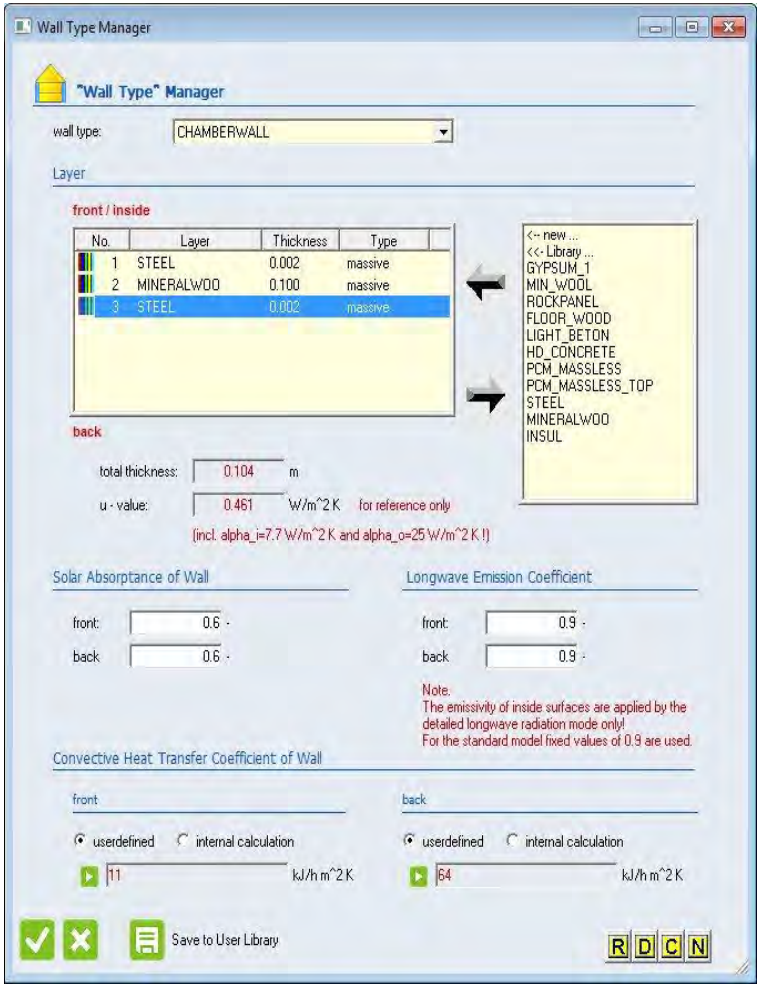

Figure 12.5 – Parameters of the walls of the climate chamber

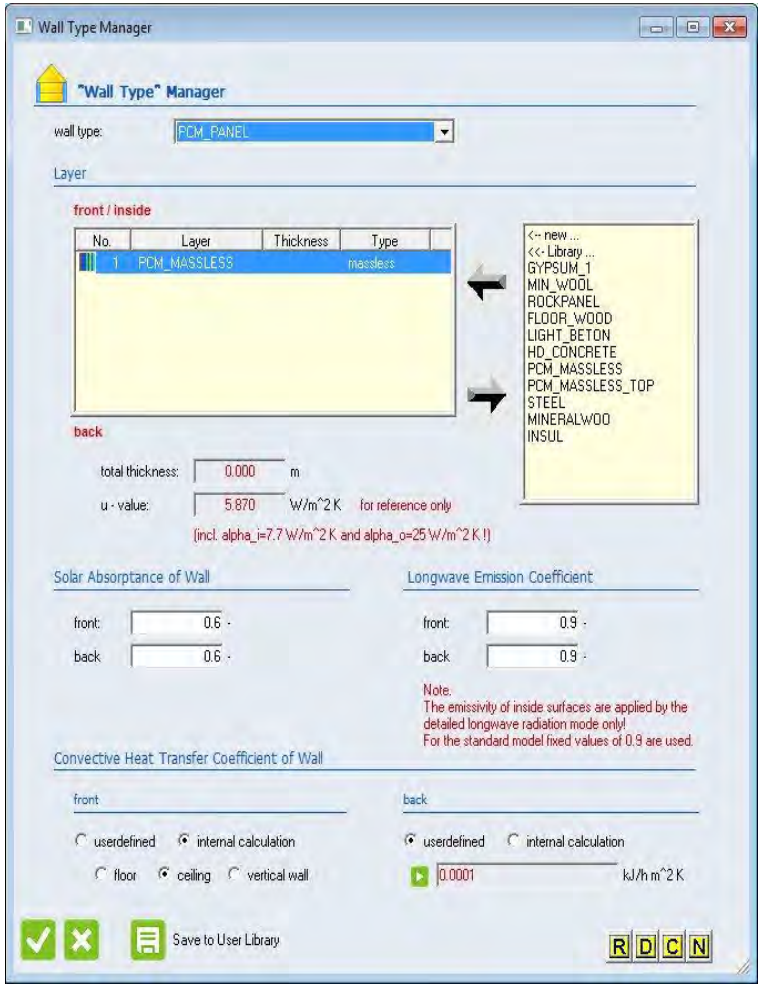

Figure 12.8 – Parameters of the bottom surface of the PCM panels

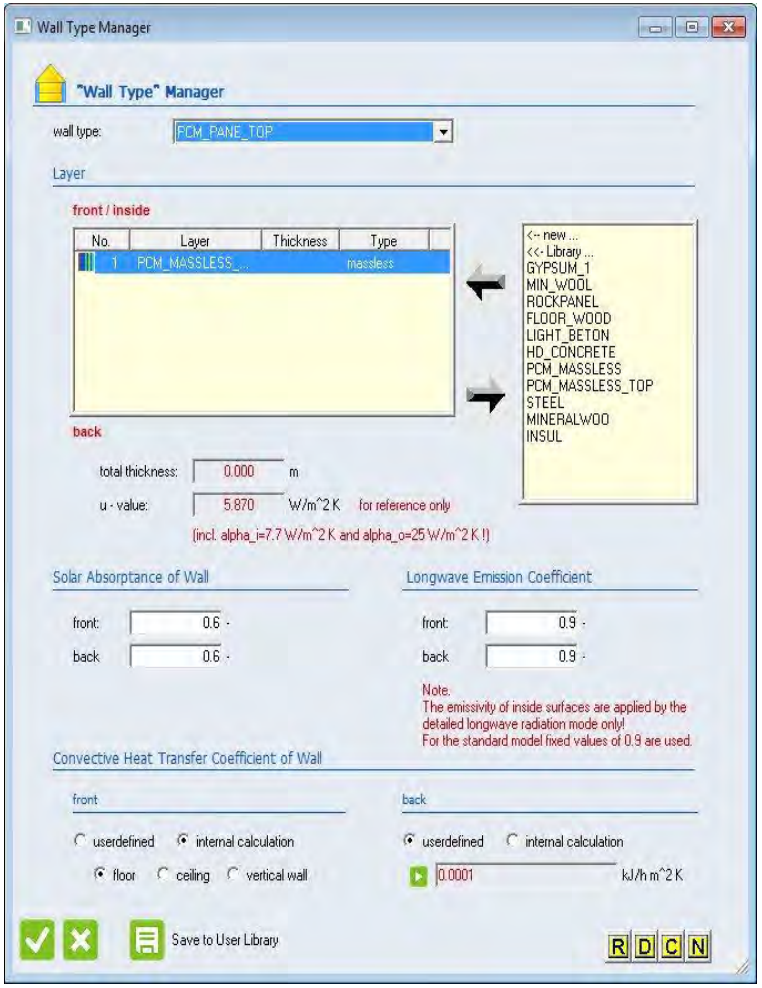

Figure 12.7 – Parameters of the top surface of the PCM panels

12.3 Envelope characteristics of the office room simulated in TRNSYS

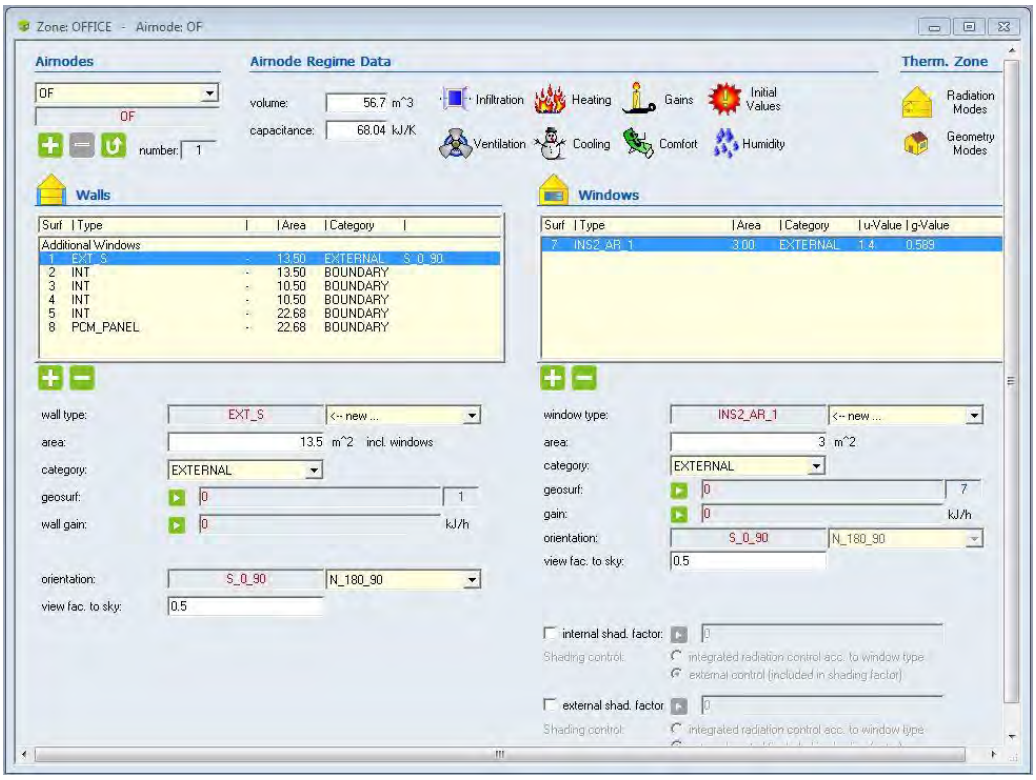

Figure 12.9 – Overview of the occupancy zone of TRNSYS building model

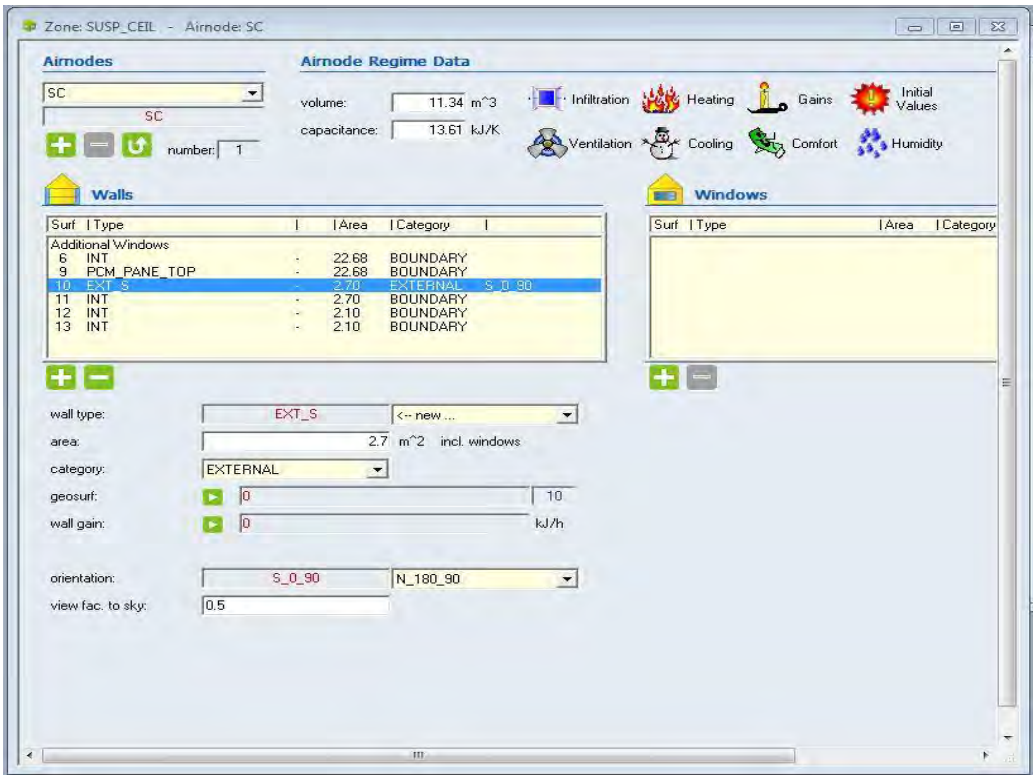

Figure 12.10 – Overview of the zone above the suspended ceiling of TRNSYS building model

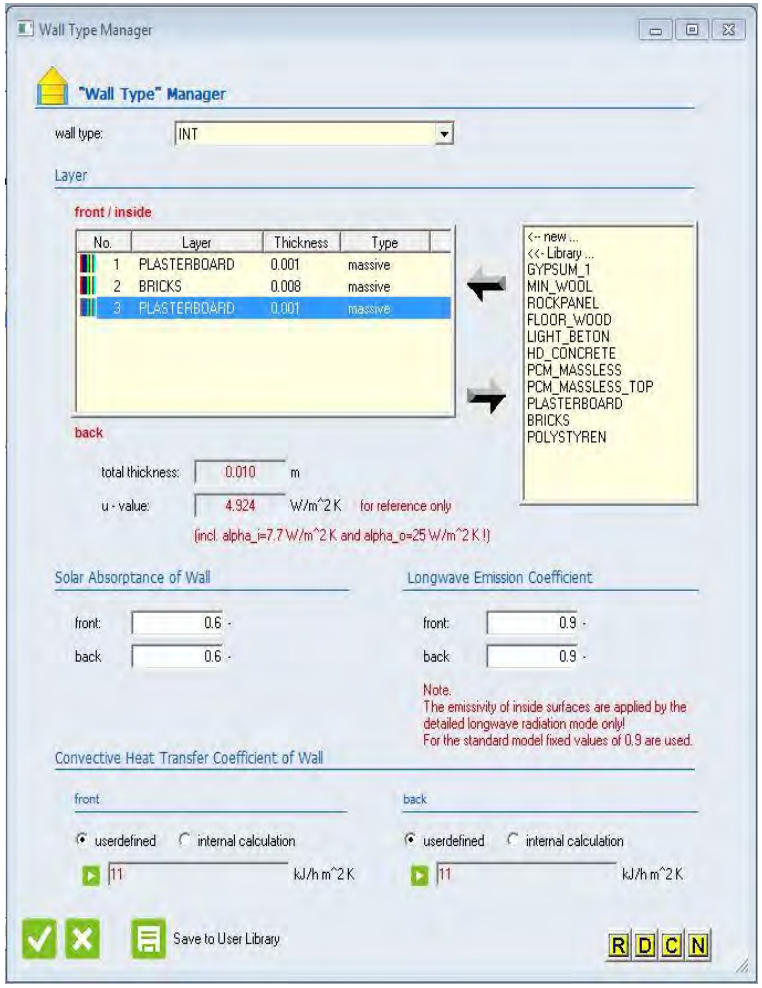

Figure 12.12 – Parameters of the internal walls of the office room

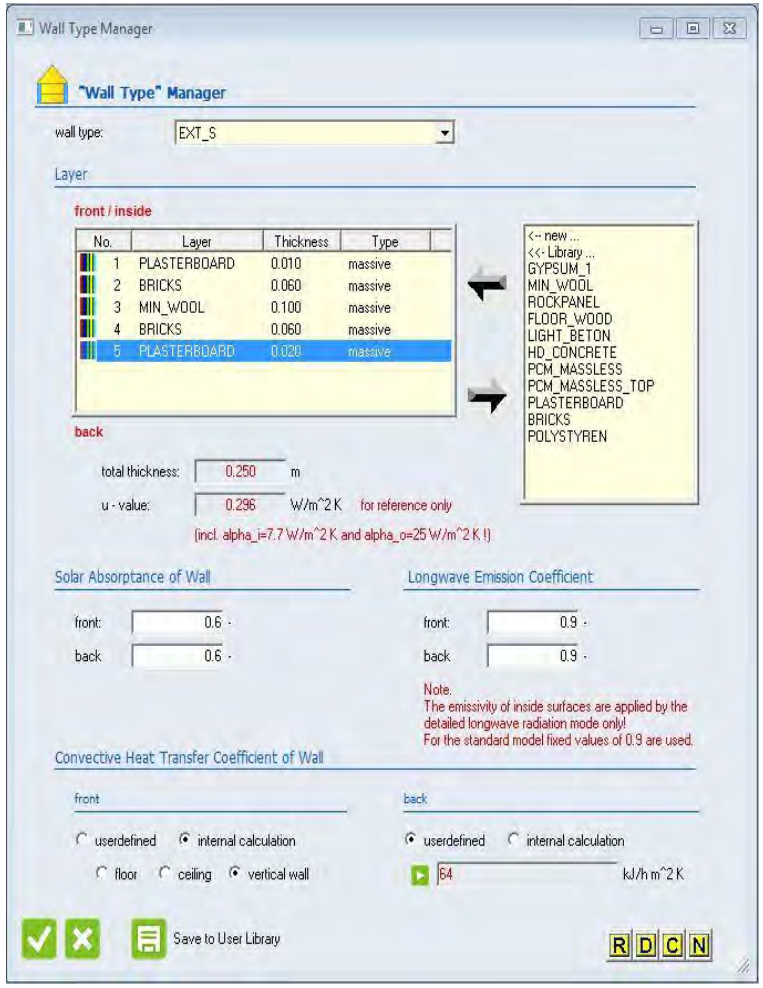

Figure 12.11 – Parameters of the external wall of the office room